

THE UNIVERSITY OF MANITOBA

LOW TEMPERATURE NUCLEAR MAGNETIC RESONANCE

AND RELAXATION IN MANGANESE FERRITE

by

JAMES H. DAVIS

A THESIS

SUBMITTED TO THE FACULTY OF GRADUATE STUDIES

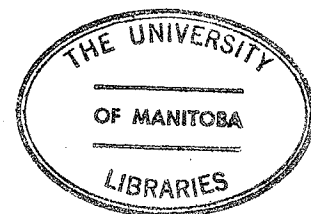
IN PARTIAL FULFILMENT OF THE REQUIREMENTS FOR THE DEGREE

OF DOCTOR OF PHILOSOPHY

DEPARTMENT OF PHYSICS

WINNIPEG, MANITOBA

February 1976



"LOW TEMPERATURE NUCLEAR MAGNETIC RESONANCE
AND RELAXATION IN MAGANESE FERRITE"

by

JAMES H. DAVIS

A dissertation submitted to the Faculty of Graduate Studies of
the University of Manitoba in partial fulfillment of the requirements
of the degree of

DOCTOR OF PHILOSOPHY

© 1975

Permission has been granted to the LIBRARY OF THE UNIVER-
SITY OF MANITOBA to lend or sell copies of this dissertation, to
the NATIONAL LIBRARY OF CANADA to microfilm this
dissertation and to lend or sell copies of the film, and UNIVERSITY
MICROFILMS to publish an abstract of this dissertation.

The author reserves other publication rights, and neither the
dissertation nor extensive extracts from it may be printed or other-
wise reproduced without the author's written permission.

PREFACE

The ^{55}Mn nuclear magnetic resonance of the A-site ions in manganese ferrites provides an opportunity to study many of the features characteristic of magnetic materials. The strong signal and the cubic symmetry of the A-sites make this a relatively easy system to study although the presence of two strongly overlapping signal components and the fairly complex structure of the spinel lattice result in some difficulty in the interpretation of the spectra.

Nuclear magnetic resonance in ordered magnetic materials has many distinctive features and some special problems, these are discussed in Chapter I, as an introduction, with particular reference to the properties of manganese ferrites. The strong magnetic hyperfine interaction, the spin-wave interactions, and the existence of domain-walls lead to most of the interesting properties of this system, including the Suhl-Nakamura or indirect nuclear spin-spin interaction, spin-wave relaxation processes, and the contrast in the behaviour of the two components of the signal (due to nuclei in domains and in domain walls).

Chapter II gives a detailed discussion of the Suhl-Nakamura interaction with particular reference to its role in the formation of multiple echoes following a two pulse rf excitation of the spin system.

Chapter III is a general discussion of relaxation processes in magnetic materials, including dipole-dipole and spin-wave relaxation as well as the dominant Suhl-Nakamura relaxation. The frequency dependent relaxation due to the Suhl-Nakamura interaction is compared to the experimental data for the first three echoes, followed by a discussion of the two-component nature of the spectrum in low external fields.

Chapter IV discusses and compares the temperature and field dependences of the two components of the spectrum. The technique of fitting a set of partially relaxed spectra to a function (made up of two independently relaxing components) of two independent variables, frequency and rf pulse separation, allows the effective separation of the spectrum into its domain and domain-wall components.

Finally, Chapter V gives a brief discussion and conclusion, pointing out some areas where the techniques used here may be usefully applied.

I would like to thank my supervisor Dr. C. W. Searle for his help and encouragement during the course of this work, and Dr. Akira Hirai of Kyoto University, Kyoto, Japan, who assembled much of the equipment and pointed out the existence of multiple echoes in manganese ferrite. The practical advice and assistance in many areas given by Dr. Iman Maartense has been especially helpful. Finally, I would like to thank my wife for her patience and for her help in drawing the figures.

TABLE OF CONTENTS

	page
Preface	i
Table of Contents	iii
Abstract	vi
I. Introduction to NMR in Magnetic Materials	1
1. Manganese Ferrite	1
2. The Magnetic Field at the Nucleus	2
2.1 The dipolar contributions--the Lorentz and demagnetizing fields	3
2.2 The electronic hyperfine field	4
3. Magnetic Ordering	6
3.1 The exchange interaction	6
3.2 Molecular field theory	8
4. Spin Waves	9
4.1 Holstein-Primakoff diagonalization	11
4.2 The diagonalized Hamiltonian	13
4.3 The ferrimagnon dispersion relation	17
4.4 Higher order terms	21
4.4.a Three-magnon dipolar Hamiltonian	21
4.4.b Four-magnon exchange Hamiltonian	22
5. Magnetocrystalline Anisotropy	23
6. Domain Walls	25
6.1 Equation of motion of a domain wall	27
7. The Coupled Equations of Motion of the Magnetic Sublattices	29
7.1 Single domain enhancement	31
7.2 Frequency pulling	31

8. Free Precession of Nuclear Moments	33
8.1 Free induction decay and spin echoes	33
8.2 Relaxation processes--longitudinal and transverse	34
9. Inhomogeneous Broadening--Instrumental Considerations	38
II. The Suhl-Nakamura Interaction and the Formation of Multiple Echoes	45
1. The Hyperfine Interaction Spin-Wave Expansion	45
2. Second-Order Effective Nuclear Spin-Spin Interaction	48
2.1 Perturbation expansion	48
2.2 Asymptotic form of the range function	49
3. Density Matrix Treatment of Pulsed Resonance	51
3.1 Form of the time development operators	55
3.2 The free-induction-decay and spin-echoes	59
4. Multiple Echoes	62
4.1 Observation of multiple echoes in manganese ferrites	62
4.2 Stimulation by nuclear spin-spin interaction	64
4.3 Density matrix calculation for the effective pulse	70
III. Relaxation Processes in Magnetically Ordered Systems	75
1.1 The approach to equilibrium	75
1.2 Line broadening	76
1.3 The method of moments	77
2. Longitudinal Dipole-Dipole Relaxation	78
3. Suhl-Nakamura and Transverse Dipole-Dipole Relaxation	81

4.	Spin-Wave Scattering Processes	88
4.1	Three-magnon relaxation	90
4.2	Exchange enhancement of the three-magnon process	93
4.3	Dipolar induced two-magnon process	99
5.	Frequency-Dependent Relaxation--Comparison with Data-- Relaxation of Multiple Echoes	104
6.	The Multi-Domain Spectra	115
IV.	Spectra from Domain Walls and Domains	122
1.	Separation of the Two Signal Components	122
2.	Spectra at $T = 1.45$ °K	126
2.1	Lineshapes of the two components	127
2.2	Field dependence of the spectra	132
3.	Temperature Dependence-- $1.45 \rightarrow 4.2$ °K	144
3.1	The shape of the spectra	145
3.2	Temperature dependent background relaxation	161
4.	Effects of Crystal Orientation on the Spectrum at $T = 4.2$ °K	173
5.	Three-Pulse Experiments--The Stimulated Echo	183
V.	Conclusion	192
	Appendix I: The Method of Moments	196
	References	203

ABSTRACT

The A-site ^{55}Mn nuclear magnetic resonance at low temperatures consists of two overlapping signal components, one due to nuclei within the domain walls, the other due to nuclei within the bulk domains. The resonance is inhomogeneously broadened and characterized by strongly frequency dependent relaxation. Two-pulse spin-echo measurements show that the Suhl-Nakamura or indirect spin-spin interaction is responsible for most of the low temperature relaxation near resonance, and provides a mechanism for the formation of multiple echoes. By studying a series of partially relaxed spectra it is possible to separate the two signal components leading to the observation of the different temperature dependences of the frequency-independent part of the relaxation of the two components. This difference is felt to be due to the narrowing of the longitudinal dipole-dipole interaction's contribution to the homogeneous linewidth of the domain-wall component but not of the domain component. Spin-wave scattering, in particular the dipolar-induced two-magnon process, provides the strongly temperature dependent contribution to the total relaxation rate.

CHAPTER I

Introduction to NMR in Magnetic Materials

The features that distinguish the nuclear magnetic resonance in magnetic materials from that in other solids are: i) the presence, in the ordered state, of strong magnetic hyperfine fields ($\sim 10^5 - 10^6$ Oe), ii) the distribution of these hyperfine fields and the subsequent severe broadening of the resonance lines, iii) the existence of domain walls in non-saturated samples and the complicated enhancement mechanisms associated with these domain walls, iv) the possibility of the existence of two signal components--one from domain walls, the other from the bulk domains--which strongly overlap each other, and v) the interaction of the nuclear spins with unpaired electronic spins or, in the ordered state, with spin waves. These strictly magnetic effects profoundly alter the nature of the nuclear resonance and, therefore, must be carefully considered and understood before any analysis of the spectra can be attempted.

1. Manganese Ferrite

Manganese ferrite (MnFe_2O_4) is a magnetic insulator and has the spinel (MgAl_2O_4) structure with the magnetic (Mn, Fe) ions located on two crystallographically inequivalent sites, the tetrahedral A-sites and the octahedral B-sites. The ionic distribution has been studied in some detail¹⁻⁴ and can be described by the formula unit $\text{Mn}_{0.8}^{2+}\text{Fe}_{0.2}^{3+}[\text{Mn}_{0.2}^{3+}\text{Fe}_{1.8}]_0_4$, where the cations outside the brackets occupy the

tetrahedral sites and the cations inside the brackets occupy the octahedral sites. The nuclear resonance of the ^{55}Mn nuclei on the two different sites have been reported and identified⁴ as being from Mn^{2+} ions on the A-sites and Mn^{3+} ions on the B-sites. The B-site resonance will be quadrupolar split into $2I = 5$ components due to the non-cubic symmetry of the octahedral sites (the octahedral symmetry does not extend beyond the O^{2-} ions forming the octahedron), while the A-site, due to its tetrahedral symmetry, has a single resonance line. The work reported here is concerned only with the ^{55}Mn resonance from ions on the A-sites.

The spinel A-site, illustrated in Figure 1, is at the center of a tetrahedron formed by four O^{2-} ions. Each of the oxygen ions is connected to three B-site cations (Mn^{3+} , Fe^{3+}) in such a way as to preserve the tetrahedral symmetry of the A-site. Because of this symmetry, the dipolar field at the A-site is expected to be zero, as is the quadrupole splitting. Some small contribution to the local field may exist due to the presence of different ions on the B-sites, however, there is no indication of this in the nuclear resonance data.

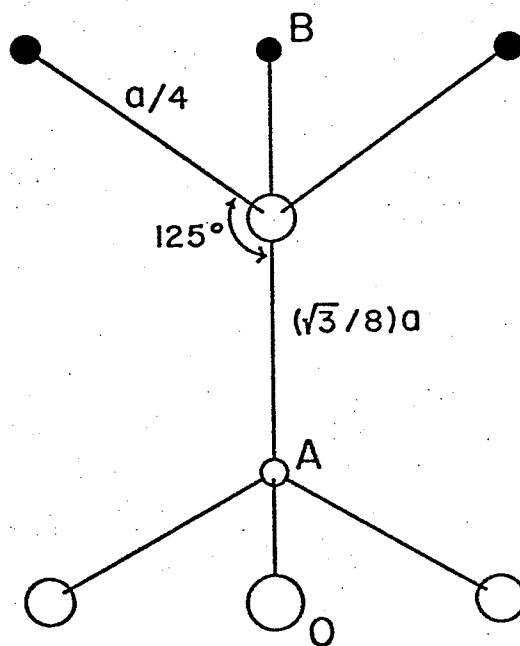


Figure 1. The spinel A-site. Large circles are oxygen ions and the dark circles are B-sites. $a = 8.5 \text{ \AA}$.

2. The Magnetic Field at the Nucleus

The magnetic field at a nucleus in a magnetic material is the sum of

the externally applied field, the magnetic field due to the distribution of the magnetic dipoles surrounding the ion containing the nucleus, and the electronic hyperfine field.

2.1 The dipolar contributions---the Lorentz and demagnetizing fields

The total dipolar contribution to the microscopic magnetic field at nucleus i in a single domain sample is

$$\vec{h}_{dd} = g\mu_B \sum_j \left(\frac{1}{r_{ij}}\right)^5 (\vec{S}_j r_{ij}^2 - 3\vec{r}_{ij} (\vec{S}_j \cdot \vec{r}_{ij})) \quad (1)$$

where \sum_j is over all spins \vec{S}_j located at position \vec{r}_{ij} with respect to spin i , g is the electronic spectroscopic splitting factor and μ_B is the Bohr magneton. (The field due to nuclear dipoles may be neglected.) This sum may be evaluated by breaking it up into the sums over spins in two regions separated by a surface, called the Lorentz sphere, such that the volume enclosed by the sphere is large by atomic dimensions but small on a macroscopic scale. Then, the sum is evaluated explicitly for spins inside the sphere and the contribution from spins outside the sphere can be evaluated as an integral over the volume enclosed by the sample's surface and the Lorentz sphere. If we define, after Keffer⁵

$$D_V^{IJ} = D_L^{IJ} + D_{V-L}^{IJ} = \sum_{\ell} (3r_{\ell}^I r_{\ell}^J - r_{\ell}^{2, IJ}) r_{\ell}^{-5}$$

for cartesian components I, J of r_{ℓ} , where D_L^{IJ} is the sum over the interior of the Lorentz sphere, then,

$$D_{V-L}^{IJ} \rightarrow \delta^{IJ} \int_{V-L} (\partial/\partial r^I) (-r^I/r^3) d\vec{r} = -\delta^{IJ} \int (r^I/r^3) \hat{I} \cdot (d\vec{S}_1 - d\vec{S}_2)$$

where $\delta^{IJ} = 0$ unless $I = J$, and S_1 is the surface of the sample, and S_2 is

the Lorentz sphere. Then, assuming an ellipsoidal sample,

$$D_{V-L}^{IJ} = \left(\frac{4\pi}{3} - N^I\right) \delta^{IJ}$$

The factor $4\pi/3$ is due to the uncompensated poles at the surface of the Lorentz sphere, while the factor N^I , called the demagnetizing factor, is due to uncompensated magnetic poles on the surface of the sample. For a spherical sample, $N^I = 4\pi/3$ and $D_{V-L}^{IJ} = 0$.

The contribution to the field from spins inside the Lorentz sphere is called the dipolar field and can be readily evaluated by direct summation over lattice sites. For sites (of the spin i) of cubic symmetry the dipolar field vanishes.

2.2 The electronic hyperfine field

By far the largest contribution to the magnetic field at the nucleus is the field produced by it's ion's own electrons--the electronic hyperfine field. The magnetic hyperfine interaction can be written as⁶

$$\mathcal{H}_{\text{hf}} = -g g_N \mu_B \mu_N \sum_i \left(\frac{8\pi}{3} \delta(r_i) \vec{S}_i \cdot \vec{I} + \frac{(\vec{L}_i - \vec{S}_i) \cdot \vec{I}}{r_i^3} + \frac{3(\vec{S}_i \cdot \vec{r}_i)(\vec{I} \cdot \vec{r}_i)}{r_i^5} \right) \quad (2)$$

where g_N is the nuclear spectroscopic splitting factor, μ_N is the nuclear magneton; \vec{L} , \vec{S} , \vec{I} are the electronic orbital angular momentum, electronic spin, and nuclear spin, respectively; r_i is the distance of the i th electron from the nucleus, and the sum is over all of the ion's electrons.

The term in \vec{L}_i will be neglected here since in many iron-group compounds (as in this case) the orbital angular momentum is almost completely quenched by the crystal field⁶. The last two terms involving \vec{S}_i are the dipole-dipole terms and will be non-zero only for unpaired electrons. The

first term, called the Fermi contact term, involves, through the delta function, the density of electrons at the nucleus. This is non-zero only for s-electrons and thus should vanish here since all s-electrons are paired. However, the presence of unpaired d-electrons causes a polarization⁶ of the s-electrons through the exchange interaction and a substantial hyperfine field results. In fact, the largest contribution to the field at the nucleus is due to s-electron polarization.

The details of the polarization of the s-electrons are very complicated and include contributions from the unpaired d-electrons of neighboring ions through polarization by them of the oxygen anions which in turn polarize the original cation's s-electrons (super-transferred hyperfine interaction)⁷.

The dipolar part of Equation 2 gives rise to an anisotropic hyperfine field. For Mn³⁺ ions on the B-sites considerable anisotropy is observed⁴ but for Mn²⁺ ions on the A-sites, since Mn²⁺ is an S-state ion (five 3-d electrons → half-filled shell), the hyperfine field is isotropic.

Writing the interaction in Equation 2 in terms of the effective hyperfine field yields

$$\mathcal{H}_{\text{hf}} = -g_N \mu_N \vec{I} \cdot \vec{H}_s = A \vec{I} \cdot \vec{S} \quad (3)$$

where, $A = -g_N \mu_N \vec{H}_s \cdot \vec{S} / (\vec{S} \cdot \vec{S})$

and S is the total spin of the ion (for Mn²⁺, S = 5/2). For the isotropic case A is simply a constant while in the anisotropic case A would be a second rank tensor.

Finally, in manganese ferrite, as in many other magnetic materials,

the hyperfine field at an A- or B-site is anti-parallel to the sublattice magnetization at that site. The A-site hyperfine field has been found to be proportional to the sublattice magnetization at low temperatures⁸, and at $T = 4.2$ °K has a magnitude of $H_{hf}^A \approx 560$ kOe, while at the same temperature, the B-site hyperfine field is $H_{hf}^B \approx 360$ kOe.

3. Magnetic Ordering

Below a temperature $T_F \approx 600$ °K the unpaired spins of the magnetic ions in manganese ferrite are spontaneously ordered in such a way that all of the A-site moments are parallel to each other and anti-parallel to the B-site moments. This type of order is called ferrimagnetic and T_F is the ferrimagnetic Neel point. The A and B sites can be considered to form sublattices whose magnetizations are oppositely directed but do not have the same magnitude⁹. This results in a net moment of $4.6 \mu_B$ per formula unit along the B-site magnetization, since there are twice as many occupied B-sites as there are A-sites. Because of this net moment many of the properties of ferromagnets are present in ferrimagnets; e.g., the existence of domains, magnetic hysteresis, etc.

3.1 The exchange interaction

The interaction responsible for the spontaneous ordering of the magnetic ions' spins is the exchange interaction, which can be described in insulators by the Heisenberg exchange Hamiltonian

$$\mathcal{H}_{ex} = - \sum_{i < j} J_{ij} \vec{S}_i \cdot \vec{S}_j \quad (4)$$

where \vec{S}_i is the spin of the i th ion, and J_{ij} is the exchange constant representing the strength of the interaction between ions i and j . In

these materials, as mentioned earlier in connection with the hyperfine interaction, the orbital contribution to the magnetic moment is quenched and therefore the contribution of the orbital angular momentum to the exchange interaction will be neglected. The exchange interaction is very short ranged and only very near neighbors in the sums over i and j in Equation 4 need to be considered.

As shown in Figure 1 there is an oxygen anion between an A-site ion and each of its nearest B-site neighbors. The exchange interaction must proceed via a polarization of the anion's electronic p-orbitals¹⁰. Such an interaction is called superexchange (analogous to the super-transferred hyperfine fields mentioned earlier) and is found to be very common in iron-group salts¹¹. Superexchange allows the exchange interaction to be effective over quite large distances when compared with direct exchange¹⁰ which would require significant overlap of the magnetic ions' d-orbitals. Even so, the strength of the superexchange is strongly dependent on distance between cations and on the angle formed by the cation-anion-cation system¹¹. Table 1 gives a list of the possible exchange couplings between cations in a spinel together with the distances and angles between the cations.¹²

Table 1: Superexchange in Spinel

Interaction	Angle	Distance	Sign
A-O-B	125° 9'	$\sqrt{11}a/8$	-
A-O-B	154° 34'	$3\sqrt{3}a/8$	-
A-O-A	79° 38'	$\sqrt{3}a/4$	+
B-O-B	90°	$\sqrt{2}a/4$	+
B-O-B	125° 2'	$\sqrt{6}a/4$	+

The minus sign corresponds to antiparallel or antiferromagnetic exchange and the plus sign to parallel or ferromagnetic exchange.

The superexchange interaction is strongest for short distances and for angles closest to 180° ¹¹, thus the A-B exchange (especially the first type shown in Table 1) is the strongest in these materials¹² and is responsible for the antiparallel alignment of the two sublattices. The other contributions (of which the 125° B-B is the largest) can be safely neglected¹² in many instances.

3.2 Molecular field theory

As postulated by Weiss¹³ the exchange interaction in a ferromagnetic material can be represented by an effective magnetic field $H_{\text{ex}} = \lambda M$, where M is the sample magnetization and λ is the molecular field constant. Extending this concept to the ferrimagnetic case^{9,14} one obtains an exchange field acting on A-site spins due to the B-sublattice magnetization and a similar field on the B-site spins due to the A-sublattice magnetization (neglecting intrasublattice interactions).

$$H_{\text{ex}}^{\text{A}} = \lambda M_{\text{B}} \quad , \quad H_{\text{ex}}^{\text{B}} = \lambda M_{\text{A}}$$

where the molecular field constant λ represents the same quantity in both cases and is given by

$$\lambda = 3k_{\text{B}} T_{\text{F}} / N g_{\text{B}}^2 \mu_{\text{B}}^2 (S_{\text{A}} (S_{\text{A}} + 1) S_{\text{B}} (S_{\text{B}} + 1))^{\frac{1}{2}} \quad (5)$$

where $S_{\text{A}} = 5/2$ is the A-site spin (both Mn^{2+} and Fe^{3+} have spin $5/2$) and $S_{\text{B}} = 2.40$ is the average B-site spin. N is the total number of magnetic ions, k_{B} is the Boltzmann constant, and T_{F} is the ferrimagnetic ordering temperature.

Since $M_B = N_B g \mu_B S_B$ and $N_B = \frac{2}{3} N$, the exchange field acting on the A-site ions is

$$H_{\text{ex}}^A = \frac{2}{3} S_B \left(\frac{3k_B T_F}{g \mu_B (S_A (S_A + 1) S_B (S_B + 1))^{1/2}} \right) \quad (6)$$

Then, for $g = 2$ and $T_F = 600$ °K, the exchange field is

$$H_{\text{ex}}^A = (2zS_B / g \mu_B) J \approx 2.6 \times 10^6 \text{ Oe}$$

where $z = 12$ is the number of magnetic nearest neighbors of the A-site ion and J is the A-B exchange constant as used in Equation 4.

4. Spin Waves

The Hamiltonian of a ferromagnet including only an isotropic exchange interaction and the electronic Zeeman interaction with an external field H_0 is

$$\mathcal{H} = - \sum_{(i,j)} J_{ij} \vec{S}_i \cdot \vec{S}_j - g \mu_B H_0 \sum_i S_i^z \quad (7)$$

where $\sum_{(i,j)}$ is the sum over all "distinct" pairs of spins. The ground state of a ferromagnet, denoted by $|\uparrow\rangle$, is the state with all spins aligned parallel. Introducing the spin raising and lowering operators $S^\pm = S^x \pm iS^y$ the Hamiltonian can be written as

$$\mathcal{H} = - \sum_{(i,j)} J_{ij} (S_i^z S_j^z + \frac{1}{2} S_i^+ S_j^- + \frac{1}{2} S_i^- S_j^+) - g \mu_B H_0 \sum_i S_i^z$$

Then, the ground state energy is given by

$$\mathcal{H} |\uparrow\rangle = - N(g \mu_B H_0 S + \frac{1}{2} S^2 \sum_j J_{ij}) |\uparrow\rangle \quad (8)$$

since $S_i^Z|\uparrow\rangle = S$, $S_i^+|\uparrow\rangle = 0$. The factor of $1/2$ preceding Σ_j is to insure that the contribution from each pair of spins is counted only once.

Then, taking the commutator of \mathcal{H} and the spin lowering operator S_i^- and applying it to $|\uparrow\rangle$ yields

$$\begin{aligned} [\mathcal{H}, S_i^-]|\uparrow\rangle &= (g\mu_B H_0 S_i^- + \sum_j J_{ij} (S_i^- S_j^Z - S_i^Z S_j^-))|\uparrow\rangle \\ &= (g\mu_B H_0 S_i^- + S \sum_j J_{ij} (S_i^- - S_j^-))|\uparrow\rangle \end{aligned} \quad (9)$$

This forms a new state which is a linear combination of states where a spin i has been flipped, $(S_i^-|\uparrow\rangle)$. Then, replacing S_i^- by its Fourier transform $\sum_i \exp(i\vec{k}\cdot\vec{r}_i) S_i^-$,

$$\begin{aligned} [\mathcal{H}, \sum_i \exp(i\vec{k}\cdot\vec{r}_i) S_i^-]|\uparrow\rangle & \\ &= (g\mu_B H_0 + S \sum_j J_{ij} (1 - \exp(i\vec{k}\cdot(\vec{r}_i - \vec{r}_j)))) \sum_i \exp(i\vec{k}\cdot\vec{r}_i) S_i^-|\uparrow\rangle \end{aligned} \quad (10)$$

it can be seen that the states

$$|k\rangle = \frac{1}{\sqrt{2SN}} \sum_i \exp(i\vec{k}\cdot\vec{r}_i) S_i^-|\uparrow\rangle \quad (11)$$

are the normalized eigenstates of the Hamiltonian \mathcal{H} with eigenvalues given by

$$E_k = E_0 + g\mu_B H_0 + S \sum_i J_{ij} \{1 - \exp(i\vec{k}\cdot(\vec{r}_i - \vec{r}_j))\} \quad (12)$$

where E_0 is the ground state energy. These new states $|k\rangle$ are called Bloch spin-wave states^{15,16} and the excitations of wavevector \vec{k} are called spin waves.

The minimum energy required to excite a spin wave ($E - E_0 = g\mu_B H_0$) is much lower than that required to flip a single spin since, for a spin-wave excitation, neighboring spins are still very nearly parallel

(on the average) and their exchange energy is only slightly increased.

The interaction of the ^{55}Mn nuclear moments with these spin waves via the hyperfine ($\vec{A}\vec{I}\cdot\vec{S}$) interaction and the effective nuclear spin-spin interaction--the Suhl-Nakamura interaction--which is a result of the virtual excitation, by the hyperfine interaction, of electronic spin waves as intermediate states, require a detailed understanding of these excitations.

4.1 Holstein-Primakoff diagonalization

The eigenstates of the Hamiltonian are expanded in terms of the eigenstates $|n_\ell\rangle$ of the spin-deviation operator η_ℓ defined by

$$\eta_\ell |n_\ell\rangle = (S - S_\ell^Z) |n_\ell\rangle = n_\ell |n_\ell\rangle$$

In this notation, the ferromagnetic ground state is $|0\rangle$, the state of zero spin deviation. Then the raising and lowering operators acting on these states give¹⁷

$$\begin{aligned} S_\ell^+ |n_\ell\rangle &= \{(S - S_\ell^Z)(S + S_\ell^Z + 1)\}^{\frac{1}{2}} |n_\ell - 1\rangle \\ S_\ell^- |n_\ell\rangle &= \{(S + S_\ell^Z)(S - S_\ell^Z + 1)\}^{\frac{1}{2}} |n_\ell + 1\rangle \end{aligned} \quad (13)$$

The spin-deviation operator η_ℓ is actually the boson occupation number operator defined by

$$\eta_\ell = a_\ell^+ a_\ell, \quad \text{with} \quad [a_\ell, a_m^+] = \delta_{\ell,m}, \quad \text{all others zero}$$

where the a_ℓ^+ and a_ℓ are the spin-deviation creation and annihilation operators. Then, since

$$a_\ell^+ |n_\ell\rangle = (n_\ell + 1)^{\frac{1}{2}} |n_\ell + 1\rangle$$

and,

$$a_\ell |n_\ell\rangle = (n_\ell)^{\frac{1}{2}} |n_\ell - 1\rangle \quad (14)$$

we may express the spin operators in the Hamiltonian in terms of these operators as

$$\begin{aligned} S_\ell^+ &= (2S)^{\frac{1}{2}} (1 - a_\ell^+ a_\ell / 2S)^{\frac{1}{2}} a_\ell \\ S_\ell^- &= (2S)^{\frac{1}{2}} a_\ell (1 - a_\ell^+ a_\ell / 2S)^{\frac{1}{2}} \\ S_\ell^z &= S - a_\ell^+ a_\ell \end{aligned} \quad (15)$$

Expanding these expressions for S_ℓ^+ , S_ℓ^- in powers of $(1/S)$ yields

$$\begin{aligned} S_\ell^+ &= (2S)^{\frac{1}{2}} \left(1 - \frac{a_\ell^+ a_\ell}{4S} - \frac{a_\ell^+ a_\ell a_\ell^+ a_\ell}{32S^2} - \dots \right) a_\ell \\ S_\ell^- &= (2S)^{\frac{1}{2}} a_\ell^+ \left(1 - \frac{a_\ell^+ a_\ell}{4S} - \frac{a_\ell^+ a_\ell a_\ell^+ a_\ell}{32S^2} - \dots \right) \end{aligned}$$

where for many applications only the terms linear in the spin-deviation operators need to be retained^{5,18,19}. When spin wave scattering becomes important, as in the derivation of spin-wave relaxation processes, higher order terms may be necessary.

For a two sublattice system, with the B-sublattice aligned along the positive z-axis (the direction of H_0), the spin operators are given by²⁰

$$\begin{aligned} S_{Bj}^+ &= (2S_B)^{\frac{1}{2}} (1 - b_j^+ b_j / 2S_B)^{\frac{1}{2}} b_j \\ S_{Ai}^+ &= (2S_A)^{\frac{1}{2}} a_i^+ (1 - a_i^+ a_i / 2S_A)^{\frac{1}{2}} \end{aligned} \quad , (\text{plus complex conjugates}) \quad (16)$$

$$S_{Bj}^z = S_B - b_j^+ b_j \quad , \quad S_{Ai}^z = -S_A + a_i^+ a_i$$

where S_A and S_B are the A- and B-site spin and the operators a_i^+ , b_j^+ create a spin-deviation on their respective sublattices.

The next step in diagonalizing the Hamiltonian is to Fourier transform the spin-deviation operators, which become

$$a_i = (N_A)^{-1/2} \sum_k \exp(i\vec{k} \cdot \vec{r}_i) a_k$$

$$b_j = (N_B)^{-1/2} \sum_k \exp(-i\vec{k} \cdot \vec{r}_j) b_k$$

4.2 The diagonalized Hamiltonian

The Hamiltonian we wish to consider is

$$\begin{aligned} \mathcal{H} &= \mathcal{H}_A^Z + \mathcal{H}_B^Z + \mathcal{H}_{A-B}^{\text{ex}} + \mathcal{H}^{\text{dd}} \\ &= -g\mu_B H \sum_i^A S_{A_i}^Z - g\mu_B H \sum_j^B S_{B_j}^Z + \frac{1}{2} J \sum_{i,j}^{\text{nn}} \vec{S}_i \cdot \vec{S}_j \\ &\quad + \frac{1}{2} \sum_{i,j} \frac{g^2 \mu_B^2}{R_{ij}^5} \left(R_{ij}^2 \{ \vec{S}_i \cdot \vec{S}_j - 3(\vec{R}_{ij} \cdot \vec{S}_i)(\vec{R}_{ij} \cdot \vec{S}_j) \} \right) \end{aligned} \quad (17)$$

This Hamiltonian consists of Zeeman, exchange, and dipole-dipole terms. The sum \sum_i^A is over all spins on the A-sublattice, \sum_j^B is over all spins on the B-sublattice, $\sum_{i,j}^{\text{nn}}$ is over all pairs (i,j) of nearest neighbor spins, and $\sum_{i,j}$ is over all spins ($i \neq j$). When the spin has a subscript it refers to a particular sublattice and when no subscript is present, S can refer to either sublattice. Thus, for example,

$$\frac{1}{2} J \sum_{i,j}^{\text{nn}} \vec{S}_i \cdot \vec{S}_j = \frac{1}{2} J \left[\sum_i^A \sum_{i+\delta}^B \vec{S}_{A_i} \cdot \vec{S}_{B_{i+\delta}} + \sum_j^B \sum_{j+\delta}^A \vec{S}_{B_j} \cdot \vec{S}_{A_{j+\delta}} \right]$$

where $\vec{\delta}$ is the vector joining nearest neighbors. Similarly, the dipole-

dipole part of the Hamiltonian can be written as

$$\begin{aligned} \frac{1}{2} \sum_{i \neq j} \mathcal{H}_{i,j}^{dd}(\vec{S}_i, \vec{S}_j) &= \frac{1}{2} \left(\sum_{i \neq \ell}^A \mathcal{H}_{i,\ell}^{dd}(\vec{S}_{A_i}, \vec{S}_{A_\ell}) \right. \\ &+ \sum_i^A \sum_j^B \mathcal{H}_{i,j}^{dd}(\vec{S}_{A_i}, \vec{S}_{B_j}) + \sum_j^B \sum_\ell^A \mathcal{H}_{j,\ell}^{dd}(\vec{S}_{B_j}, \vec{S}_{A_\ell}) \\ &\left. + \sum_{j \neq m}^B \mathcal{H}_{j,m}^{dd}(\vec{S}_{B_j}, \vec{S}_{B_m}) \right) \end{aligned}$$

The factor of $\frac{1}{2}$ on both sides of these equations is to insure that the interaction between any two spins is included only once.

By breaking up the Hamiltonian in this manner we can more easily carry out the steps in diagonalization of the total Hamiltonian. The dipole-dipole Hamiltonian can be written in terms of spin operators S^+ , S^- , and S^z as

$$\begin{aligned} \mathcal{H}_{dd} &= \frac{1}{2} \sum_{i \neq j} \left\{ A_{i,j}^{(z,z)} S_i^z S_j^z + A_{i,j}^{(+,-)} (S_i^+ S_j^- + S_i^- S_j^+) \right. \\ &- A_{i,j}^{(z,+)} (S_i^z S_j^+ + S_i^+ S_j^z) - A_{i,j}^{(z,-)} (S_i^z S_j^- + S_i^- S_j^z) \\ &\left. - A_{i,j}^{(+,+)} S_i^+ S_j^+ - A_{i,j}^{(-,-)} S_i^- S_j^- \right\} \end{aligned} \quad (18)$$

where,

$$A_{i,j}^{(z,z)} = \frac{g^2 \mu_B^2}{5 R_{ij}^2} (R_{ij}^2 - 3(R_{ij}^z)^2)$$

$$A_{i,j}^{(+,-)} = \frac{1}{2} \frac{g^2 \mu_B^2}{5 R_{ij}^2} (R_{ij}^2 - \frac{3}{2} R_{ij}^+ R_{ij}^-) \quad (19)$$

$$A_{i,j}^{(z,\pm)} = \frac{3}{2} \frac{g^2 \mu_B^2}{5 R_{ij}^2} R_{ij}^z R_{ij}^\mp$$

$$A_{i,j}^{(\pm,\pm)} = \frac{3}{4} \frac{g^2 \mu_B^2}{R_{ij}^5} (R_{ij}^{\mp})^2$$

Each of the four parts (A-A, A-B, B-A, B-B) of the dipole-dipole Hamiltonian will be written in this fashion, where the sums involved will be over a particular sublattice.

Applying the Holstein-Primakoff transformation to the Zeeman and exchange terms leads, to second order in magnon operators, to

$$\mathcal{H}'^{(2)} = \sum_k (\mu_{AA}^0 a_k^+ a_k + \mu_{AB}^0 a_k^+ b_k + \mu_{BA}^0 a_k b_k + \mu_{BB}^0 b_k^+ b_k) + \text{const.} \quad (20)$$

where,

$$\begin{aligned} \mu_{AA}^0 &= -g\mu_B H + \hat{z} J S_B (N_B/N_A)^{1/2} \\ \mu_{AB}^0 &= \frac{1}{2} J (S_A S_B)^{1/2} \{ Z_B (N_B/N_A)^{1/2} \gamma_{-k}^B + Z_A (N_A/N_B)^{1/2} \gamma_{-k}^A \} \\ \mu_{BA}^0 &= \frac{1}{2} J (S_A S_B)^{1/2} \{ Z_B (N_B/N_A)^{1/2} \gamma_k^B + Z_A (N_A/N_B)^{1/2} \gamma_k^A \} \\ \mu_{BB}^0 &= g\mu_B H + \hat{z} J S_A (N_A/N_B)^{1/2} \end{aligned} \quad (21)$$

$$\text{with, } \hat{z} = \frac{1}{2} \{ (N_B/N_A)^{1/2} Z_B + (N_A/N_B)^{1/2} Z_A \}$$

$$\text{and } \gamma_k^{A,B} = Z_{A,B}^{-1} \sum_{\delta}^{A,B} \exp(i\vec{k} \cdot \vec{\delta})$$

where $\vec{\delta}$ is the vector joining nearest neighbors and N_A, N_B, Z_A, Z_B are the numbers of A-, B-site ions and the number of A-, B-site nearest neighbors.

The dipole-dipole Hamiltonian can be transformed in the same fashion to obtain the total Hamiltonian to second-order in magnon operators

$$\mathcal{H}^{(2)} = \sum_k (\mu_{AA}^0 a_k^+ a_k + \mu_{AB}^0 a_k^+ b_k + \mu_{BA}^0 a_k b_k + \mu_{BB}^0 b_k^+ b_k) \quad (23)$$

In this equation we have neglected terms such as $a_k a_{-k}, a_k^+ b_{-k}, b_k^+ b_{-k}$,

etc., which arise from terms in S^+S^+ , S^-S^- and are expected to be small compared to the remaining terms^{5,20}. The coefficients in this Hamiltonian are

$$\begin{aligned}
\mu_{AA} &= \mu_{AA}^o + \mu_{AA}^{dd}, & \mu_{AB} &= \mu_{AB}^o + \mu_{AB}^{dd}, & \text{etc., and} \\
\mu_{AA}^{dd} &= S_A \{ (C_{AA}^{(+,-)}(-\vec{k}) + C_{AA}^{(+,-)}(\vec{k})) - C_{AA}^{(z,z)}(0) \} \\
&\quad + (S_A S_B)^{1/2} (N_B/N_A)^{1/2} \{ (N_A/N_B)^{1/2} C_{AB}^{(z,z)}(0) + (N_B/N_A)^{1/2} C_{BA}^{(z,z)}(0) \} \\
\mu_{AB}^{dd} &= (S_A S_B)^{1/2} \{ (N_A/N_B)^{1/2} C_{AB}^{(+,-)}(-\vec{k}) + (N_B/N_A)^{1/2} C_{BA}^{(+,-)}(\vec{k}) \} \\
\mu_{BA}^{dd} &= (S_A S_B)^{1/2} \{ (N_A/N_B)^{1/2} C_{AB}^{(+,-)}(\vec{k}) + (N_B/N_A)^{1/2} C_{BA}^{(+,-)}(-\vec{k}) \} \\
\mu_{BB}^{dd} &= S_B \{ (C_{BB}^{(+,-)}(\vec{k}) + C_{BB}^{(+,-)}(-\vec{k})) - C_{BB}^{(z,z)}(0) \} \\
&\quad + (S_A S_B)^{1/2} (N_A/N_B)^{1/2} \{ (N_A/N_B)^{1/2} C_{AB}^{(z,z)}(0) + (N_B/N_A)^{1/2} C_{BA}^{(z,z)}(0) \}
\end{aligned} \tag{24}$$

Here we have defined the expressions $C_{XY}^{(\mu,\nu)}$ by

$$C_{XY}^{(\mu,\nu)}(\vec{k}) = \sum_{\vec{\delta}_X}^Y A_{\vec{\delta}_X}^{(\mu,\nu)} \exp(i\vec{k} \cdot \vec{\delta}_X) \tag{25}$$

where the sum $\sum_{\vec{\delta}_X}^Y$ is over all vectors $\vec{\delta}_X$ originating on a site on the X-sublattice ($X = A$ or B) and terminating on the Y-sublattice, and the $A_{\vec{\delta}}^{(\mu,\nu)}$ are as defined in Equation 19 with $\vec{\delta} = R_{ij}$.

The Hamiltonian in Equation 23 is still not diagonal since it contains terms coupling the operators a_k and b_k . To bring the Hamiltonian into normal-mode form, the transformation to normal-mode operators α_k , β_k is made.

$$b_k = u_k \alpha_k - v_k \beta_k^+ \quad (26)$$

$$a_k = -v_k \alpha_k^+ + u_k \beta_k$$

$$[\alpha_k, \alpha_k^+] = [\beta_k, \beta_k^+] = 1, \text{ all others zero.}$$

The transformation coefficients u_k, v_k are chosen to bring the Hamiltonian into diagonal decoupled form. The Hamiltonian then takes the form

$$\mathcal{H}^{(2)} = \sum_k (\hbar\omega_\alpha \alpha_k^+ \alpha_k + \hbar\omega_\beta \beta_k^+ \beta_k) \quad (27)$$

which is the desired result.

4.3 The ferrimagnon dispersion relation

The normal-mode energies in Equation 27 are given by

$$\begin{aligned} \hbar\omega_\alpha &= \mu_{BB} u_k^2 - (\mu_{AB} + \mu_{BA}) u_k v_k + \mu_{AA} v_k^2 \\ \hbar\omega_\beta &= \mu_{BB} v_k^2 - (\mu_{AB} + \mu_{BA}) v_k u_k + \mu_{AA} u_k^2 \\ &= \hbar\omega_\alpha - (\mu_{BB} - \mu_{AA}) \end{aligned} \quad (28)$$

The transformation coefficients are determined from the equations of motion of the magnon operators $\alpha_k, \beta_k, a_k, b_k$, i.e.,

$$i \frac{d\alpha_k}{dt} = [\alpha_k, \mathcal{H}_k] = \omega_\alpha \alpha_k \quad (29)$$

and since, from Equation 26, $u_k^2 - v_k^2 = 1$, we obtain the equation

$$\begin{pmatrix} \mu_{BB} - \omega & -\mu_{BA} \\ \mu_{AB} & -\mu_{AA} - \omega \end{pmatrix} \begin{pmatrix} u_k \\ v_k \end{pmatrix} = 0 \quad (30)$$

and the coefficients may be defined by the relations

$$u_k = \{1 - (v_k/u_k)^2\}^{-\frac{1}{2}}, \quad v_k = (v_k/u_k)\{1 - (v_k/u_k)^2\}^{-\frac{1}{2}}$$

To obtain the dispersion relation (Equation 29) in terms of recognizable quantities we must substitute for the μ 's from Equations 21 and 24. First we consider the ratio of the transformation coefficients.

$$(v_k/u_k) = \frac{\mu_{BB} - \omega}{\mu_{BA}} \approx \frac{\hat{z}(N_A/N_B)^{\frac{1}{2}} (S_A/S_B)^{\frac{1}{2}}}{\frac{1}{2} \{Z_B(N_B/N_A)^{\frac{1}{2}} \gamma_k^B + Z_A(N_A/N_B)^{\frac{1}{2}} \gamma_k^A\}} = \eta(S_A/S_B)^{\frac{1}{2}}$$

This equation is used to define a parameter η which, since it depends on N_A , N_B , Z_A , Z_B , describes the nonequivalence of the two sublattices. For small k , $\eta \approx (N_A/N_B)^{\frac{1}{2}}$. Then, we find that

$$u_k^2 = \frac{S_B}{S_B - \eta^2 S_A}, \quad u_k v_k = \frac{\eta(S_A S_B)^{\frac{1}{2}}}{S_B - \eta^2 S_A}, \quad v_k^2 = \frac{\eta^2 S_A}{S_B - \eta^2 S_A} \quad (31)$$

To put the α -mode dispersion relation in a more understandable form we rewrite it as

$$\hbar\omega_\alpha = -\mu_{AA} + (\mu_{AA} + \mu_{BB})u_k^2 - (\mu_{AB} + \mu_{BA})u_k v_k$$

Now, from Equations 21 and 24,

$$\begin{aligned} \hbar\omega_\alpha^0 &= -\mu_{AA}^0 + (\mu_{AA}^0 + \mu_{BB}^0)u_k^2 - (\mu_{AB}^0 + \mu_{BA}^0)u_k v_k \\ &= g\mu_B H + Z' J S_{\text{eff}} \{ \eta^2 (N_B/N_A) - 1 \} \end{aligned} \quad (32)$$

$$\text{with } Z' = (N_B/N_A)^{\frac{1}{2}} \hat{z}, \quad S_{\text{eff}} = \frac{N_A}{N_B} \left(\frac{S_A S_B}{S_A - \eta^2 S_B} \right)$$

For small k , $\eta^2 \approx (N_A/N_B)(1 + \frac{1}{3} a_{nn}^2 k^2)$, for a cubic lattice, where a_{nn} is the nearest neighbor distance. In this approximation the dispersion relation assumes the familiar ferromagnetic form given by

$$\hbar\omega_{\alpha}^0 = g_{\mu_B}^H + \frac{1}{3} Z' JS_{\text{eff}} a_{\text{nn}}^2 k^2$$

with, for a spinel, $Z' = Z_A = 12$ and $a_{\text{nn}} = (\sqrt{11}/8)a$, where a is the lattice constant ($a \approx 8.5 \text{ \AA}$).

The dipole-dipole terms can be treated analogously yielding

$$\begin{aligned} \hbar\omega_{\alpha}^d = & \frac{N_A}{N_B} S_{\text{eff}} \left[\{ (S_B/S_A) K_{BB}^{(+,-)}(\vec{k}) - \eta(K_{BA}^{(+,-)}(\vec{k}) + K_{AB}^{(+,-)}(\vec{k})) \right. \\ & + \eta^2 (S_A/S_B) K_{AA}^{(+,-)}(\vec{k}) \} - \frac{1}{2} \{ (S_B/S_A) K_{BB}^{(z,z)}(0) - \eta(K_{BA}^{(z,z)}(0) \\ & \left. + K_{AB}^{(z,z)}(0)) + \eta^2 (S_A/S_B) K_{AA}^{(z,z)}(0) \} \right] \quad (33) \end{aligned}$$

where

$$K_{XY}^{(\mu,\nu)}(\vec{k}) = (N_X/N_Y)^{\frac{1}{2}} C_{XY}^{(\mu,\nu)}(\vec{k}) + (N_Y/N_X)^{\frac{1}{2}} C_{YX}^{(\mu,\nu)}(-\vec{k})$$

These dipole-wave sums can be directly evaluated for $k = 0$, and can be approximately evaluated for $k \neq 0$, assuming $kR > 10$, where R is the sample radius⁵. For example,

$$\begin{aligned} C_{XY}^{(z,z)}(0) &= g_{\mu_B}^2 \sum_{\delta_X}^Y \{ R_{\delta_X}^2 - 3(R_{\delta_X}^z)^2 \} / R_{\delta_X}^5 \\ &= -g_{\mu_B}^2 \bar{N}_Y D^{(z,z)}(0) \quad , \quad \bar{N}_Y = N_Y/N_u \end{aligned}$$

where \bar{N}_Y is the number of Y-sublattice ions per unit cell and N_u is the number of unit cells, and

$$D^{(I,J)}(\vec{k}) = \bar{N}^{-1} \sum_{\ell} (3r_{\ell}^{IJ} - r_{\ell}^2 \delta^{IJ}) r_{\ell}^{-5} \exp(i\vec{k} \cdot \vec{r}_{\ell})$$

are the dipole-wave sums discussed by Keffer⁵. For $k = 0$, these sums give the Lorentz and demagnetizing fields

$$D^{IJ}(0) = L^{IJ} - N_{\delta}^{IJ}$$

where $L^{IJ} = \frac{4\pi}{3} \delta^{IJ} + \{D^{IJ}(0)\}_L$

is the Lorentz factor with $\{D^{IJ}(0)\}_L$ the sum over all points on the interior of the Lorentz sphere. N^I is the demagnetizing factor along the I th direction.

For $\vec{k} \neq 0$, $kR > 10$, the sum may be approximated by an integral⁵ which for \vec{k} not too large gives, with $I, J = x, y, z$

$$D^{IJ}(\vec{k}) \approx L^{IJ} - 4\pi k^I k^J / k^2$$

An example of this is

$$\begin{aligned} K_{AA}^{(+,-)}(\vec{k}) &= \frac{1}{4} g^2 \mu_B^2 \sum_{\delta_A}^A \{2R_{\delta_A}^2 - 3R_{\delta_A}^+ R_{\delta_A}^-\} / R_{\delta_A}^5 \\ &\quad \times \{\exp(i\vec{k} \cdot \vec{R}_{\delta_A}) + \exp(-i\vec{k} \cdot \vec{R}_{\delta_A})\} \\ &= -\frac{1}{2} g^2 \mu_B^2 \bar{N}_A \{L^{XX} + L^{YY} - 4\pi \sin^2 \theta_{\vec{k}}\} \end{aligned} \quad (34)$$

where $\theta_{\vec{k}}$ is the angle \vec{k} makes with the z -axis.

Using these expressions we obtain the dipole-dipole part of the dispersion relation

$$\hbar\omega_{\alpha}^d = \frac{1}{2} g\mu_B (4\pi M') \sin^2 \theta_{\vec{k}} - g\mu_B N^z M' \quad (35)$$

with

$$M' = g(N_B/N_A) \{(S_B N_B - S_A N_A)^2 / S_A N_A S_B N_B\} \mu_B S_{\text{eff}} \bar{N}_A \quad (36)$$

as the effective magnetization per unit volume.

Finally, then, the ferrimagnetic dispersion relation can be written as

$$\hbar\omega_{\alpha} = g\mu_B (H - N^z M') + Z' J S_{\text{eff}} \{n^2 (N_B/N_A) - 1\} + \frac{1}{2} g\mu_B (4\pi M') \sin^2 \theta_{\vec{k}} \quad (37)$$

The β -mode dispersion relation can be written down by inspection, ignoring dipole-dipole effects, giving

$$\begin{aligned} \hbar\omega_{\beta}^0 &= \hbar\omega_{\alpha}^0 - (\mu_{BB}^0 - \mu_{AA}^0) \\ &= Z'J(S_B - (N_A/N_B)S_A) - g\mu_B H + Z'JS_{\text{eff}}\{\eta^2(N_B/N_A) - 1\} \end{aligned}$$

The first term, proportional to J , provides a large energy gap between the α - and β -modes. Thus, at low temperatures there will not be any appreciable number of β -mode magnons.

4.4 Higher order terms

There are two terms arising from higher order in the expansion of the total Hamiltonian in spin-wave operators which are of considerable importance in spin-wave relaxation processes at low temperatures. These higher order terms give rise to the second-order dipolar-induced two-magnon and the exchange-enhanced three-magnon processes.

4.4.a Three-magnon dipolar Hamiltonian

The first of these, the dipolar-induced process, arises from the $S^z S^{\pm}$ terms of the dipolar Hamiltonian of Equation 18. When expanded in terms of the spin-deviation operators $a_{\mathbf{k}}$, $b_{\mathbf{k}}$ these terms give a three-magnon contribution to the Hamiltonian

$$\begin{aligned} \mathcal{H}_{\text{dd}}^{(3)} &= - \sum_{\mathbf{k}_1, \mathbf{k}_2, \mathbf{k}_3} \delta(\vec{\mathbf{k}}_1 - \vec{\mathbf{k}}_2 - \vec{\mathbf{k}}_3) \left\{ (S_A/2N_A)^{\frac{1}{2}} \left\{ \frac{1}{2} C_{AA}^{(z,-)}(0) \right. \right. \\ &\quad \left. \left. + K_{AA}^{(z,-)}(\vec{\mathbf{k}}_2) - \frac{1}{2} (S_B/S_A)(N_B/N_A)^{\frac{1}{2}} K_{AB}^{(z,-)}(0) \right\} a_{\mathbf{k}_1}^+ a_{\mathbf{k}_2} a_{\mathbf{k}_3} \right. \\ &\quad \left. + (2S_B/N_A)^{\frac{1}{2}} K_{AB}^{(z,-)}(-\vec{\mathbf{k}}_3) a_{\mathbf{k}_1}^+ a_{\mathbf{k}_2} b_{\mathbf{k}_3}^+ \right\} \end{aligned} \quad (38)$$

$$\begin{aligned}
& - (2S_A/N_B)^{\frac{1}{2}} K_{AB}^{(z,-)}(\vec{k}_3) b_{k_1} b_{k_2}^+ a_{k_3} - (S_B/2N_B)^{\frac{1}{2}} \left\{ \frac{1}{2} C_{BB}^{(z,-)}(0) \right. \\
& \left. + K_{BB}^{(z,-)}(\vec{k}_2) - \frac{1}{2} (S_A/S_B) (N_A/N_B)^{\frac{1}{2}} K_{AB}^{(z,-)}(0) \right\} b_{k_1}^+ b_{k_2}^+ b_{k_3} \\
& + (\text{complex conjugate})
\end{aligned}$$

4.4.b Four-magnon exchange Hamiltonian

The second of these processes, the exchange-enhanced three-magnon process, results from the expansion of the exchange Hamiltonian to fourth order in spin-deviation operators. Then, to order $(1/S)$,

$$\begin{aligned}
\mathcal{H}_{\text{ex}}^{(4)} &= -\frac{1}{8} J \sum_{\substack{k_1, k_2 \\ k_3, k_4}} \delta(\vec{k}_1 + \vec{k}_2 - \vec{k}_3 - \vec{k}_4) \\
& \times \left(4(Z_A/N_B) \gamma_{-3-4}^A a_{k_1}^+ a_{-k_2} b_{k_3}^+ b_{-k_4} + 4(Z_B/N_A) \gamma_{-3-4}^B b_{k_1}^+ b_{-k_2} a_{k_3}^+ a_{-k_4} \right. \\
& + Z_A (S_B/S_A N_A N_B)^{\frac{1}{2}} \gamma_{-4}^A (a_{k_1}^+ a_{-k_2} a_{k_3} b_{-k_4} + a_{k_1}^+ a_{k_2}^+ a_{k_3} b_{k_4}^+) \\
& + Z_B (S_A/S_B N_A N_B)^{\frac{1}{2}} (\gamma_{-2+3+4}^B a_{k_1} b_{k_2}^+ b_{k_3} b_{k_4} + \gamma_{2-3-4}^B a_{k_1}^+ b_{-k_2}^+ b_{k_3}^+ b_{-k_4}) \\
& + Z_A (S_A N_A / S_B N_B^3)^{\frac{1}{2}} (\gamma_{1+2-3}^A b_{-k_1}^+ b_{k_2} b_{-k_3} a_{k_4} + \gamma_{-1-2+3}^A b_{k_1}^+ b_{k_2}^+ b_{k_3} a_{k_4}^+) \\
& \left. + Z_B (S_B N_B / S_A N_A^3)^{\frac{1}{2}} (\gamma_1^B b_{k_1} a_{k_2}^+ a_{k_3} a_{k_4} + \gamma_1^B b_{-k_1}^+ a_{k_2}^+ a_{-k_3}^+ a_{k_4}) \right)
\end{aligned} \quad (39)$$

In addition, some four-magnon terms will arise from the six-magnon terms on commuting all creation operators to the left (since, $aa^+ = a^+a + 1$). These terms are $\sim (1/S)^2$ however, and will be neglected here¹⁹.

A more detailed discussion of these terms will be made in Chapter 3 in connection with the spin-lattice relaxation via spin-wave scattering.

5. Magnetocrystalline Anisotropy

The preceding discussion has introduced the concept of an anisotropy field due to dipolar interactions. The magnetic anisotropy describes the preference of the sample magnetization for a certain set of crystallographic directions (e.g., the $[111]$ directions of MnFe_2O_4), and its reluctance to lie along other directions. This can be effectively described by an anisotropy energy which for cubic symmetry has the form²¹

$$E_K = K_1(\alpha_1^2\alpha_2^2 + \alpha_2^2\alpha_3^2 + \alpha_3^2\alpha_1^2) + K_2\alpha_1^2\alpha_2^2\alpha_3^2 + \dots \quad (40)$$

where the α_i are the direction cosines locating the magnetization \vec{M}_s with respect to the principal cubic axes. The energy of a magnetization \vec{M}_s in a field \vec{H}_K is ($\theta \ll \pi$)

$$E_K = -\vec{M}_s \cdot \vec{H}_K \approx \frac{1}{2} M_s H_K \theta^2 \quad (+ \text{constant}) \quad (41)$$

where θ is the angle between \vec{M}_s and \vec{H}_K . In spherical polar coordinates the expression in Equation 40 becomes, approximately, ($\theta \ll \pi$)

$$E_K \approx K_1\{\theta^4 \sin^2\phi \cos^2\phi + (1 - \frac{1}{2}\theta^2)^2 \theta^2\} + K_2\{\theta^4 \cos^2\phi \sin^2\phi (1 - \frac{1}{2}\theta^2)^2\} \approx K_1\theta^2 \quad (42)$$

Comparing these last two equations, where θ is the same angle in both, we find,

$$H_K \approx 2K_1/M_s$$

Thus the effective anisotropy field H_K can be used to describe the crystal-

line anisotropy (from Eqn. 41 H_K is seen to be an effective field directed along the magnetically preferred direction).

Table 2 lists the preferred directions for the possible ranges of K_1 and K_2 in cubic crystals as well as values of F_K and H_K along these directions (from Smit and Wijn¹²).

Table 2: Magnetocrystalline anisotropy in cubic crystals

Direction	100	110	111
F_K	0	$\frac{1}{4}K_1$	$\frac{1}{3}K_1 + \frac{1}{27}K_2$
Preferred direction if	$K_1 \begin{cases} > 0 \\ > -\frac{1}{9}K_2 \end{cases}$	$0 > K_1 > -\frac{4}{9}K_2$	$K_1 \begin{cases} < -\frac{4}{9}K_2 \\ < -\frac{1}{9}K_2 \end{cases}$
H_K	$2K_1/M_s$	$\begin{cases} (100): -2K_1/M_s \\ (110): (K_1+K_2)/M_s \end{cases}$	$-(\frac{4}{3}K_1 + \frac{4}{9}K_2)/M_s$

From ferromagnetic resonance measurements²² at $T = 4.2^\circ\text{K}$ on a single crystal of MnFe_2O_4 the anisotropy constants were determined to be $K_1 \approx -2.02 \times 10^5$ ergs/cc and $K_2 \approx 0.34 \times 10^5$ ergs/cc, in good agreement with values reported elsewhere²³. This corresponds to an effective anisotropy field

$$H_K = -\frac{2}{3} \left(\frac{2K_1}{M_s} + \frac{2}{3} \frac{K_2}{M_s} \right) \approx 520 \text{ Oe.} \quad (44)$$

where $M_s = 560$ emu/cc is the saturation magnetization at $T = 0^\circ\text{K}$.

While the dipolar field as given in Equation 1 vanishes classically for sites of cubic symmetry, it has been shown^{24,25} that the dipole-dipole interaction contributes to the anisotropy. In partic-

ular the off-diagonal terms in the dipole-dipole Hamiltonian of Equation 18 give a small contribution to the cubic anisotropy²⁵. The main contribution to the magnetic anisotropy, however, in manganese ferrites appears to be from the interaction of the cations' ground state electron distribution with the crystal field, including the effects of the spin-orbit coupling, as discussed by Yosida and Tachiki²⁵. In particular, the octahedral site Fe^{3+} and Mn^{3+} ions (especially for Mn-rich compositions) provide the largest contributions to the anisotropy²⁶.

The anisotropy constants K_1 and K_2 may exhibit very strong temperature dependences for some compositions and, at very low temperatures K_2 may become comparable to K_1 ²³.

6. Domain Walls

In the absence of an external magnetic field a ferromagnetic (or ferrimagnetic) material can exist in an unmagnetized state (i.e., no net magnetization). This is accomplished by the division of the sample volume into small magnetically saturated regions called domains whose moments are randomly distributed among the various preferred axes. The existence of domains was postulated by Weiss¹³ in 1907 and has become an accepted and fundamental part of the physics of magnetic materials²⁷.

The domains are formed to minimize the total free energy of the system, consisting essentially of magnetostatic energy, due to uncompensated magnetic poles at the sample surface, and exchange energy. The individual domains are separated by narrow regions called domain walls in which the direction of the spin, as a function of position in the wall, rotates smoothly between the easy directions of the domains

on either side of the wall. The width of these walls is determined by competition between exchange, anisotropy, and magnetostriction energies²⁷. For the simple case of a 180° wall, neglecting magnetostriction, the exchange and anisotropy energies can be written as

$$\sigma_{\text{ex}} \approx k_B T_F / a' \delta_w \quad \text{and} \quad \sigma_K \approx \frac{1}{2} K \delta_w$$

where a' is the distance between nearest magnetic neighbors, K is the anisotropy constant, and δ_w is the domain wall width. Then,

$$\delta_w \approx (2k_B T_F / a' K)^{1/2} \quad (45)$$

For manganese ferrite with $T_F = 600^\circ \text{K}$, $K = 2 \times 10^5 \text{ erg/cc}$, $a' \approx 3 \times 10^{-8} \text{ cm}$, this gives

$$\delta_w \approx 530 \text{ \AA} \approx 180 \times a'$$

When an external magnetic field is applied to the multidomain sample, those domains whose magnetizations lie most nearly parallel to the field will increase in size at the expense of those whose moments lie more antiparallel to the field. The domain walls then will move under the influence of the field until the increase in the sample magnetization is sufficient to set up a demagnetizing field $H_D = -NM$ large enough to cancel the effects of the applied field H_0 . Thus, for external fields smaller than that required to effectively saturate the sample (remove all domain walls), the net internal magnetic field is $H_0 - H_D = 0$ (except, as noted earlier, for microscopic fields such as the Lorentz and dipolar fields as well as the electronic hyperfine field, which are always present). Above the field H_S required for saturation the net internal field is $H_0 - H_S$. The demagnetizing field determined by the demagnetization fac-

tor N is due to uncompensated surface poles, as discussed in Section 2.1. A magnetically saturated sample in an external field $H_0 > H_s$ is equivalent to a single-domain sample in an external field $H_0 - H_s$.

6.1 Equation of motion of a domain-wall

If we consider the example of a spherical sample of volume V which is divided into two domains by a single 180° wall, we see from the preceding discussion that if a magnetic field H_x is applied parallel to the wall, it responds by moving a distance z perpendicular to the wall such that the change in the net magnetization is $\Delta M = 2M_s Az/V$, where A is the wall area. The equation of motion of the wall is^{28,29}

$$\mu(d^2z/dt^2) + \beta(dz/dt) + \alpha z = 2M_s H_x - \delta U \quad (46)$$

where μ , the effective mass per unit area, β , the wall damping constant, and α , the stiffness constant, are given by²⁹

$$\mu = 1/8\pi\gamma_e^2\delta_w, \quad \alpha = 4M_s^2/\chi_0\ell, \quad \beta = 2(\Delta H_{fmr})M_s/\delta_w(\gamma_e H_{res}), \quad (47)$$

Here, γ_e is the electronic gyromagnetic ratio, χ_0 is the initial susceptibility, (ΔH_{fmr}) is the ferromagnetic resonance linewidth, $(\gamma_e H_{res})$ is the ferromagnetic resonance frequency, and ℓ is the wall length.

The expression on the right-hand side of Equation 46 is the pressure exerted on the wall; the first term is due to the applied field H_x and the second to the hyperfine interaction.

Neglecting the term in δU , the solution to Equation 46 is

$$z = \frac{2M_s H_x}{\left[(\alpha - \mu\omega^2)^2 + \beta^2\omega^2 \right]} \left(\frac{(\alpha - \mu\omega^2) - i\beta\omega}{2} \right)$$

The rf field acting on the nucleus is

$$H_1 \approx H_N \frac{d\theta}{dz}, \quad z \approx H_N \left(\frac{\sin\theta}{\delta} \right) z, \quad \text{for a } 180^\circ \text{ wall.}$$

Thus, there is an enhancement of the applied field H_x by a factor

$$\eta_1 = \left| \frac{H_1}{H_x} \right| = \frac{2H_N M_s \sin\theta}{\mu \delta \{ (\omega_w^2 - \omega_N^2)^2 + (\beta/\mu)^2 \omega_N^2 \}^{1/2}} \quad (48)$$

where $\omega_w = (\alpha/\mu)^{1/2}$ is the domain-wall resonance frequency and ω_N is the nuclear resonance frequency.

In pulsed spin-echo experiments, after the rf field has been removed there will be a component of nuclear magnetization in the plane perpendicular to the nuclear hyperfine field (and therefore the electronic magnetization). In this case the second term on the right in Equation 46 becomes important. The energy density can be written as²⁸

$$U = - (H_N/M) \int (\vec{M} \cdot \vec{m}) dz'$$

where M is the sublattice electronic magnetization and m is the nuclear magnetization. Then there will be an effective pressure on the domain wall given by

$$- \frac{dU}{dz} = \left(\frac{H_N}{M} \right) \int \frac{d}{dz'} (\vec{M} \cdot \vec{m}) dz' = \left(\frac{H_N}{M} \right) \int \frac{d\theta}{dz'} (\vec{M} \times \hat{z}) \cdot \vec{m} dz' \quad (49)$$

$$\delta U = H_N \int \left(\frac{d\theta}{dz'} \right) m_{\perp}(z') dz'$$

where \hat{z} is a unit vector in the z -direction. The solution to Equation 46 is now

$$z = H_N \langle m_{\perp} \rangle \frac{(\alpha - \mu\omega^2) - i\beta\omega}{(\alpha - \mu\omega^2)^2 + \beta^2\omega^2}$$

with $\langle m_{\perp} \rangle = \frac{1}{\delta} \int m_{\perp}(z') \sin\theta dz' .$

The oscillatory part of the total magnetization is

$$M' = 2M_S Az/V$$

and there is an enhancement of the nuclear magnetization by the factor

$$\eta_2 = \frac{M'}{\langle m_{\perp} \rangle} = 2H_N M_S \left(\frac{A\delta}{V} \right) \frac{1}{\mu\delta \{ (\omega_w^2 - \omega_N^2)^2 + (\beta/\mu)^2 \omega_N^2 \}^{1/2}} \quad (50)$$

Thus, when observing the nuclear resonance of nuclei within domain walls the signal will be doubly enhanced, once on application of the rf pulse, and again when the nuclear magnetization refocuses in the plane perpendicular to the hyperfine field.

For manganese ferrite, with $\chi_0 \approx .1 \text{ emu/cm}^3 \text{Oe}$, $M_S \approx 560 \text{ emu/cm}^3$, $l \approx .1 \text{ cm}$, the constants in Equation 46 are

$$\alpha = 2.5 \times 10^7 \text{ gm/cm}^2 \text{sec}^2$$

$$\beta = 0.4 \text{ gm/cm}^2 \text{sec}$$

$$\mu = 2.6 \times 10^{-11} \text{ gm/cm}^2$$

then,

$$\nu_w = \frac{\omega_w}{2\pi} \approx 50 \text{ MHz}$$

Using values of $2\Delta H_{\text{fmr}} = 150 \text{ Oe}$ and $H_{\text{res}} = 2.3 \text{ kOe}$,

$$\eta_1 \approx 2 \times 10^5, \quad \eta_2 = \left(\frac{A\delta}{V} \right) \eta_1 \quad (51)$$

The ratio $(A\delta/V)$ is simply the ratio of domain wall volume to sample volume.

7. The Coupled Equations of Motion of the Magnetic Sublattices

To obtain the nuclear resonance condition for ^{55}Mn ions on the A-sites we solve the coupled sublattice equations of motion³⁰

$$\begin{aligned}
(d\vec{M}_A/dt) &= \gamma_e \{ \vec{M}_A \times (\vec{H} - \lambda \vec{M}_B + \vec{H}_A - \alpha \vec{m}) \} \\
(d\vec{M}_B/dt) &= \gamma_e \{ \vec{M}_B \times (\vec{H} - \lambda \vec{M}_A + \vec{H}_B) \} \\
(d\vec{m}/dt) &= \gamma_N \{ \vec{m} \times (\vec{H} - \alpha \vec{M}_A) \}
\end{aligned} \tag{52}$$

where $\vec{M}_{A,B}$ are the A,B sublattice electronic magnetizations, λ is the molecular field constant describing the A-B exchange interaction, γ_e and γ_N are the electronic and nuclear gyromagnetic ratios, $\alpha = |H_N/M_A^0|$, $\vec{H}_{A,B}$ are the A,B sublattice effective anisotropy fields, and \vec{H} is the effective applied field (including demagnetizing effects). \vec{m} is the A-sublattice nuclear magnetization. The effect of the B-site nuclei on the A-site resonance condition will be very small and can be neglected.

Transforming the M's and m to M^+ , M^- , and m^+ , m^- , these equations become

$$\begin{aligned}
(\omega/\gamma_e)M_A^+ - (H - \lambda M_B^0 - H_A - \alpha m^0)M_A^+ - \lambda M_B^0 M_A^+ - \alpha m^+ M_A^0 &= 0 \\
(\omega/\gamma_e)M_B^+ - (H + \lambda M_A^0 + H_B)M_B^+ + \lambda M_B^0 M_A^+ &= 0 \\
(\omega/\gamma_N)m^+ - (H + \alpha M_A^0)m^+ + \alpha m^0 M_A^+ &= 0
\end{aligned} \tag{53}$$

assuming $M(t) = M^0 e^{-i\omega t}$. The solution for low frequencies (neglecting terms like ω/γ_e) is

$$\omega_N = \gamma_N (H_0 - H_D) + \gamma_N H_N \{ 1 - \eta' (m^0/M_A^0) \} \tag{54}$$

where

$$\eta' = H_N / \{ (H_0 - H_D)(\beta - 1) + (\beta H_B + H_A) + \alpha m^0 \} \tag{55}$$

($\beta = M_B/M_A$). Here H has been replaced by $H_0 - H_D$, the difference between the applied field and the demagnetizing field.

7.1 Single domain enhancement

The factor η' in Equations 54 and 55 is a result of the coupling of the electronic and nuclear magnetizations and is, in fact, the enhancement factor for nuclei not in domain walls. In general the rf field felt by the nucleus will be, with H_x applied perpendicular to H_N ,

$$H_1 = H_x (H_N / H_{K'})$$

where $H_{K'}$ acts as an effective anisotropy field acting to prevent the "rocking" of H_N by the applied field H_x . For $H_{K'} = H_K = \beta H_B + H_A \approx 1 \text{ kOe}$, $H_O - H_D = 0$, $\beta = 1.9$, with (at $T \approx 1.5 \text{ }^\circ\text{K}$) $m^0 \approx 1 \text{ Oe}$, $H_N = 560 \text{ kOe}$,

$$\eta' \approx 560$$

This enhancement occurs both as a response to an external rf field and as a response to an internally generated field, i.e., to the refocused nuclear magnetization.

7.2 Frequency pulling

Since the net nuclear magnetization varies with temperature as

$$m^0 \approx N(\gamma_N \hbar I) \left(\frac{I+1}{3} \right) \left(\frac{\gamma_N \hbar H_N}{kT} \right)$$

while M_A^0 is nearly constant (for $T \leq 4.2 \text{ }^\circ\text{K}$) the resonance frequency ω_N will be pulled to lower values as the temperature is lowered. This effect, known as frequency pulling³¹, is very strong in some materials due to the low anisotropy. In manganese ferrites the effect is small but still visible^{8,30}. Another effect of frequency pulling is illustrated in Figure 2-a where the resonance frequency for ^{55}Mn in a single crystal sample of $\text{Ni}_{.03}\text{Mn}_{.62}\text{Fe}_{2.36}\text{O}_4$ is plotted versus external field at $T = 1.5 \text{ }^\circ\text{K}$.

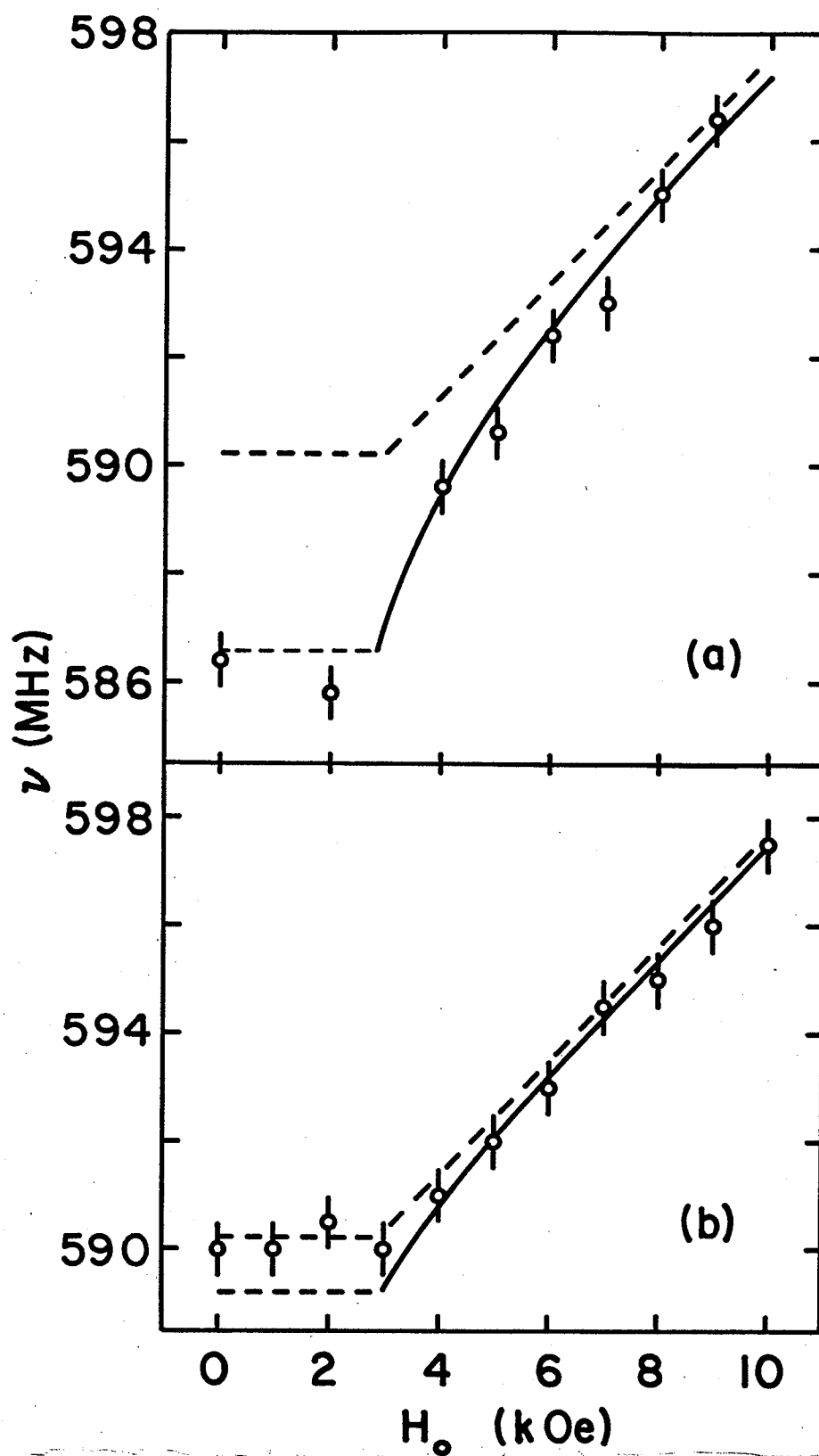


Figure 2. Frequency pulling, a) $T = 1.5$ °K, b) $T = 4.2$ °K.

The dashed line has a slope of $\gamma_{\text{Mn}} = 1.055 \times 10^3 \text{ (sec Oe)}^{-1}$ and an $H_0 - H_D = 0$ value of $\gamma_{\text{Mn}} \times 559.5 \text{ kOe}$. The solid curve is the resonance frequency calculated from Equations 54 and 55 using $H_K = 0.7 \text{ kOe}$. Figure 2.b is for the spectrum at 4.2°K . The solid curve in this case is the calculated resonance frequency using the same hyperfine field as in part (a) of the figure but with $H_K = 1.0 \text{ kOe}$.

When the enhancement factor η' is very large, an external rf field can become so strong that it destroys the resonance condition³¹. This is especially true in pulsed NMR where the rf fields are already very strong, and it may be impossible to observe the resonance unless an external static field large enough to significantly weaken the enhancement factor is applied.

8. Free Precession of Nuclear Moments

The free precession³² techniques in magnetic resonance, since they involve the response of the magnetic system to a number of rf pulses, allow the observation of the precessing magnetization (about the static magnetic field) in the absence of continuous external driving fields, and, therefore, are ideally suited for the study of relaxation effects and the interactions which cause them.

8.1 Free induction decay and spin echoes

In the vector model of pulsed resonance^{32,33}, viewed in a reference frame rotating at the Larmor precessional frequency ω_L , an rf field of frequency $\omega_0 = \omega_L$ and strength H_1^x applied perpendicular to the static magnetic field H^z (and the net equilibrium nuclear magnetization), will

exert a torque on the nuclear magnetization ($\vec{H}_1 \times \vec{m}$) and will rotate it in the plane perpendicular to H_1^x . If the rf field is left on for a time δt such that $\gamma_N H_1^x \delta t = \pi/2$, the nuclear magnetization will lie along the y-direction when the pulse is removed. In the laboratory frame this will produce a rotating field in the plane perpendicular to the static field. This rotating field can be detected by a coil or cavity and gives the familiar free induction decay (fid). If the individual nuclear spins have slightly different Larmor frequencies ($\omega_i - \omega_L \ll \omega_L$) this free induction signal will decrease in intensity due to the gradual loss of phase coherence in the total spin system.

If at a time τ later a second rf pulse is applied along the same direction in the rotating frame the components of the individual nuclear moments perpendicular to H_2^x will again experience a torque and will be rotated out of the plane. If this second pulse has a length δt such that $\gamma_N H_2^x \delta t = \pi$, these components will have been effectively reflected through the x-axis. Then, due to the spread in Larmor frequencies, the individual moments will regain their phase coherence temporarily at a time τ following the application of the second pulse. This results in a net moment along the -y direction in the rotating frame, which can again be detected as a rotating field in the laboratory frame. This is the two-pulse spin-echo experiment described by Hahn³² ($\pi/2 - \pi/2$ sequence) and by Carr-Purcell³³ ($\pi/2 - \pi$ sequence), and has been the primary tool in this study of the nuclear magnetic resonance in manganese ferrites.

8.2 Relaxation processes--longitudinal and transverse

Due to interactions between nuclear spins and between the spins and their surroundings the free precession signals (fid and spin echo) do not

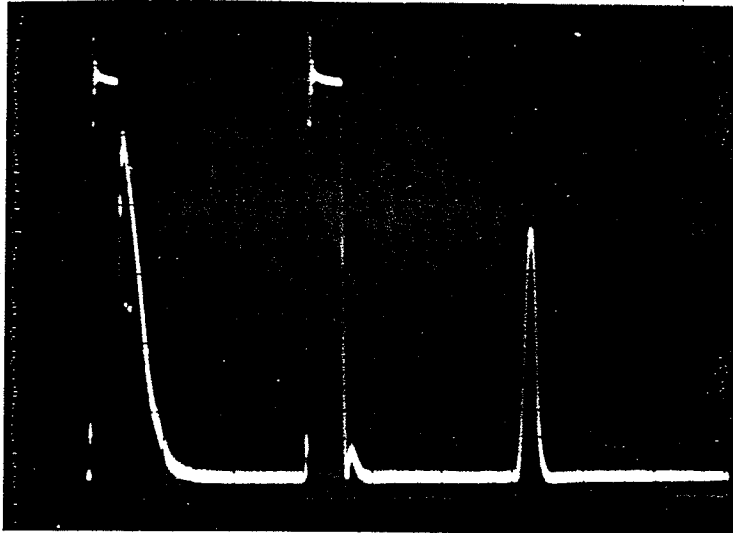


Figure 3. Free induction decay and spin echo in MnFe_2O_4 . $T = 4.2^\circ\text{K}$.

persist indefinitely. There are two basic types of relaxation possible: the longitudinal processes which bring the magnetization out of the x-y plane and back along the z-axis, and transverse processes which involve the destruction of phase coherence of the moments rotating in the x-y plane. The longitudinal and transverse relaxation rates are usually described in terms of characteristic relaxation times T_1 and T_2 respectively.

If the time between the two rf pulses is varied the spin-echo amplitude will vary due to relaxation processes, as shown in Figure 4-a. The data for this figure were taken at 1.45°K in an external field of $H_0 = 8.0 \text{ kOe}$. The clearly exponential behaviour of the spin-echo decay implies that the relaxation can be well described by a single relaxation time. This relaxation time can, however, represent the sum of several relaxation processes--of both longitudinal and transverse type. The spin-echo amplitude for this simple two-pulse experiment can be written as

$$A(2\tau) = A(\tau = 0)\exp(-2\tau/T) \quad (56)$$

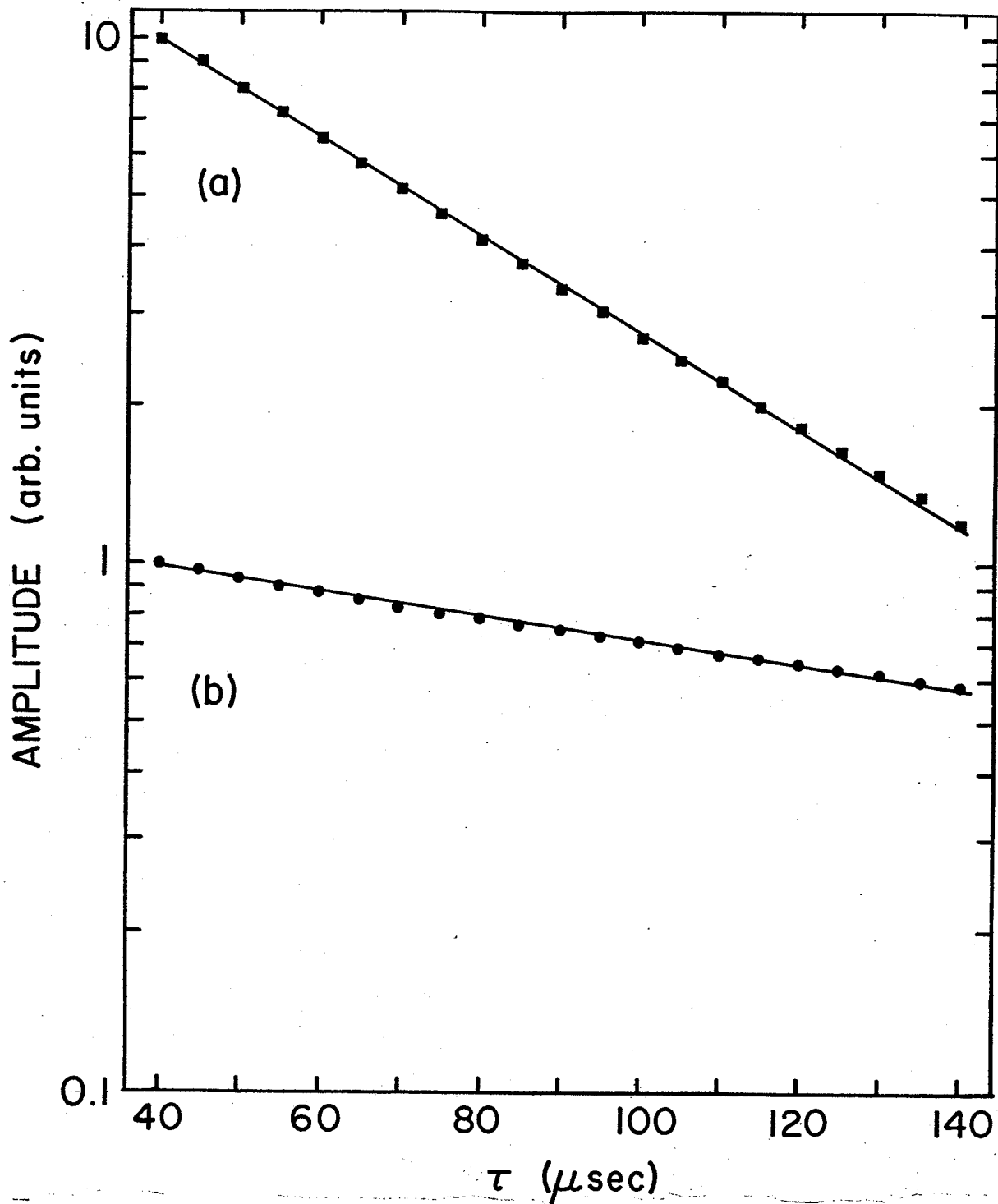


Figure 4. Spin echo decay envelopes at $T = 1.45$ $^{\circ}\text{K}$ in $H_0 = 8$ kOe; a) two-pulse echo, b) three-pulse stimulated echo.

where T includes effects from all different relaxation processes.

To separate T_1 processes from T_2 processes various techniques have been devised^{32,33,34} using larger numbers of pulses. A simple technique to determine T_1 independent of T_2 , consists in applying a third rf pulse (length corresponding to a rotation of $\frac{\pi}{2}$) at a time τ_2 after the second pulse. Under these conditions several spin-echoes appear, as shown in Figure 5. The echo occurring at a time $t = \tau_1 + \tau_2$ is of

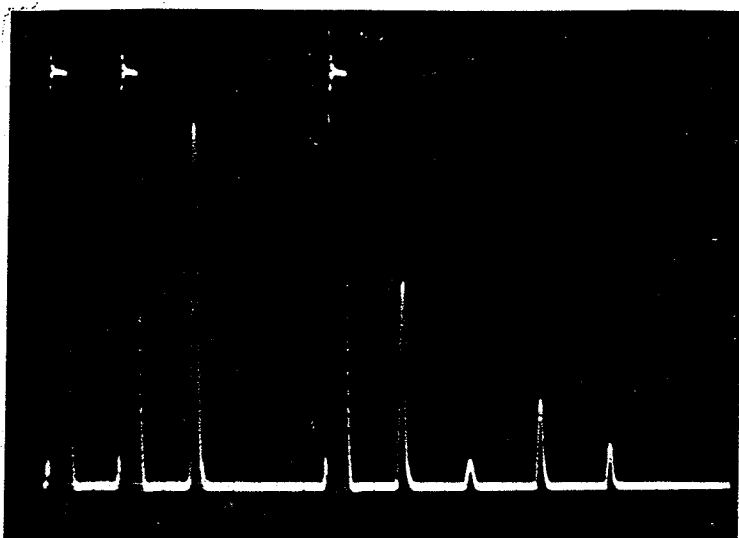


Figure 5. Response to three rf pulses showing stimulated echo and secondary echoes.

particular interest since its amplitude as a function of τ_1 and τ_2 is given (in the absence of diffusion effects) by

$$A'(\tau_1 + \tau_2) = A'_0 \exp\left\{-\tau_1\left(\frac{1}{T_1} + \frac{2}{T_2}\right)\right\} \times \exp(-\tau_2/T_1) \quad , (57)$$

Then, if τ_1 is held constant while τ_2 is varied the plot of echo amplitude versus τ_2 gives the longitudinal relaxation time T_1 , as illustrated in Figure 4-b. The transverse relaxation rate can be obtained from $(1/T_2) = (1/T) - (1/T_1)$.

9. Inhomogeneous Broadening--Instrumental Considerations

In a case where spin diffusion (whether actual particle diffusion or spectral diffusion) and relaxation effects can be neglected during the rf pulses and during the fid or spin-echo, if the resonance line is narrower than the bandwidth of the rf pulse the free induction and spin-echo can be viewed as the Fourier transform of the resonance line³⁵. In ordered magnetic materials, however, the resonance is strongly broadened by sample inhomogeneities and is usually much broader than the rf pulse bandwidth. Thus, the echo and fid will reflect the frequency spectrum of the pulse rather than that of the actual nuclear resonance spectrum. To obtain information about the entire spectrum then we must sample it as a function of frequency in a step by step fashion. Figure 6 shows a spectrum obtained in this manner. The pulse bandwidth is $\sim 1/\delta t \approx 0.5$ MHz, while the resonance line's half-width at half-maximum is $\delta \approx 3$ MHz.

Such strong inhomogeneous broadening creates some special instrumental problems. First, the pulse spectrometer must be a variable frequency type (sometimes over a very broad range) and one must insure that the rf pulse amplitude and receiver sensitivity remain constant over the entire spectrum. Second, because of the large hyperfine fields and subsequent high resonant frequencies, the rf wavelengths are of the order of meters and uhf techniques should be used. Third, since the enhancement factor for nuclei in domain walls is a function of the nucleus' position in the wall, the tuning conditions (for a $\pi/2$ or π pulse) will change with the positions in the wall being sampled at a given frequency.

In the case of ^{55}Mn resonance at the A-sites in MnFe_2O_4 these problems are not so severe as they are in other cases (e.g., ^{55}Mn resonance

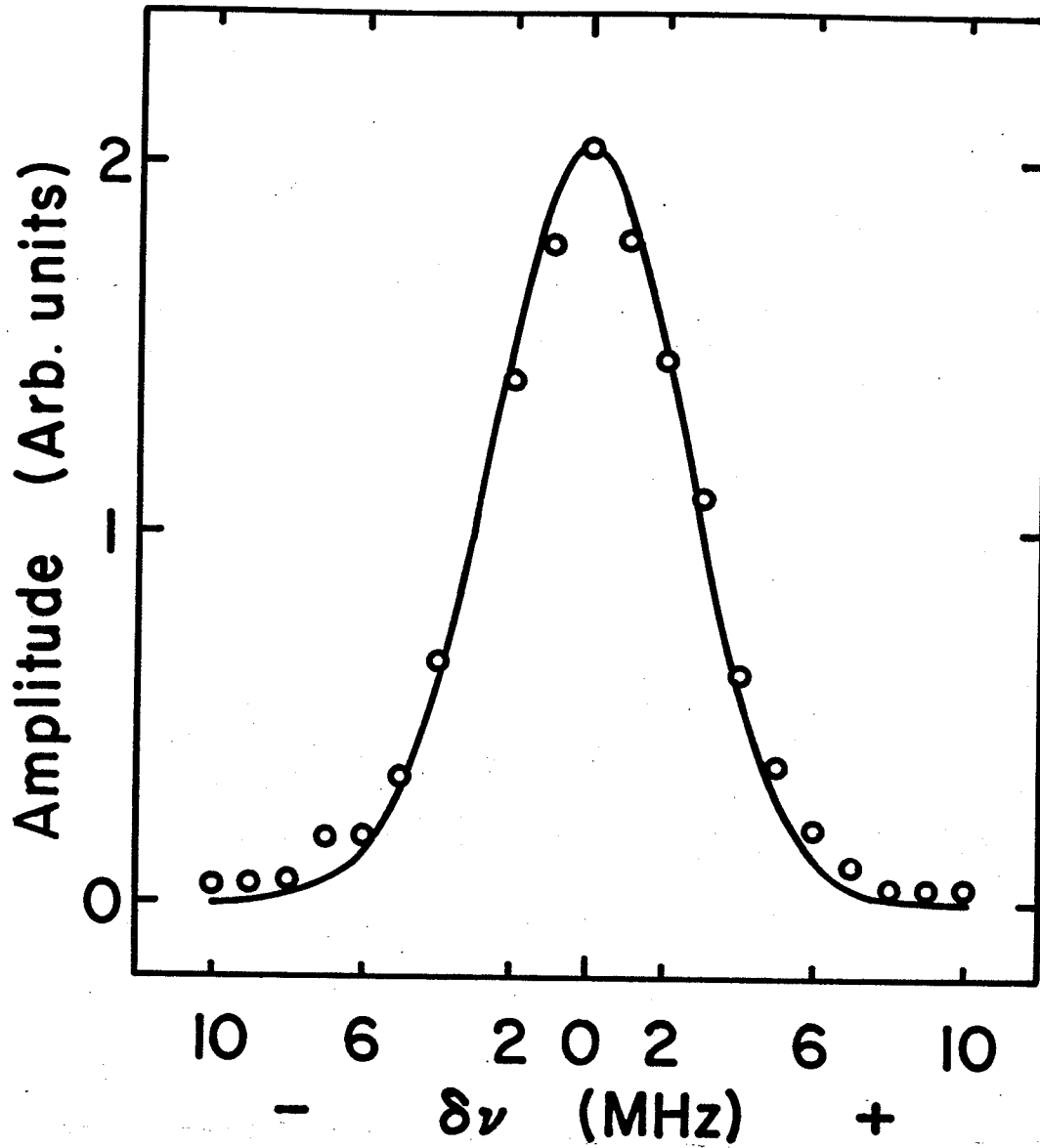


Figure 6. Spectrum extrapolated to $\tau = 0.0$ at $T = 1.5$ °K in $H_0 = 3.0$ kOe for a single crystal of $\text{Ni}_{0.03}\text{Mn}_{0.62}\text{Fe}_{2.36}\text{O}_4$.

for nuclei at the B-sites), since the linewidth is ~ 3 MHz while the resonance frequency is ≈ 600 MHz ($f/\Delta f \approx 200$). RF pulse power output is assumed constant over this range while receiver sensitivity is easily calibrated using an rf pulse of known amplitude (obtained from an rf signal generator). To minimize cable reflections, and since maximum power transfer was not a consideration, the rf cables were made long (> 10 meters) to approximate an infinite transmission line. For more critical applications, variable stub stretchers should be utilized.

The enhancement mechanisms discussed earlier depend both on the amount of nuclear magnetization at the particular frequency being sampled and on the applied magnetic field. Thus, the condition for optimum pulse widths will be a function of frequency and field. For each new frequency and field the pulse width must be readjusted. This should help to cancel any frequency variation of pulse amplitude since, in the vector model, a change in H_1^x may be compensated for by a change in pulse width.

Because of the strong enhancement of the applied rf field it is never clear that the pulses form a true $(\pi/2, \pi)$ pair. Very large turning angles are possible³⁶ for strong pulses, particularly for nuclei within domain walls. The very large enhancement factors for nuclei in domain walls (compared to the enhancement for nuclei in domains) introduces a severe experimental difficulty since it is impossible to satisfy the $(\pi/2, \pi)$ condition for both nuclei within domain walls and domains simultaneously. Thus, as the proportion of domain wall nuclei contributing to the signal changes with frequency, coupled with the changing enhancement factor, the tuning conditions (pulse widths) sometimes change drastically introducing considerable experimental uncertainty. At higher values of external field the situation is considerably simplified since then the

domain walls have been almost entirely removed and the sample is a single domain. At low fields, however, several experimental runs were necessary before reproducible results were obtained, and it was found that the situation was much improved at low rf pulse powers. For this reason, and to insure a well-shaped pulse from the pulsed oscillator, a rather low pulse amplitude was used throughout, being only large enough to allow good signal to noise ratio throughout the frequency, field, and temperature ranges of interest. Even so, it is expected that a large part of the difficulty in the interpretation of the spectra at low fields is due to this problem (see the discussion in Chapter IV).

Two types of resonant cavities were used in these experiments, one which was inserted into the cryostat and allowed the sample to be rotated about an axis perpendicular to the external field, and the other which was outside the dewar. Both are coaxial cavities whose resonant frequencies

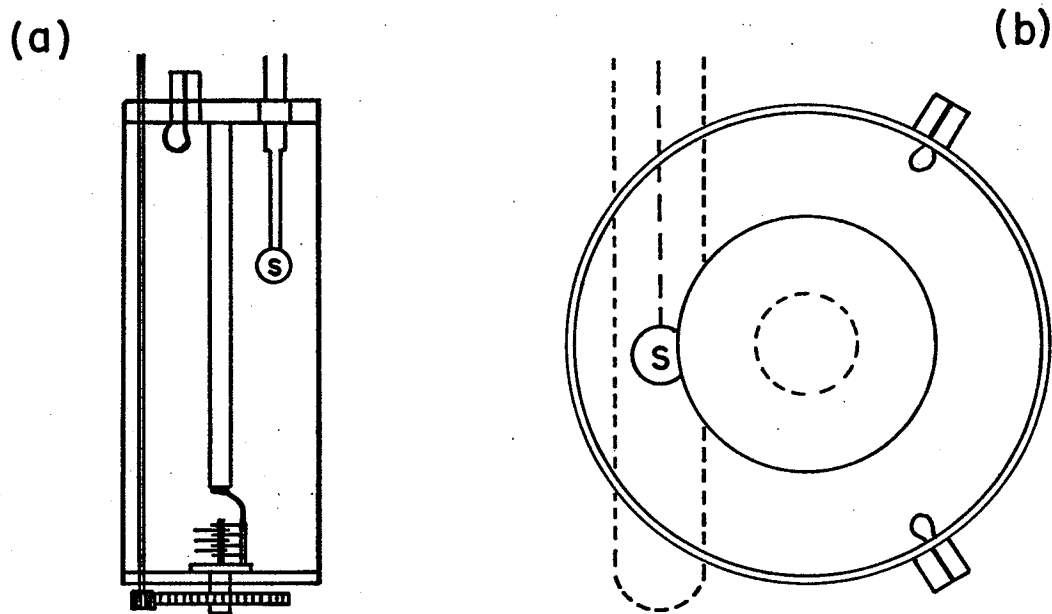


Figure 7. The cavities used in the pulsed NMR experiments. a) side view of cavity placed inside cryostat, b) front view of external cavity showing cryostat tip inserted. S is sample.

are varied by adjusting a capacitance at one end. The in-dewar cavity is illustrated in Figure 7-a where the capacitor at the bottom is a 15 pf trimmer. The external cavity, illustrated in Figure 7-b, uses a brass disc fastened to the top of the central post, and the cavity front, which screws into the cavity on very fine threads, to form the variable capacitance. This latter configuration was very successful because there is no rf current flowing across the points where the cavity front makes contact with the body of the cavity. The tip of the dewar containing the sample was inserted into the cavity as shown in the figure.

In both of these cavities the rf magnetic field is in a mode cylindrically symmetric with respect to the axis of the cavity. The rf pulse is applied to a single loop of wire as shown in the figure, and the signal is detected by a similar loop on the opposite side of the cavity.

Figure 8 is a block diagram of the system for measuring the spectra when the echo decay envelope is nearly exponential (used for spectra taken on the $\text{Ni}_{.03}\text{Mn}_{.62}\text{Fe}_{2.36}\text{O}_4$ sample). The exponential generator uses an

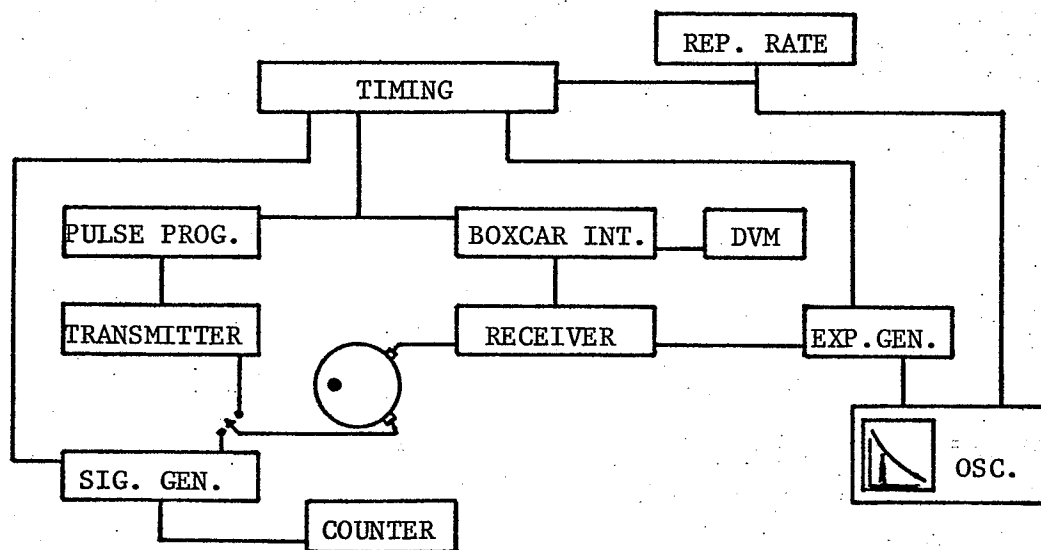


Figure 8. Block diagram of spectrometer system for comparing echo decay envelope to an exponential of known time constant.

R-C circuit to generate an exponential of known time constant to which the echo amplitude is compared while varying the time between rf pulses. The receiver is calibrated using the pulse modulated rf signal generator whose output is applied at the transmitter side of the cavity. The signal generator's output voltage is selected and fixed throughout the experiment so that its output pulse will not saturate the receiver even at those parts of the spectrum where the receiver gain is the highest (i.e., far from resonance). The gate of the boxcar integrator is placed at the position ($t \approx 2\tau$) of the echo maximum and has a width (≈ 20 nanoseconds) which is much less than the width of the echo. The signal generator output pulse is timed to occur at the same position as the echo so that the boxcar integrator and the digital voltmeter can be used to measure the receiver gain as well as the echo amplitude, depending on the position of the switch to the cavity. By measuring the decay time, echo amplitude, and receiver gain as a function of frequency the resonance spectrum is obtained. The spectrum shown in Figure 6 was obtained in this manner.

As discussed earlier, for low values of external field, domain walls exist in sufficient quantity that the echo will consist of two components with different amplitudes and relaxation times. In this case the echo decay envelope will not appear exponential. For this condition the system described by the block diagram in Figure 9 was used. Here the triggers for the two rf pulses as well as the box-car's gate positioning pulse are derived from a square wave whose frequency is varied by applying a ramp voltage to the VCG input of the square wave generator. In this way the separation between pulses can be continuously varied over a range of > 100 μsec , and the boxcar gate position automatically tracks the echo position (at 2τ). The area of the square wave is proportional to the

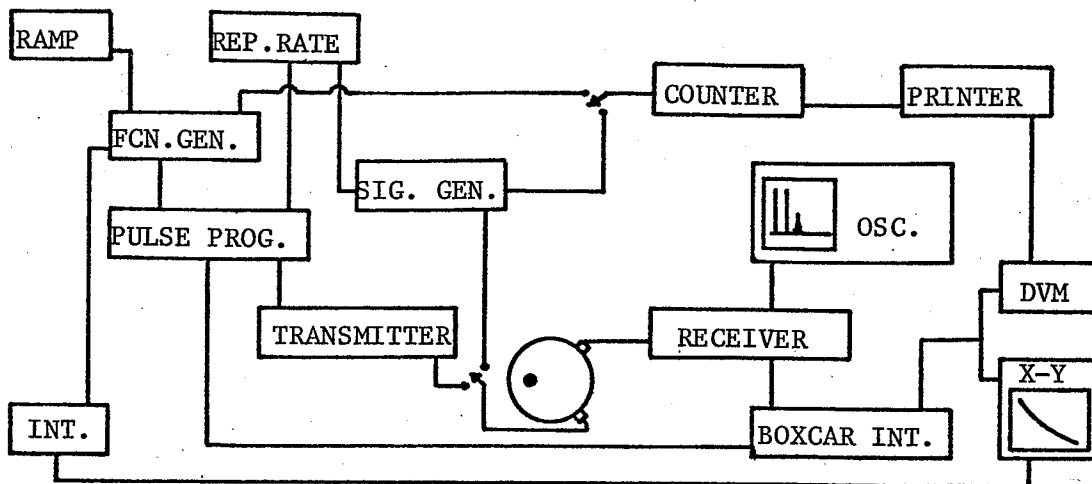


Figure 9. Block diagram of spectrometer system used in the case of non-exponential decay.

period of the square wave, thus, the output of the square-wave integrator is applied in analog form to the x-axis of an x-y recorder and in digital form to the digital printer. The boxcar output is similarly applied to the output units and a continuous record of echo amplitude versus time between pulses is obtained. This, together with receiver gain, is sufficient to obtain the complete spectrum when repeated over the entire frequency range. The spectra taken on the MnFe_2O_4 single crystal sphere were done in this way.

CHAPTER II

The Suhl-Nakamura Interaction

and the Formation of Multiple Echoes

When there is a high density of nuclear spins in a material, whether liquid³⁷, solid³⁸, metal³⁹, or magnetically ordered^{40,41}, there exists an effective nuclear spin-spin interaction which may be of either pseudo-dipolar or pseudo-exchange form^{38,42}. This interaction proceeds through a partial polarization of the electronic states by the electron-nucleus interaction, and its form may be obtained through a second-order perturbation treatment of the electronic energy levels with the electron-nucleus interaction as the perturbing Hamiltonian. In liquids the interaction is restricted to a single molecule while in insulating solids near neighbors may interact. In metals the perturbation sets up a localized spin-density wave which extends over many atomic distances ($\mathcal{H}_{\text{eff}} \sim \cos(2k_{\text{F}}R)/R^3$), and in magnetic materials, due to the strong exchange and hyperfine interactions, the effective spin-spin interaction ($\mathcal{H}_{\text{eff}} \sim R^{-1} \exp(-\alpha R)$) can have a very long range and, therefore, a strong effect.

1. The Hyperfine Interaction--Spin-Wave Expansion

At low temperatures, where the spin-wave theory outlined in Chapter I can be effectively applied, the hyperfine interaction (Equation I.3) for the isotropic case (applicable to the A-site ions) can be written as

$$\mathcal{H}_{\text{hf}} = \frac{1}{2} A \sum_{\mathbf{n}}^{\text{A}} (I_{\mathbf{n}}^+ S_{\mathbf{n}}^- + I_{\mathbf{n}}^- S_{\mathbf{n}}^+) + A \sum_{\mathbf{n}}^{\text{A}} I_{\mathbf{n}}^z S_{\mathbf{n}}^z \quad (1)$$

with $A = -g_N \mu_N \vec{H}_{hf} \cdot \vec{S} / (\vec{S} \cdot \vec{S})$, where S is the A-site electronic spin. Then, the Holstein-Primakoff transformations allow the hyperfine interaction to be written in terms of the spin-wave operators defined in Chapter I. Up to third order in spin-wave operators the hyperfine interaction may be written as

$$\mathcal{H}_{hf} = \mathcal{H}_{hf}^{(0)} + \mathcal{H}_{hf}^{(1)} + \mathcal{H}_{hf}^{(2)} + \mathcal{H}_{hf}^{(3)} \quad (2)$$

where,

$$\mathcal{H}_{hf}^{(0)} = -AS_A \sum_n I_n^z \quad (3)$$

is the zero-magnon term representing an energy shift due to the net z-polarization of the nuclear spin system. The one-magnon term,

$$\mathcal{H}_{hf}^{(1)} = \frac{1}{2} A(2S_A)^{\frac{1}{2}} \sum_k (I_k^+ a_k + I_k^- a_k^\dagger) \quad (4)$$

gives rise to the effective spin-spin interaction when treated as a perturbation. Here the nuclear spin operators I_n^\pm have been transformed to

$$I_k^\pm = (1/\sqrt{N_A}) \sum_n I_n^\pm \exp(\pm i\vec{k} \cdot \vec{r}_n)$$

The two-magnon term is

$$\mathcal{H}_{hf}^{(2)} = (A/N_A) \sum_n \sum_{k_1, k_2} I_n^z \exp\{-i(\vec{k}_1 - \vec{k}_2) \cdot \vec{r}_n\} a_{k_1}^\dagger a_{k_2} \quad (5)$$

while the three-magnon term is written as

$$\mathcal{H}_{hf}^{(3)} = -\frac{1}{2} A(2S_A)^{\frac{1}{2}} (1/4N_A^{3/2} S_A) \sum_n \sum_{k_1, k_2, k_3} (I_n^+ \exp\{-i(\vec{k}_1 - \vec{k}_2 - \vec{k}_3) \cdot \vec{r}_n\} \times a_{k_1}^\dagger a_{k_2} a_{k_3} + I_n^- \exp\{-i(\vec{k}_1 + \vec{k}_2 - \vec{k}_3) \cdot \vec{r}_n\} a_{k_1}^\dagger a_{k_2}^\dagger a_{k_3}) \quad (6)$$

These higher order terms (Equations 5 and 6) will be of considerable

importance in relation to the spin-wave relaxation processes to be discussed in Chapter III.

The one, two, and three-magnon expressions in Equations 4, 5, and 6 when written in terms of the magnon normal-mode operators α_k , β_k become

$$\mathcal{H}_{\text{hf}}^{(1)} = \frac{1}{2} A(2S_A)^{\frac{1}{2}} \sum_k \left(I_k^- (-v_k \alpha_k + u_k \beta_k^+) + I_k^+ (-v_k \alpha_k^+ + u_k \beta_k) \right) \quad (7)$$

$$\begin{aligned} \mathcal{H}_{\text{hf}}^{(2)} = & (A/N_A) \sum_n \sum_{k_1, k_2} I_n^Z \exp\{i(\vec{k}_1 - \vec{k}_2) \cdot \vec{r}_n\} \\ & \times \left(v_{k_1} v_{k_2} \alpha_{k_1} \alpha_{k_2}^+ - u_{k_1} v_{k_2} \beta_{k_1}^+ \alpha_{k_2}^+ \right. \\ & \left. - v_{k_1} u_{k_2} \alpha_{k_1} \beta_{k_2} + u_{k_1} u_{k_2} \beta_{k_1}^+ \beta_{k_2} \right) \quad (8) \end{aligned}$$

$$\begin{aligned} \mathcal{H}_{\text{hf}}^{(3)} = & - (2S_A)^{\frac{1}{2}} (A/8N_A^{3/2} S_A) \sum_n \sum_{k_1, k_2, k_3} \left(\exp\{-i(\vec{k}_1 + \vec{k}_2 - \vec{k}_3) \cdot \vec{r}_n\} I_n^- \right. \\ & \times \left(-v_1 v_2 v_3 \alpha_1 \alpha_2 \alpha_3^+ + u_1 v_2 v_3 \beta_1^+ \alpha_2 \alpha_3^+ + v_1 u_2 v_3 \alpha_1 \beta_2^+ \alpha_3^+ + v_1 v_2 u_3 \alpha_1 \alpha_2 \beta_3 \right. \\ & \left. - v_1 u_2 u_3 \alpha_1 \beta_2^+ \beta_3 - u_1 v_2 u_3 \beta_1^+ \alpha_2 \beta_3 - u_1 u_2 v_3 \beta_1^+ \beta_2^+ \alpha_3^+ + u_1 u_2 u_3 \beta_1^+ \beta_2^+ \beta_3 \right) + \\ & \left. \exp\{i(\vec{k}_1 + \vec{k}_2 - \vec{k}_3) \cdot \vec{r}_n\} I_n^+ \left(-v_1 v_2 v_3 \alpha_1^+ \alpha_2^+ \alpha_3 + u_1 v_2 v_3 \beta_1 \alpha_2^+ \alpha_3 + v_1 u_2 v_3 \alpha_1^+ \beta_2 \alpha_3 \right. \right. \\ & \left. \left. + v_1 v_2 u_3 \alpha_1^+ \alpha_2^+ \beta_3 - v_1 u_2 u_3 \alpha_1^+ \beta_2 \beta_3 - u_1 v_2 u_3 \beta_1 \alpha_2^+ \beta_3 - u_1 u_2 v_3 \beta_1 \beta_2 \alpha_3 \right. \right. \\ & \left. \left. + u_1 u_2 u_3 \beta_1 \beta_2 \beta_3^+ \right) \right) \quad (9) \end{aligned}$$

In these expressions, $\alpha_i = \alpha_{k_i}$, $v_i = v_{k_i}$, etc., and

$$a_k = -v_k \alpha_k^+ + u_k \beta_k$$

as given in Equation I.26. The transformation coefficients are

$$u_k^2 = \frac{S_B}{S_B - \eta^2 S_A}, \quad v_k^2 = \frac{\eta^2 S_A}{S_B - \eta^2 S_A} \quad (10)$$

$$\eta = \frac{\hat{z} N_A}{\frac{1}{2} \{ N_A Z_A \gamma_k^A + N_B Z_B \gamma_k^B \}}$$

Equations 8 and 9 will be discussed further in Chapter III.

2. Second-order Effective Nuclear Spin-Spin Interaction

2.1 Perturbation expansion

The second-order shift in the energy levels, using the usual perturbation expansion with the one-magnon term of Equation 7 as the perturbing Hamiltonian, is given by

$$\Delta E = - \sum_k \frac{\langle 0 | \mathcal{H}_{hf}^{(1)} | k \rangle \langle k | \mathcal{H}_{hf}^{(1)} | 0 \rangle}{E_k - E_0} \quad (11)$$

where the state $|k\rangle$ is the state with one spin-wave (either α or β) of wave vector \vec{k} and $|0\rangle$ is the state with no spin-waves. Since the magnon dispersion relation has two branches (Equation I.28) the one-magnon hyperfine interaction is written

$$\mathcal{H}_{hf}^{(1)} = \mathcal{H}_\alpha^{(1)} + \mathcal{H}_\beta^{(1)}$$

$$\mathcal{H}_\alpha^{(1)} = - \frac{1}{2} A (2S_A)^{\frac{1}{2}} \sum_k \{ I_{k k}^+ v_k \alpha_k^+ + I_{k k}^- v_k \alpha_k \} \quad (12)$$

$$\mathcal{H}_\beta^{(1)} = + \frac{1}{2} A (2S_A)^{\frac{1}{2}} \sum_k \{ I_{k k}^+ u_k \beta_k + I_{k k}^- u_k \beta_k^+ \}$$

and the energy shift becomes

$$\Delta E = - \sum_k \left[\frac{\langle 0 | \mathcal{H}_\alpha^{(1)} | k \rangle \langle k | \mathcal{H}_\alpha^{(1)} | 0 \rangle}{\hbar\omega_\alpha} + \frac{\langle 0 | \mathcal{H}_\beta^{(1)} | k \rangle \langle k | \mathcal{H}_\beta^{(1)} | 0 \rangle}{\hbar\omega_\beta} \right] \quad (13)$$

$$= \Delta E_\alpha + \Delta E_\beta$$

Then, since $\alpha_k |0\rangle = 0$, $\beta_k^+ |0\rangle = |k\rangle$, etc., the energy shifts can be written as

$$\Delta E_\alpha = - \frac{1}{2} A^2 S_A \sum_k \left(\frac{I_k^- I_k^+}{\hbar\omega_\alpha} \right) v_k^2 \quad (14)$$

$$\Delta E_\beta = - \frac{1}{2} A^2 S_A \sum_k \left(\frac{I_k^+ I_k^-}{\hbar\omega_\beta} \right) u_k^2$$

Since the gap between the α and β branches of the spin-wave spectrum is quite large for ferrimagnets, the energy denominator $\hbar\omega_\beta$ is large and ΔE_β may be neglected, giving $\Delta E \approx \Delta E_\alpha$. Thus, the form of the Suhl-Nakamura effective spin-spin interaction for ferrimagnets is the same as that for ferromagnets⁴⁰.

2.2 Asymptotic form of the range function

Transforming the expression in Equation 14 for ΔE_α back to the nuclear spin operators I_n^\pm , the effective nuclear spin-spin interaction takes the form

$$\mathcal{H}_{S-N} = - \frac{1}{2} A^2 S_A \sum_{i \neq j} \left\{ (1/N_A) \sum_k \left(\frac{v_k^2}{\hbar\omega_\alpha} \right) \exp\{i\vec{k} \cdot (\vec{r}_i - \vec{r}_j)\} I_j^- I_i^+ \right\} \quad (15)$$

omitting from the summation self-energy terms where a magnon is emitted and then reabsorbed by the same nucleus. The expression

$$B_{ij} = (A^2 S_A / N_A) \sum_k \left(\frac{v_k^2}{\hbar\omega_\alpha} \right) \exp\{i\vec{k} \cdot (\vec{r}_i - \vec{r}_j)\} \quad (16)$$

is called the Suhl-Nakamura range function. The α -mode dispersion relation is, for MnFe_2O_4 ,

$$\hbar\omega_\alpha = g\mu_B H' + 4JS_{\text{eff}} a^2 k^2 \quad (11/64) \quad (17)$$

where

$$S_{\text{eff}} = \frac{N_A}{N_B} \left(\frac{S_A S_B}{S_B - \eta^2 S_A} \right) \approx \frac{1}{2} \left(\frac{S_A S_B}{S_B - \frac{1}{2} S_A} \right)$$

The sum over \vec{k} in Equation 16 can be replaced by an integral in the long wavelength approximation. Then, with

$$\sum_{\vec{k}} \left(\frac{v_{\vec{k}}^2}{\hbar\omega_\alpha} \right) e^{i\vec{k} \cdot \vec{r}_{ij}} \approx (S_{\text{eff}}/S_B) \int_{\vec{k}} \left(\frac{e^{i\vec{k} \cdot \vec{r}_{ij}}}{c + dk^2} \right)$$

since $v_{\vec{k}}^2 \approx \frac{1}{2} S_A / (S_B - \frac{1}{2} S_A)$, (which amounts to neglecting a term like $g\mu_B H' k^2$ compared to $g\mu_B H_{\text{ex}} k^2$), the range function, on transforming to an integral, becomes

$$\begin{aligned} B_{ij} &= A^2 S_A (S_{\text{eff}}/S_B) (\hat{a}^3 / 2\pi)^3 \int_0^{2\pi} d\phi \int_{-1}^1 d\cos\theta \int_0^\infty dk k^2 \left(\frac{e^{i\vec{k} \cdot \vec{r}_{ij}}}{c + dk^2} \right) \quad (18) \\ &= A^2 S_A (S_{\text{eff}}/S_B) (\hat{a}^3 / (2\pi)^2) (1/2dr) \text{Im} \left[\int_{-\infty}^\infty dz \frac{ze^{iz}}{c/d + z^2} \right] \\ &= A^2 S_A (S_{\text{eff}}/S_B) (\hat{a}^3 / 4\pi d) (1/r) \exp\{-(c/d)^{1/2} r\} \end{aligned}$$

Then, as a function of the effective internal field H' (including externally applied fields, anisotropy and demagnetizing fields) and the exchange energy $\hbar\omega_e$, where \hat{a}^3 is the volume per A-site ion,

$$B_{ij} = \left(\frac{2A^2 S_A}{z\hbar\omega_e} \right) \left(\frac{S_{\text{eff}}}{S_B} \right) (1/\bar{N}_A) f(r_{ij})$$

where z is the number of A-site nearest magnetic neighbors and \bar{N}_A is the number of A-site ions per unit cell, $\hbar\omega_e = 4JS_{\text{eff}} (11/64)$, and the function $f(r_{ij})$ is given by

$$f(r_{ij}) = \frac{1}{4\pi\alpha} \frac{a}{r} \exp\{-(g\mu_B H' / \hbar\omega_e)^{1/2} (r/a)\} \quad (19)$$

with the constant $\alpha = (2/z) = 1/6$.

In Figures 1-a,b the asymptotic range function is plotted as a function of distance (r/a_{nn}) and as a function of the effective field H' . The effective range of the interaction, R , is defined as the distance where $(r/a_{nn}) = R = (g\mu_B H' / \hbar\omega_e)^{-1/2}$. For the values $\hbar\omega_e = 1.29 \times 10^{-15}$ ergs and $H' = 1.0$ kOe, the range is $R = 21.4 \times a_{nn} = 76 \text{ \AA}$.

Even though the interaction would appear to be quite weak due to its second order nature, its very long range makes it the strongest inter-nuclear interaction in these materials and it provides the most effective nuclear magnetic relaxation channel at low temperatures.

The Suhl-Nakamura Hamiltonian of Equation 15 describes an interaction between the transverse (I^+ , I^-) components of the nuclear spin; therefore, when there are a large number of nuclear spins in the x-y plane, as is the case in the usual pulsed NMR experiments, the spins will interact strongly. The result of this interaction, other than the transverse relaxation to be discussed in Chapter III, is an effective magnetic field at one nucleus due to the x, y components of the spin of another nucleus. This effect will be discussed in connection with the formation of multiple echoes after a brief discussion of the density matrix treatment of pulsed nuclear resonance.

3. Density Matrix Treatment of Pulsed Resonance

The density matrix formalism provides a straightforward and powerful method of calculating the response of the nuclear spin system to an external excitation^{43,44}. Given a general state of the system ψ which is a linear superposition of the orthonormal eigenstates u_m of the Hamiltonian

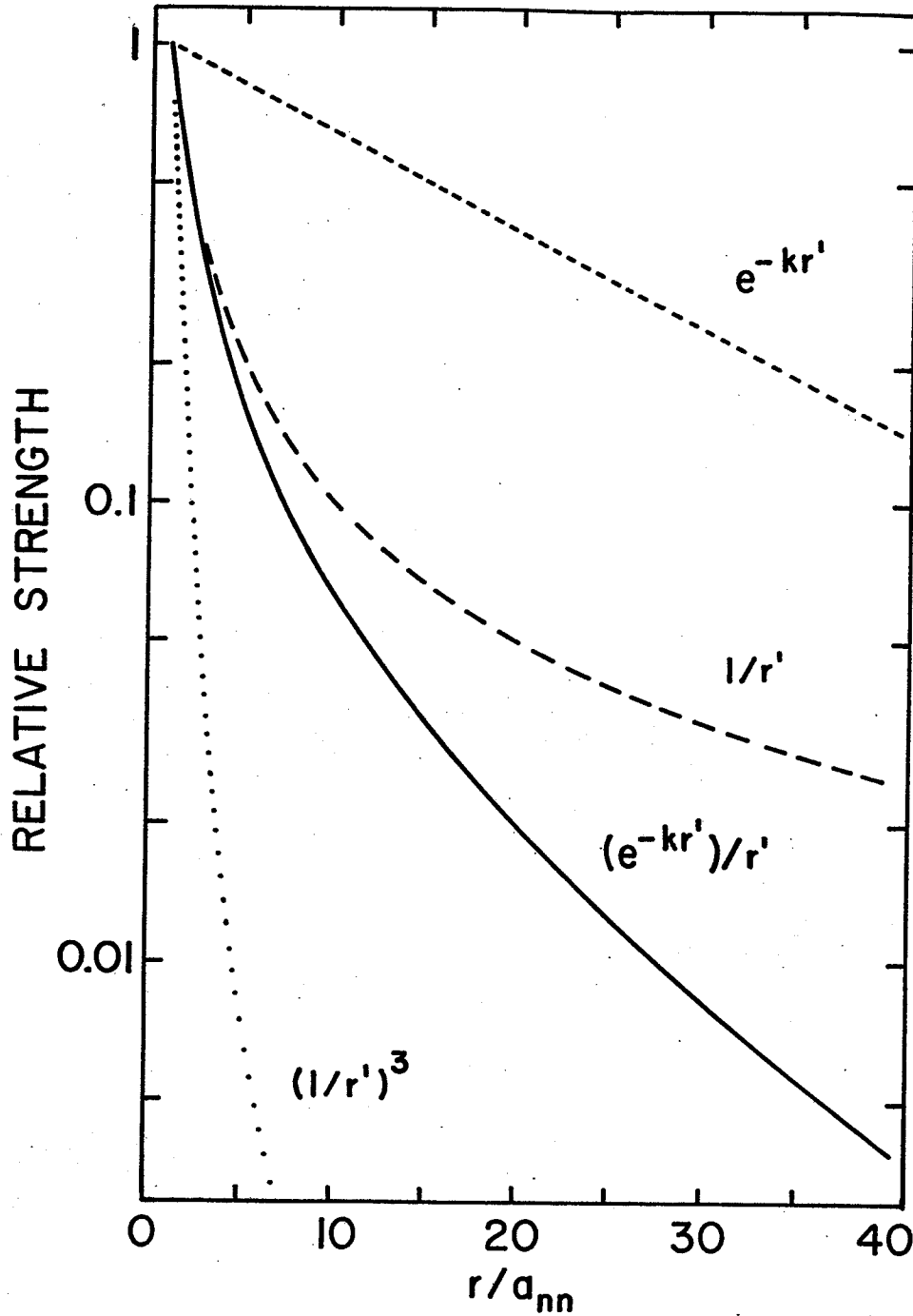


Figure 1a. Distance dependence of Suhl-Nakamura asymptotic range function compared to other range functions. $r' = r/a_{nn}$, $k = 4.6 \times 10^{-2}$

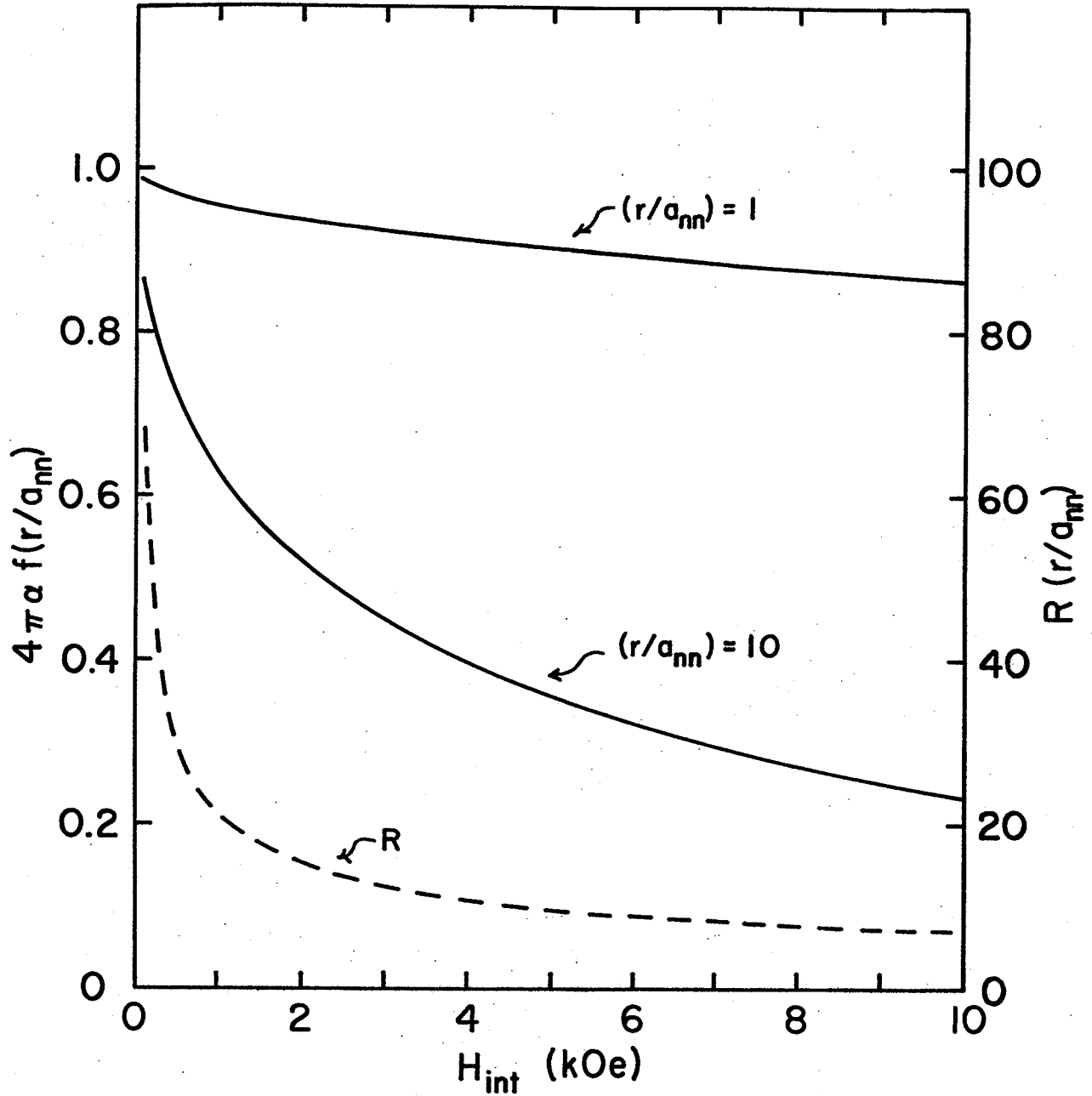


Figure 1b. Field dependence of Suhl-Nakamura asymptotic range function and effective range R for $\hbar\omega_e = 1.32 \times 10^{-15}$

the expectation value of an operator M_z in the state ψ is

$$\langle M_z \rangle = (\psi^*, M_z \psi) = \sum_{n,m} a_n^* a_m \langle u_n | M_z | u_m \rangle = \sum_{n,m} \langle m | P | n \rangle \langle n | M_z | m \rangle, \quad (20)$$

where $\langle m | P | n \rangle = a_m a_n^*$ defines an operator P . From Equation 20 we have that the average value of M_z is

$$\langle M_z \rangle = \sum_m \langle m | P M_z | m \rangle$$

The density operator ρ is defined as the ensemble average⁴³ of matrix elements of P

$$\langle m | \rho | n \rangle = \overline{a_m a_n^*} = \overline{\langle m | P | n \rangle}$$

Then, in general, the expectation value of any operator T is

$$\langle T \rangle = \text{Tr}(\rho T) = \sum_m \langle m | \rho T | m \rangle \quad (21)$$

From the Schrödinger equation for the state ψ

$$(-\hbar/i)(\partial\psi/\partial t) = \mathcal{H}\psi = (-\hbar/i) \sum_n (\partial a_n / \partial t) | u_n \rangle$$

with Hamiltonian \mathcal{H} , the density matrix ρ can be seen to satisfy the equation

$$d\rho/dt = (i/\hbar)[\rho, \mathcal{H}] \quad (22)$$

with solution, if \mathcal{H} is not a function of t ,

$$\rho(t) = \exp(-i\mathcal{H}t/\hbar) \rho(0) \exp(i\mathcal{H}t/\hbar) \quad (23)$$

where the $t = 0$ matrix elements can be defined by the Boltzmann factor and therefore,

$$\rho(0) = \exp(-\mathcal{H}_0/k_B T) / \left(\sum_n \exp(-iE_n/k_B T) \right) \quad (24)$$

where $\mathcal{H}|n\rangle = E_n|n\rangle$. For the equilibrium density matrix in the absence of external rf fields

$$\rho(0) \propto \exp\{\hbar(\omega_0 I_z + aI_z^2)/k_B T\}$$

in the presence of Zeeman ($\hbar\omega_0 I_z$) and quadrupole (aI_z^2) Hamiltonians. In the high temperature approximation $k_B T \gg \hbar(\omega_0 I_z + aI_z^2)$, valid for all but the very lowest temperatures ($\sim 10^{-3}$ oK),

$$\rho(0) \sim 1 + (\hbar\omega_0 I_z/k_B T) \quad (25)$$

if $\hbar a I_z^2 \ll \hbar\omega_0 I_z$. The constant term in this expression can be neglected since it will not affect any of the calculated properties.

If $\mathcal{H} = \mathcal{H}_0 + \mathcal{H}_1$, where \mathcal{H}_1 is a function of time, then the equation of motion becomes

$$d\rho^*/dt = (i/\hbar) [\rho^*, \mathcal{H}_1^*(t)] \quad (27)$$

where $\rho(t) = \exp(-i\mathcal{H}_0 t/\hbar) \rho^*(t) \exp(i\mathcal{H}_0 t/\hbar)$

and $\mathcal{H}_1^*(t) = \exp(i\mathcal{H}_0 t/\hbar) \mathcal{H}_1(t) \exp(-i\mathcal{H}_0 t/\hbar)$

Then the time development of $\rho^*(t)$ can be solved by iteration⁴² yielding, to second order in $\mathcal{H}_1^*(t)$,

$$d\rho^*(t)/dt = (i/\hbar) [\rho^*(0), \mathcal{H}_1^*(t)] + (i/\hbar)^2 \int_0^t [[\rho^*(0), \mathcal{H}_1^*(t)], \mathcal{H}_1^*(t')] dt' \quad (28)$$

This approach is very useful in cases where there is a fluctuating internal field, etc.⁴²

3.1 Form of the time development operators

In the case where \mathcal{H} is time-independent the time development operators can be evaluated from the knowledge of the Hamiltonian. In the case of a

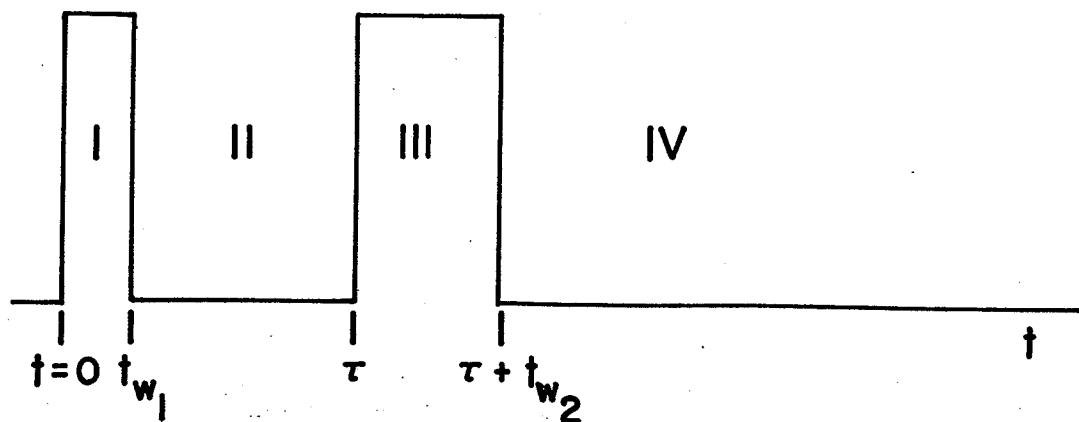


Figure 2. Division of time axis in a two pulse experiment.

two pulse NMR experiment, time can be divided as shown in Figure 2. Before $t = 0$ the spin system is in equilibrium described by the density matrix $\rho(0)$. In region I in the figure, during the first pulse (of length t_{w1} and strength $H_1 = \omega_1/\gamma$), the Hamiltonian, in the frame rotating about the z-axis at a frequency ω' equal to the frequency of the applied rf pulse, is given by

$$\mathcal{H}_I = \hbar(\omega_0 - \omega')I_z + \hbar a I_z^2 + \hbar\omega_1 I_y$$

if the pulse is applied along the y-axis in the rotating frame. Then, with $\Delta\omega = \omega_0 - \omega'$, the time development operator in the first region is

$$U_I = \exp\{-i(\Delta\omega I_z + \omega_1 I_y + a I_z^2) t_{w1}\} \quad (29)$$

and, $\rho_2 = U_I \rho_1 U_I^{-1}$

is the density matrix immediately following the first rf pulse, where $\rho_1 = \hbar\Delta\omega I_z$ is the $t = 0$ density matrix in the rotating frame.

From the expansion

$$U(t) = \exp(-i\mathcal{H}t/\hbar) = \sum_{n=0}^{\infty} \frac{(-i)^n}{n!} \mathcal{H}^n t^n$$

and since $\langle m|\mathcal{H}|m'\rangle = (-1)^{m-m'} \langle m'|\mathcal{H}|m\rangle$ and $\langle -m|\mathcal{H}| -m'\rangle = \langle m'|\mathcal{H}|m\rangle$

whenever $\mathcal{H} \sim$ any of the spin angular momentum operators, by induction, if

$$\langle m | \mathcal{H}^k | m' \rangle = (-1)^{m-m'} \langle m' | \mathcal{H}^k | m \rangle$$

and

$$\langle -m | \mathcal{H}^k | -m' \rangle = \langle m' | \mathcal{H}^k | m \rangle$$

then for $k + 1$,

$$\mathcal{H}^{k+1} = \frac{1}{2}(\mathcal{H}^k \mathcal{H} + \mathcal{H} \mathcal{H}^k)$$

$$\langle m | \mathcal{H}^{k+1} | m' \rangle = (-1)^{m-m'} \langle m' | \frac{1}{2}(\mathcal{H} \mathcal{H}^k + \mathcal{H}^k \mathcal{H}) | m \rangle$$

and

$$\langle -m | \mathcal{H}^{k+1} | -m' \rangle = \langle m' | \frac{1}{2}(\mathcal{H} \mathcal{H}^k + \mathcal{H}^k \mathcal{H}) | m \rangle$$

Thus, in general the operators have the form (shown here for $I = 5/2$)

$$U = \begin{pmatrix} A & B & C & D & E & F \\ -B & G & H & I & J & E \\ C & -H & K & L & I & D \\ -D & I & -L & K & H & C \\ E & -J & I & -H & G & B \\ -F & E & -D & C & -B & A \end{pmatrix} \quad (30)$$

and they have only 12 distinct elements.

In region I, during the first pulse, for nuclei with Larmor frequencies ω_0 such that $\omega_0 - \omega' \ll \omega_1$, and assuming that the quadrupole coupling constant a is small, the first time development operator is given by

$$U_I = \exp(-i\omega_1 t \frac{I_y}{\omega_1}) \quad (31)$$

which represents a rotation¹⁷ about the y-axis through an angle $\omega_1 t \frac{I_y}{\omega_1}$. If the quadrupole coupling constant a is not small compared to ω_1 , the operators can be evaluated iteratively using the identity⁴⁴

$$\exp(\beta A) \exp(-\beta(A+B)) = 1 - \int_0^\beta d\lambda \exp(\lambda A) B \exp(-\lambda(A+B))$$

for the two cases $a < \omega_1$, and $a > \omega_1$. The matrices will still have the form of Equation 30. For the nuclei at the tetrahedral sites in MnFe_2O_4 , there should be no quadrupole splitting and the quadrupole coupling constant a may be neglected. The expressions for the observed signal to be evaluated in this section will be valid in the presence of quadrupole splitting since these expressions only require that the operators have the form of Equation 30.

At a time $t > t_{w_1}$, i.e., in region II in Figure 2, the density matrix is given by

$$\begin{aligned} \rho_3(t) &= U_{\text{II}} \rho_2(t_{w_1}) U_{\text{II}}^{-1} = U_{\text{II}}^{(1)} U_{\text{II}}^{(2)} \rho_2 (U_{\text{II}}^{(2)})^{-1} (U_{\text{II}}^{(1)})^{-1} \\ &= U_{\text{II}}^{(1)} \rho_2' (U_{\text{II}}^{(1)})^{-1} \end{aligned} \quad (32)$$

where,

$$U_{\text{II}} = U_{\text{II}}^{(1)} U_{\text{II}}^{(2)} = \exp\{-i\Delta\omega(t - t_{w_1}) I_z\} \exp\{-ia(t - t_{w_1}) I_z^2\} \quad (33)$$

since $[I_z, I_z^2] = 0$, and the matrix elements of this operator may be immediately evaluated.

During the time interval immediately following the first pulse the spin system is not in equilibrium and the Hamiltonian used in the time-development operator in Equation 33 should contain the terms describing the relaxation of the spin system towards equilibrium. These terms include the Suhl-Nakamura and dipole-dipole interactions, but if their main effect is to cause relaxation, they may be described by a relaxation time T such that the transverse magnetization at a time t following a single rf pulse is given by

$$S_3^*(t) = c_n e^{-t/T} \text{Tr}(I^+ \rho_3) \quad (34)$$

where ρ_3 is given by Equation 32, and c_n is a normalization constant.

3.2 The free induction decay and spin echoes

From the form of the time development operator given in Equation 33 the transverse magnetization, in the rotating frame, following a single rf pulse can be rewritten as

$$S_3^*(t) = c_n e^{-t/T} \exp(ia_3) \text{Tr}(I^+ \rho_2^+) \quad (35)$$

where $a_3 = \Delta\omega(t - t_{w1})$. The trace in this equation can be easily evaluated once the matrix elements of U_I have been determined.

To obtain an expression for the free induction decay we must average Equation 35 over the distribution $g(\omega_s)$ of spins excited by the rf pulse. The function $g(\omega_s)$ will be the product of the lineshape function $f(\omega_o)$ of the inhomogeneously broadened resonance and the rf pulse shape function $h(\omega_s)$. The observed spectrum will then be the convolution⁴⁵ of the two functions $f(\omega_o)$ and $h(\omega_s)$ while the free induction decay and spin echoes at a given spectrometer frequency ω_s will have a shape determined by the product function $g(\omega_s)$. Taking the average over $g'(\omega'_o) = g(\omega_s + \omega'_o)$ and transforming back to the laboratory frame, the free induction decay will be proportional to

$$S_3(t) = \exp\{i\omega_s(t - t_{w1})\} \int_{-\infty}^{\infty} d\omega'_o g'(\omega'_o) \exp\{i\omega'_o(t - t_{w1})\} \\ \times \text{Tr}(I^+ \rho_2^+) \exp(-t/T) c_n \quad (36)$$

Since the functions $f(\omega_o)$ and $h(\omega_s)$, while they may both be symmetric about their central frequencies, have in general different shapes and different central frequencies, the free induction and spin-echo shape

function will, in the case of strong inhomogeneous broadening (when the spread in Larmor frequencies in the sample is much greater than the pulse bandwidth, $\delta\omega_0 \gg \delta\omega_s$), change on varying the spectrometer frequency ω_s through the spectrum described by $f(\omega_0)$.

Defining the shape function by

$$G(t) = \int d\omega'_0 \exp(i\omega'_0 t) g(\omega_s + \omega'_0) \quad (37)$$

the signal following one pulse is

$$S_3(t) = \exp\{i\omega_s(t-t_{w_1})\} \text{Tr}(I^+\rho_2) G(t-t_{w_1}) \exp(-t/T) c_n \quad (38)$$

The signal will thus have a frequency ω_s and, for a symmetric $g(\omega_s)$ (i.e., at $\omega_s = \omega_{00}$), will have a maximum at $t-t_{w_1} = 0$.

If, after allowing the spin system to develop according to Equation 32 until a time $t = \tau_1$, a second rf pulse, of strength ω_2/γ and length t_{w_2} , is applied, the operator U_{III} describing this pulse will be of the same form as U_{I} in Equation 31, namely,

$$U_{\text{III}} = \exp(-i\omega_2 t_{w_2} I_z) \quad (39)$$

assuming that both pulses are applied along the same direction in the rotating frame (for the case of an incoherent pulse spectrometer with all pulses applied at the same point in the cavity this is always true, however, for coherent pulse spectrometers if the phase of the two rf pulses is shifted, a transformation such as that applied in the discussion of Section 4.3 to the case of the effective refocusing pulse due to the first echo must be employed). Again, the more general form given for U_{I} in Equation 29 may be used for U_{III} . The matrix elements of the density operator during the second pulse are

$$(\rho_4)_{ij} = (U_{III} \rho_3 U_{III}^{-1})_{ij} = \sum_k \sum_l (U_{III})_{ik} (U_{III})_{jl}^* (\rho_2)_{kl} \exp(i(k-l)a_3) \quad (40)$$

Then,

$$\text{Tr}(I^+ \rho_4) = \sum_n \sum_m (I^+)_{nm} (\rho_4)_{nm} = \sum_{r=0}^{2I} M_r^{(3)} \exp(ria_3) \quad (41)$$

(r=k-1)

where

$$M_r^{(3)} = \sum_{i=1}^{2I} \sigma_i \sum_k (U_{III})_{i+1,k} (U_{III})_{i,k-r}^* (\rho_2)_{k,k-r} \quad (42)$$

with $\sigma_i = (I^+)_{i,i+1}$, and the sum \sum_k is over k such that $k-r \geq 1$, $k \leq 2I+1$

Following the second pulse,

$$\rho_5 = U_{IV} \rho_4 U_{IV}^{-1}$$

$$\text{with } U_{IV} = \exp\{-i(\Delta\omega I_z + a I_z^2)(t - \tau_1 - t_{w_2})\} = U_{IV}^{(1)} U_{IV}^{(2)} \quad (43)$$

and the response of the spin system will be given by

$$\text{Tr}(I^+ \rho_5) = \exp(ia_5) \text{Tr}(I^+ \rho_4') \quad (44)$$

where $a_5 = \Delta\omega(t - \tau_1 - t_{w_2})$ and $\rho_4' = U_{IV}^{(2)} \rho_4 U_{IV}^{(2)}$, similar to the definition of ρ_2' . The transverse magnetization and the signal in the laboratory frame are then given by

$$S_{(5)}(t) = c_n' \sum_{r=0}^{2I} \exp(i\omega_s(a_5 + ra_3)) M_r^{(3)} G\left(\frac{a_5 + ra_3}{\Delta\omega}\right) e^{-t/T} \eta^2(H_{\text{ext}}) \quad (45)$$

with $M_r^{(3)}$ given by Equation 42 and $G(t)$ defined in Equation 37. The factor $\eta^2(H_{\text{ext}})$ is included to give the field dependence of echo amplitude due to the enhancement mechanisms⁴⁶ discussed in Chapter I, Sections 6 and 7. In the case where the quadrupole constant $a \neq 0$, the $\text{Tr}(I^+ \rho_4')$ will contain terms which depend on time (like e^{iat}).

These modulation terms⁴⁴ do not change the form of $G(t)$ since they do not enter the averaging process.

From Equation 45 it can be seen that in general $2I$ echoes can be observed, occurring at times $(a_5 + ra_3)/\Delta\omega$. These echoes may occur as a result of a quadrupole interaction by the introduction into the operators U_I and U_{III} of non-zero elements more than one position off the diagonal⁴⁴ or by a generalized excitation condition wherein the rf pulses do not represent pure rotations.

For pure rotations in the absence of a quadrupole interaction, the expression in Equation 45 is non-zero only for times near

$$t = \tau_1 + t_{w_2}$$

and

$$t = 2\tau_1 + t_{w_2} - t_{w_1} \quad (46)$$

These mark the occurrence of the free induction decay and first spin-echo following the second pulse.

4. Multiple Echoes

Multiple spin echoes have been observed in various materials and several explanations have been applied to the different cases^{44,47-51}. As shown above for nuclei with $I > \frac{1}{2}$ quadrupole effects can cause as many as $2I$ echoes following a two pulse excitation^{44,47,49}. Also, external processes⁴⁸ requiring the active participation of the resonant cavity can cause a refocusing of the spin and consequently, multiple echoes.

4.1 Observation of multiple echoes in manganese ferrites⁵⁰

In manganese ferrites, as illustrated in Figure 3, the application

ECHO AMPLITUDE (arb. units)

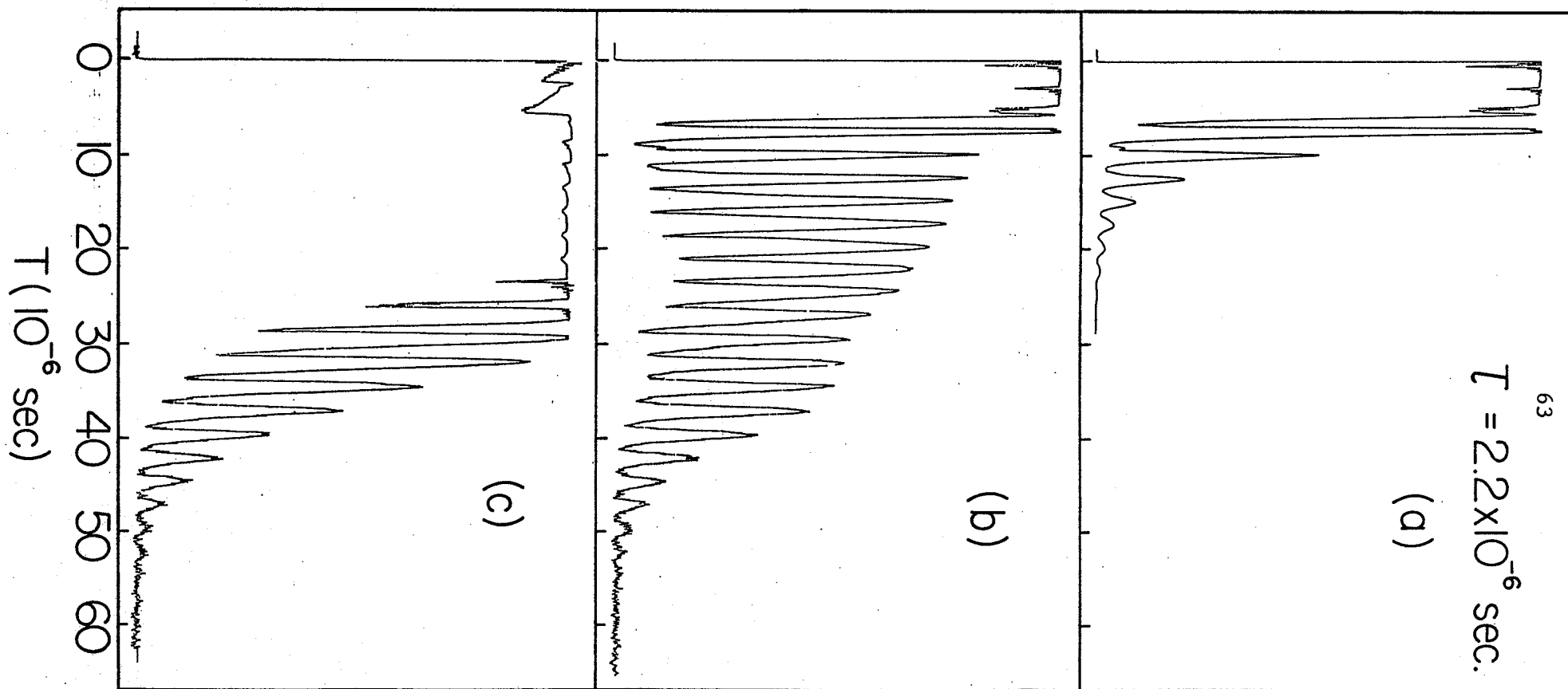


Figure 3. Response of spin system to two rf pulses at $T = 1.6 \text{ }^{\circ}\text{K}$, $H_0 = 0.0 \text{ kOe}$, and $\nu = 587 \text{ MHz}$. a) minimum receiver gain, b) varying gain to exhibit the echoes clearly, c) maximum gain.

of two rf pulses results in a very large number of spin echoes^{50,51}. The number of echoes observed increases rapidly on lowering the temperature of the sample from 4.2 to 1.5 °K due to the increase in relaxation times at lower temperatures. At 1.5 °K more than 20 spin echoes are observed, while from Equation 45 above, for generalized excitation conditions or with quadrupole interactions, only $2I = 5$ echoes are expected. From Figure 3-a it can be seen that the envelope of the multiple echoes is exponential with a decay time of $\sim 4 \mu\text{sec}$ at $\nu = 587 \text{ MHz}$ ⁵⁰.

In Figure 4 this decay rate is plotted as a function of frequency, showing that the refocusing mechanism, whatever its origin, is most efficient at the resonance frequency ($\nu_{00} \approx 587 \text{ MHz}$) of the nuclear spin system. This characteristic frequency dependence suggests that a transverse spin-spin interaction, such as the Suhl-Nakamura interaction, is responsible for the refocusing.

4.2 Stimulation by nuclear spin-spin interaction

The formation of multiple echoes in the present case can be easily visualized if one considers the reaction of a single spin j' to the partial polarization of the rest of the spin system. During the formation of the first echo, spin j' will feel the net nuclear magnetization in the rotating frame. Since this magnetization represents an internal field, nucleus j' will respond to this field in much the same way that it would respond to the application of an rf pulse along the direction of echo formation. The reaction of the spin system will be to refocus again at a time $\Delta t \approx \tau$ after the first echo. This process then continues with ever decreasing amplitude resulting in the multiple refocusing of the spin system.

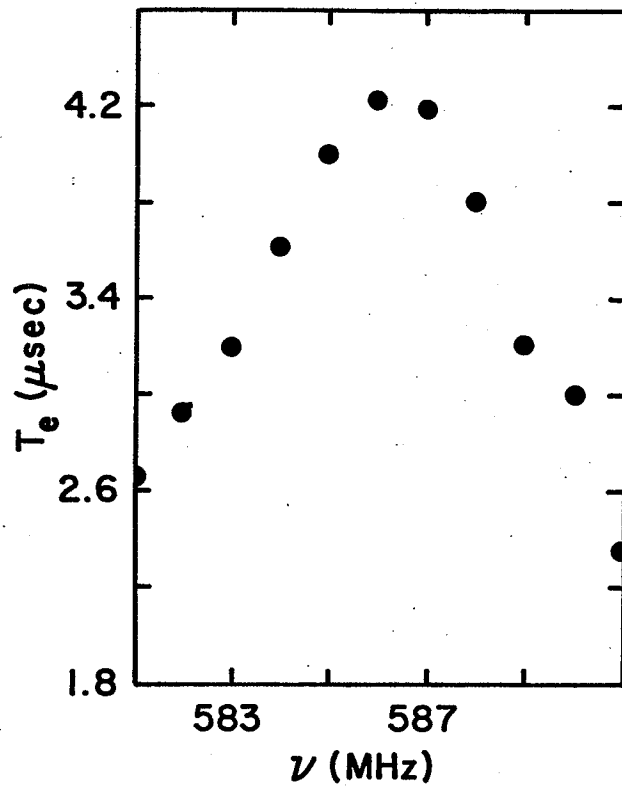


Figure 4. Characteristic time of multiple echo envelope versus frequency.

What is necessary in this process is an interaction between nuclei of sufficient strength to allow repetitive refocusing. The dipole-dipole interaction with its r^{-3} dependence is too weak, but the long-range nature of the Suhl-Nakamura interaction makes it sufficient for multiple echo formation when there is a large abundance of identical spins.

From Equations 14 and 19 the interaction between the transverse components of a spin j' and the rest of the spin system can be written as

$$\mathcal{H}_{S-N}^{j'} = -C \sum_j f(r_{jj'}) (I_j^+ I_{j'}^- + I_j^- I_{j'}^+) \quad (47)$$

where the sum \sum_j is over $j \neq j'$. This interaction can be visualized as an interaction between a magnetic field H_{S-N} and a magnetic moment $\hbar \gamma I_{j'}$. The Hamiltonian can be written as

$$\mathcal{H}_{S-N}^{j'} = -C \left(\left(\sum_j f(r_{jj'}) I_j^+ \right) I_{j'}^- + \left(\sum_j f(r_{jj'}) I_j^- \right) I_{j'}^+ \right) \quad (48)$$

and, when the spin system is in equilibrium, $\sum_j f(r_{jj'}) I_j^\pm = 0$. Following the application of a $\pi/2$ pulse and a π pulse at a time τ_1 later, both along the y-axis, the magnetization in the x-y plane is no longer zero and, therefore, the sums above do not vanish and there will be an interaction between the spins. At a time $t = 2\tau_1 + t_{w_2} - t_{w_1}$ the components of spin in the x-y plane will refocus along the negative x-axis. At this time, neglecting relaxation, $I_j^+ = I_j^x = I_j^-$, and

$$\mathcal{H}_{S-N}^{j'} = -2C \left(\sum_j f(r_{jj'}) I_j^x \right) (I_{j'}^- + I_{j'}^+) \quad (49)$$

or, writing the effective field H_{S-N} as

$$H_{S-N} = (\omega_{S-N}/\gamma) = -4(C/\hbar) \sum_j f(r_{jj'}) I_j^x$$

the interaction takes the form

$$\mathcal{H}_{S-N} = H_{S-N} (\hbar\gamma I_j^x) = \hbar\omega_{S-N} I_j^x,$$

In general, if $g_e(t)$ is the function describing the x-component of nuclear magnetization, i.e., the echo shape function,

$$\mathcal{H}_{S-N} = \hbar g_e(t) \omega_{S-N}^{\max} I_j^x,$$

and the time development operator following the second pulse will be of the form

$$U_{IV} = \exp\{-i(\Delta\omega I_z + a I_z^2)(t - \tau_1 - t_{w_2}) - ig_e(t)\omega_{S-N}^{\max} I_j^x\}, \quad (51)$$

The function $g_e(t)$ has a maximum at $t = 2\tau_1 + t_{w_2} - t_{w_1}$ and is zero for times far from this value. Thus, the spin system sees an effective pulse along the direction of formation of the first echo, in this case, the negative x-axis. This pulse is due to the Suhl-Nakamura interaction and causes the refocusing of the spin-system to form a second echo and is partly responsible for the formation of a third echo.

An upper bound on the strength of this pulse can be estimated from the observed transverse relaxation time assuming that the Suhl-Nakamura interaction is the primary relaxation channel. Then,

$$E_{S-N} T_{S-N} \sim \hbar \quad \text{or} \quad \omega_{S-N} T_{S-N} \sim 1$$

and, for $T_{S-N} \approx 25 \mu\text{sec}$ at $T = 4.2 \text{ }^\circ\text{K}$, $\omega_{S-N} \approx 4 \times 10^4 \text{ (sec)}^{-1}$. If the echo shape function $g_e(t)$ is assumed to be a Gaussian with amplitude h , replacing it by a rectangular pulse of height h with the same area as $g_e(t)$ gives for the turning angle of the effective pulse at $t = 2\tau_1 + t_{w_2} - t_{w_1}$ with $\delta_e \approx 2.8 \times 10^{-7} \text{ sec}$ (the half-width at half-maximum of the

$$\text{echo)} \quad \omega_{S-N}^{\max} h \delta_e \sqrt{(\pi/2 \ln 2)} \eta \approx \eta h \cdot 2.4 \times 10^{-2} \text{ radians} \quad (52)$$

The factor η is the enhancement factor as discussed in Sections I.6 and I.7, which for the single-domain or saturated sample case is ~ 500 .

The height of the echo, h , depends on the absolute magnitude of the re-focused magnetization and is difficult to estimate directly. However,

the data shown in Figure 5 showing

the $t = 0$ amplitudes of the

first four echoes suggest that

the effective pulse must be strong

enough to provide a rotation of

nearly π radians about the x-axis,

since each echo is $\sim 2/3$ the amp-

litude of the preceding echo.

Recall that while the second echo

is due solely to the refocusing

by the first echo, the third and

fourth (and higher) echoes have

contributions from more than one

source. Thus,

$$\eta h \cdot 2.4 \times 10^{-2} \approx 12h \lesssim \pi$$

giving a value of $h \lesssim 1$ as expected since the value for ω_{S-N} determined from the relaxation time should provide a good estimate of the strength of the interaction (with $h = 1$). The data in Table 1, taken in $H_{\text{ext}} = 0$ at $T = 1.5$ °K show quite clearly the frequency dependence expected for a refocusing mechanism depending on the number of spins in the x-y plane, i.e., a transverse spin-spin interaction, as the first echo is far less

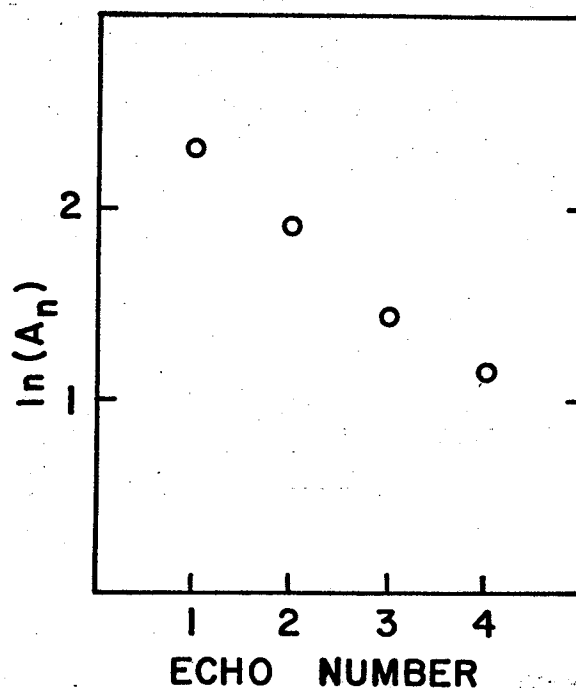


Figure 5. Logarithm of echo amplitude versus echo number at $T=1.5$ °K, $H = 0.0$ kOe, and $\nu=587$ MHz.

Table 1. Frequency dependence of multiple echoes at $T = 1.5^{\circ}\text{K}$ in $H = 0$.
 A_n and T_n are the amplitudes and relaxation times of the n th echo.

ν (MHz)	T_e (μsec)	Echo #	T_n (μsec)	A_n^0 (arb. units)	A_{n+1}/A_n
581.0	2.65	1	140.	0.257	0.25
		2	70.0	0.064	0.22
		3	57.5	0.014	0.21
		4	57.5	0.003	
583.0	3.20	1	100.	0.440	0.35
		2	45.0	0.153	0.32
		3	40.0	0.049	0.37
		4	32.5	0.018	
585.0	4.00	1	40.0	0.816	0.50
		2	24.0	0.405	0.46
		3	22.0	0.187	0.58
		4	17.0	0.108	
587.0	4.20	1	26.0	1.000	0.67
		2	14.0	0.668	0.62
		3	12.0	0.415	0.75
		4	10.0	0.312	
589.0	3.20	1	26.0	0.552	0.53
		2	13.0	0.292	0.49
		3	11.0	0.143	0.81
		4	8.0	0.116	
591.0	2.40	1	45.0	0.210	0.26
		2	24.0	0.054	0.31
		3	16.0	0.017	0.35
		4	12.0	0.006	

effective in refocusing the spins at frequencies far from the central frequency of $\nu = 587$ MHz. (The frequency dependence of the relaxation time will be discussed in Chapters III and IV.)

In this connection it should be noted that near 587 MHz the pulse tuning conditions (pulse widths) required to maximize the first echo are different from those required to maximize the second echo and that for some tuning conditions the third echo is larger than the second echo. These effects are due to the extreme strength of the refocusing mechanism, i.e., the first echo when maximized is apparently equivalent to a pulse whose width is greater than π radians, thus the decrease in second echo amplitude on increasing the first echo.

4.3 Density matrix calculation for the effective pulse⁵¹

Continuing the discussion of Section II.3 by treating the first echo as an rf pulse occurring along the x-axis at a time $t = 2\tau_1 + t_{w_1} - t_{w_1} = \tau_1 + \tau_2$, of strength ω_e and length $t_{w_e} = \delta_e \sqrt{(\pi/2) \ln 2}$. Neglecting $\Delta\omega$ and during the first echo, the operator describing this effective pulse is

$$U_V = D_z(\pi/2) \exp(-i\omega_e t_{w_e} I'_y) D_z(-\pi/2) = D_z(\pi/2) \Theta D_z(-\pi/2) \quad (53)$$

representing a rotation through an angle $\omega_e t_{w_e}$ about the negative x-axis, where the $D_z(\pm\pi/2)$ are rotations of $\pm\pi/2$ radians about the z-axis. The density matrix during this pulse is

$$\rho_6 = U_V \rho_5 U_V^{-1}$$

with $(U_V)_{jk} = \exp(-i(k-j)) \Theta_{jk}$

Then the response of the spin system to this effective pulse is given by

$$\text{Tr}(I^+ \rho_6) = \sum_{r=-2I}^{2I} \sum_{s=-2I}^{2I} M_{r,s}^{(4)} \exp(sia_5) \exp(ria_3) \quad , (54)$$

where as before $a_3 = \Delta\omega(t-t_{w_1})$, $a_5 = \Delta\omega(t-\tau_1-t_{w_2})$, also,

$$M_{+|r|,s}^{(4)} = \sum_{p=1}^{2I+1-|r|} \delta_{p,p+|r|} \sum_{\ell}^{2I} (U_{III})_{p+|r|,\ell+s} (U_{III})_{p,\ell}^* (\rho_2)_{\ell+s,\ell} \quad , (55)$$

and

$$M_{-|r|,s} = \sum_{p=1}^{2I+1-|r|} \delta_{p+|r|,p} \sum_{\ell}^{2I} (U_{III})_{p,\ell+s} (U_{III})_{p+|r|,\ell}^* (\rho_2)_{\ell+s,\ell} \quad , (56)$$

with
$$\delta_{ij} = \sum_{k=1}^{2I} \sigma_k \theta_{k+1,j} \theta_{k,i}^*$$

and, as before, $\sigma_k = (I^+)_{k,k+1}$.

Then following the first echo, at time t , with $\tau_2 = \tau_1 + t_{w_2} - t_{w_1} - \frac{1}{2}t_{w_e}$, the time development operator is

$$U_{VI} = \exp\{-i\Delta\omega(t-\tau_1-\tau_2-t_{w_e})I_z\} \exp\{-ia(t-\tau_1-\tau_2-t_{w_e})I_z^2\} \quad , (57)$$

$$= U_{VI}^{(1)} U_{VI}^{(2)} = \exp(-ia_7 I_z) U_{VI}^{(2)}$$

and, defining
$$\rho_6' = U_{VI}^{(2)} \rho_6 (U_{VI}^{(2)})^{-1}$$

then,
$$\rho_7 = U_{VI}^{(1)} \rho_6' (U_{VI}^{(1)})^{-1}$$

and
$$\text{Tr}(I^+ \rho_7) = \exp(ia_7) \text{Tr}(I^+ \rho_6') \quad , (58)$$

Finally, the observed signal following two external pulses and the first echo will be proportional to

$$S^{(7)}(t) = c_n' \sum_{r=-2I}^{2I} \sum_{s=-2I}^{2I} M_{r,s}^{(4)} \exp\{i\omega_s(a_7+sa_5+ra_3)\} G\left(\frac{a_7+sa_5+ra_3}{\Delta\omega}\right) e^{-t/T} \eta^2 \quad , (59)$$

The factor $\eta^2(H_{\text{ext}})$ is again included to give the field dependence of echo

amplitudes due to enhancement mechanisms. However, due to the dependence of the effective strength of this pulse (given by ω_e), on the amplitude of the first echo, and to the inclusion of the enhancement factor η in Equation 52 for the turning angle of the effective pulse, the second echo amplitude should decrease more strongly with field than the first echo. Figure 6 shows the amplitude of the first two echoes as a function of the effective internal magnetic field $H' = 1/\eta$ for the two temperatures $T = 1.5$ and 4.2 °K. As expected the first echo's amplitude goes roughly as $(1/H')^2$ while the second echo's amplitude varies more nearly like $(1/H')^3$. The higher echoes (echoes 3, 4, etc.) will have more complicated behaviour with field, all falling off more rapidly than $(1/H')^2$.

The expression in Equation 59 for the signal following the first echo can also be applied to the case of a third external pulse applied at a time τ_2 following the second pulse. This method can be applied to the calculation of the spin-system's response to an arbitrary number of rf pulses applied along any axes if transformations such as that used with U_V above are applied.

In general the expression in Equation 59 allows the formation of a large number of echoes, however, the assumption of pure rotations and no quadrupole interaction reduces these allowed echoes to only two, occurring for times

$$t = 2\tau_1 + \tau_2 - t_{w_1} + t_{w_e}$$

and

$$t = 2\tau_1 + 2\tau_2 - t_{w_2} - t_{w_1} + t_{w_e}$$

These are the second and third echoes, respectively. As mentioned earlier, the third echo, which appears here due to the refocusing of the spin system by the first echo, will also receive a contribution due to the refocus-

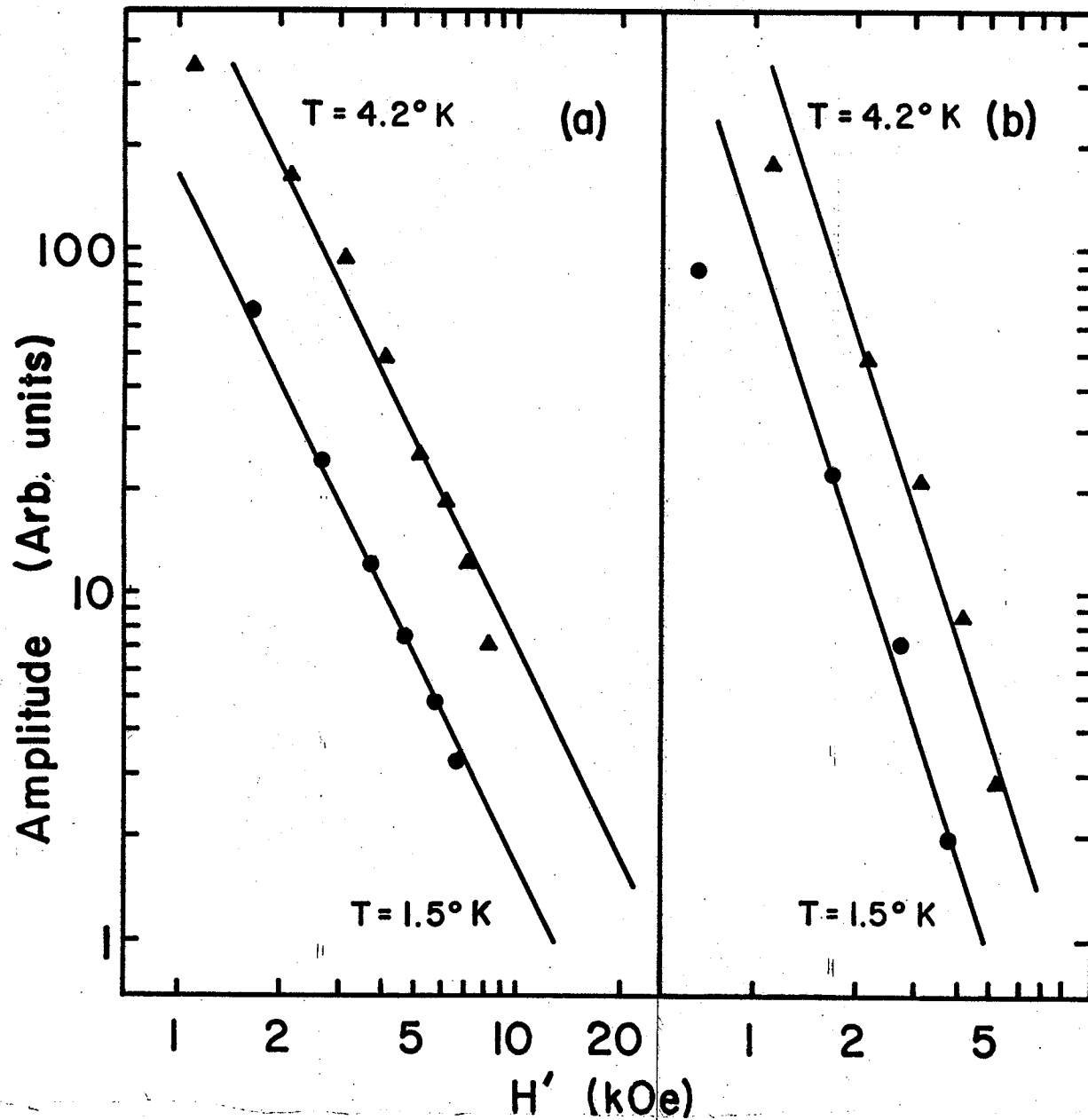


Figure 6. Signal amplitude versus effective internal field, a) first echo, b) second echo.

ing effect of the second echo, and in general all higher numbered echoes will have such multiple contributors. This should explain why the ratios of echo amplitudes (A_{n+1}/A_n) shown in Table 1 do not appear to decrease for higher numbered echoes.

In conclusion it should be mentioned that any material with a large concentration of identical nuclear moments which undergo a strong spin-spin coupling can exhibit the multiple echo phenomenon, for example ^{59}Co resonance in cobalt powders exhibits a similar sequence of echoes in both the fcc and hexagonal cobalt phases. The relaxation processes described in the next chapter will provide further verification of this model of multiple echo formation.

CHAPTER III

Relaxation Processes in Magnetically Ordered Systems

One of the most interesting and informative aspects of magnetic resonance is the process of relaxation. The free precession or pulse techniques discussed in Chapter I are ideally suited to the study of relaxation since they allow, after the initial pulse excitation, the direct observation of the spin system's approach to equilibrium. The form and strength of the various interactions responsible for the relaxation of the spin system can be determined by measuring the relaxation rate over a suitable range of the experimentally controlled variables, such as temperature, frequency, and external magnetic field.

1.1 The approach to equilibrium

The relaxation processes allowing the spin-system to come to equilibrium can be conveniently classified as either spin-lattice or spin-spin processes. In magnetic insulators at low temperatures electronic spin-wave scattering processes provide the most effective spin-lattice mechanism while the nuclear spin-spin relaxation is a result of the nuclear dipole-dipole and the Suhl-Nakamura interactions. The dipole-dipole interaction must be further separated into its transverse (mutual spin flip) and longitudinal parts, while the Suhl-Nakamura interaction is basically transverse (for high density of identical nuclei).

Basically, the experimental measurement, as discussed in Chapter I, of the relaxation times consists of a measurement of echo amplitude as a function of rf pulse separation in a two pulse experiment. The echo

decay envelope if exponential, as it is for the Mn^{2+} resonance in $MnFe_2O_4$ at high fields, can be described by a single relaxation rate ($1/T_{tot}$) which is the sum of the relaxation rates due to each of the different spin interactions. The temperature, frequency, and field dependences of the various interactions make it possible to separate and identify the individual contributions to the total decay rate.

The spin system's approach to equilibrium can be most easily visualized by considering a simple pulse experiment in which a $\pi/2$ pulse is applied perpendicular to the z-axis (the axis of quantization). This pulse rotates a significant part of the nuclear magnetization into the x-y plane. Transverse relaxation then corresponds to a loss of phase coherence of the precessing spins in the plane while longitudinal relaxation corresponds to the return of the nuclear magnetization to the z-axis. The energy absorbed by the spins during the rf pulse must eventually be absorbed by the lattice--in the present case via spin-wave relaxation processes.

1.2 Line broadening

The width of a nuclear resonance line can be due either to homogeneous broadening by interactions between spins or to inhomogeneous broadening by sample inhomogeneities, such as the broad distribution of hyperfine fields common to magnetic materials, or inhomogeneous external fields. Homogeneous broadening is a result of the interactions responsible for the spin relaxation, and the relaxation rate characteristic of a given interaction is a measure of its contribution to the total linewidth. Thus, in the absence of inhomogeneous broadening, the resonance linewidth is given by $\delta\omega \sim 1/T_{tot}$. In the presence

of inhomogeneous broadening⁵², however, the linewidth does not reflect the relaxation effects and other methods, such as the free precession techniques, must be used to measure the relaxation rate. The extreme inhomogeneous broadening in magnetic materials permits the measurement of the frequency dependence of the relaxation rate and, therefore, simplifies the identification of the interactions responsible.

The contributions of the various interactions to the homogeneous linewidth and the relaxation rate can be calculated, at least in principle, by the method of moments⁵³⁻⁵⁵, as outlined in Appendix I, and in the next section.

1.3 The method of moments

The moments of the spectral distribution function in principle give all the information necessary for complete determination of the resonance lineshape. However, higher order moments become increasingly difficult to evaluate and, in practice, one must be satisfied in most cases with the first two even moments, M_2 and M_4 (although the sixth moment for the dipole-dipole interaction has been calculated^{56,57}).

The second moment of the homogeneously broadened resonance line, where \mathcal{H}' is the Hamiltonian describing the interaction responsible for the line broadening, is given by

$$M_2 = - \text{Tr}\{[\mathcal{H}', I_x]^2\} / \text{Tr}\{I_x^2\} \quad (1)$$

and the fourth moment is

$$M_4 = \text{Tr}\{[\mathcal{H}', [\mathcal{H}', I_x]]^2\} / \text{Tr}\{I_x^2\} \quad (2)$$

where I_x is the x-component of the nuclear spin. If the lineshape func-

tion $f(\omega)$ is a Gaussian, the half-width at half-maximum is given by

$$\delta = \sqrt{2 \ln 2} M_2^{\frac{1}{2}} \quad (3)$$

while for a cut-off Lorentzian

$$\delta = \frac{1}{6} \pi \sqrt{3} (M_2^2/M_4)^{\frac{1}{2}} M_2^{\frac{1}{2}} \quad (4)$$

Thus, the ratio (M_2^2/M_4) will indicate which lineshape is more nearly correct (see Appendix I for a more detailed discussion of the moment method). In the next section the moments of the longitudinal part of the dipole-dipole interaction will be discussed, while the treatment of the Suhl-Nakamura and the transverse dipole-dipole interactions will be presented in Section 3.

2. Longitudinal Dipole-Dipole Relaxation

The total dipole-dipole Hamiltonian for the interaction between two nuclei labeled 1 and 2 (from Equations I.18, 19) can be written in the form^{58,59} (using the notation of reference 58)

$$\mathcal{H}_{dd} = \frac{\gamma_1 \gamma_2 \hbar}{3 r_{12}} \{A + B + C + D + E + F\} \quad (5)$$

with

$$\begin{aligned} A &= I_1^z I_2^z (1 - 3 \cos^2 \theta) \\ B &= -\frac{1}{4} \{I_1^+ I_2^- + I_1^- I_2^+\} (1 - 3 \cos^2 \theta) \\ C &= -\frac{3}{2} \{I_1^+ I_2^z + I_1^z I_2^+\} \sin \theta \cos \theta e^{-i\phi} \\ D &= -\frac{3}{2} \{I_1^- I_2^z + I_1^z I_2^-\} \sin \theta \cos \theta e^{i\phi} \\ E &= -\frac{3}{4} I_1^+ I_1^+ \sin^2 \theta e^{-2i\phi} \end{aligned} \quad (6)$$

$$F = -\frac{3}{4} I_1^- I_2^- \sin^2 \theta e^{2i\phi}$$

where r_{12} , θ , ϕ are the usual spherical polar coordinates, r_{12} joining nuclei 1 and 2.

The term A represents the longitudinal interaction between the two nuclei (not necessarily identical), while the B term is the transverse or spin-flip part of the dipole-dipole interaction which is effective only for nuclei whose Larmor frequencies are close together (within an energy \sim the dipole-dipole interaction energy). Thus, the B term is an interaction between what can be called identical nuclei, much like the Suhl-Nakamura interaction, and will be considered in the next section. The remaining terms, C - F, do not conserve energy in zeroth order and will not be considered in the moment analysis. These terms however can be of importance when considering higher order processes, in particular, spin-wave scattering, and will be discussed in this connection in Section 4. (See reference 59 for a discussion of the physical significance of these terms.)

The second moment of the longitudinal part of \mathcal{H}_{dd} is the sum of two contributions, from like nuclei and from unlike nuclei. In the present case this means first a contribution from the Mn^{2+} nuclei on the A-sites and secondly, contributions from $^{57}Fe^{3+}$ ions on the A- and B-sites as well as Mn^{3+} nuclei on the B-sites. Since we are dealing only with term A in this section, all of these contributions to the second moment have the same form. The commutator $[\mathcal{H}', I_x]$ in Equation 1 is, summing over j, k

$$\begin{aligned} [\mathcal{H}', I_x] &= \gamma_1 \gamma_2 \hbar \sum_{j < k} \frac{1}{r_{jk}^3} (1 - 3\cos^2 \theta_{jk}) [I_j^z I_k^z, \sum_{\ell} I_{\ell}^x] \\ &= i\gamma_1 \gamma_2 \hbar \sum_{j < k} \left(\frac{1 - 3\cos^2 \theta_{jk}}{r_{jk}^3} \right) (I_j^z I_k^y + I_k^z I_j^y) \end{aligned} \quad (7)$$

and the second moment for nuclei of type 1 ⁵⁴ interacting with nuclei of type 2 is given by

$$M_2(1,2) = \frac{1}{3} \gamma_1^2 \gamma_2^2 I_2(I_2 + 1) \hbar^2 \sum_k \left(\frac{1 - 3\cos^2\theta_{jk}}{r_{jk}^3} \right)^2 \quad (8)$$

where the sum \sum_k is over nuclei of type 2. Then, the total longitudinal second moment can be written

$$M_2 = M_2(\text{Mn}^A, \text{Mn}^A) + M_2(\text{Mn}^A, \text{Fe}^A) + M_2(\text{Mn}^A, \text{Mn}^B) + M_2(\text{Mn}^A, \text{Fe}^B) = M_2^A + M_2^B$$

the superscripts A, B signifying the sublattice the nuclei belong to.

The separate sublattice contributions are

$$M_2^A = \frac{1}{3} \gamma_{\text{Mn}}^2 \hbar^2 (C_{\text{Mn}}^A \gamma_{\text{Mn}}^2 (35/4) + C_{\text{Fe}}^A \gamma_{\text{Fe}}^2 (3/4)) \sum_k^A \left\{ (1 - 3\cos^2\theta_{jk}) / r_{jk}^3 \right\}^2, \quad (9)$$

and

$$M_2^B = \frac{1}{3} \gamma_{\text{Mn}}^2 \hbar^2 (C_{\text{Mn}}^B \gamma_{\text{Mn}}^2 (35/4) + C_{\text{Fe}}^B \gamma_{\text{Fe}}^2 (3/4)) \sum_k^B \left\{ (1 - 3\cos^2\theta_{jk}) / r_{jk}^3 \right\}^2$$

where now the sums are over all nuclei on the individual sublattices and $C_{\text{Mn}}^{A,B}$ is the manganese concentration on the A, B sublattice while $C_{\text{Fe}}^{A,B}$ is the ⁵⁷Fe concentration on the respective sublattices. These sums may be easily carried out on a computer since, because of the $(1/r^3)^2$ behaviour, they converge quite rapidly. The results for MnFe_2O_4 are

$$M_2^A = 2.31 \times 10^7 \quad (\text{sec})^{-2}, \quad M_2^B = 0.57 \times 10^7 \quad (\text{sec})^{-2}$$

$$M_2 = 2.88 \times 10^7 \quad (\text{sec})^{-2}$$

This total second moment, assuming a Gaussian lineshape, corresponds to a relaxation rate

$$1/T_{\text{dfl}} = \sqrt{2\ln 2} M_2^{1/2} \approx 6.32 \times 10^3 \quad (\text{sec})^{-1} \quad (10)$$

or $T_{d\ell} \approx 158 \text{ } \mu\text{sec}$

For a more nearly Lorentzian lineshape, the fourth moment must be calculated and used as in Equation 4, and the resonance linewidth will appear narrower than that estimated from the second moment alone. Thus, the result in Equation 10 is an upper limit on the linewidth due to the longitudinal dipole-dipole interaction and the value of $T_{d\ell}$ given is the lower bound for the relaxation time. Since this time is already much longer than the total relaxation time observed near resonance, over the entire field and temperature range, it will be sufficient to neglect the contribution of this interaction to the total relaxation rate except in including it as a frequency independent background relaxation process whose magnitude can be obtained from the experimental data. Because of this the fourth moment need not be calculated.

A proper treatment of the dipole-dipole relaxation processes requires the calculation of the second and fourth moments of the total dipole-dipole Hamiltonian including the frequency dependent behaviour of the transverse part of the interaction⁶⁰. In fact, the Suhl-Nakamura and dipole-dipole interactions should also be treated at the same time to avoid dropping the cross terms since, e.g.,

$$M_2^{\text{tot}} = M_2^{\text{S-N}} + M_2^{\text{dd}} - 2 \frac{\text{Tr}\{\mathcal{H}_{\text{S-N}, I_x} \mathcal{H}_{\text{dd}, I_x}\}}{\text{Tr}\{I_x^2\}} \quad (11)$$

These points will be discussed further in the next section.

3. Suhl-Nakamura and Transverse Dipole-Dipole Relaxation

The Suhl-Nakamura interaction

$$\mathcal{H}_{\text{S-N}} = -\frac{1}{2} A^2 S_A \sum_{j \neq j'} B_{jj'} (I_j^+ I_{j'}^- + I_j^- I_{j'}^+) \quad (12)$$

and the transverse dipole-dipole interaction

$$\mathcal{H}_{td} = \gamma^2 \hbar \sum_{j \neq j'} d_{jj'} (I_j^+ I_{j'}^- + I_j^- I_{j'}^+) \quad (13)$$

have the same general form and can be treated in the same manner, except as outlined at the end of the last section. The second and fourth moments of this "spin-flip" form of interaction have been calculated, for the case of a strictly homogeneously broadened line, by Van Vleck⁵³. The second moment, where $V_{jj'}$, can be either $-\frac{1}{2} A^2 S_A B_{jj'}$, or $\gamma^2 \hbar d_{jj'}$, is

$$M_2^h = \frac{1}{3} I(I+1) \sum_{j'}' V_{jj'}^2 \quad (14)$$

where the sum is over spins $j' \neq j$ and the superscript h identifies this as the second moment of the homogeneously broadened line. The prime on the summation symbol is to indicate that for spin-flip terms the sums are over identical nuclei only. In the case of an inhomogeneously broadened line the definition of "identical" spins must be modified⁶¹ to include all those identical nuclei whose Larmor frequencies, ω_i and ω_j for nuclei i and j , are such that $|(\omega_i - \omega_j)| < |V_{ij}|$. For strong inhomogeneous broadening, $\delta \gg (M_2^{S-N})^{1/2}$, where δ is the half-width of the resonance line, the probability that spin j has a Larmor frequency within $|V_{ij}|$ of ω_i is $g(\omega_i) |V_{ij}|$. Figure 1 illustrates the essential features of this model. Here, the fraction of spins within $\pm \Delta$ of ω_j is approximately $g(\omega_j) \cdot \Delta$. Thus, if the homogeneous Suhl-Nakamura linewidth, Δ , is much less than the inhomogeneous linewidth, δ , $|B_{jk}| \Delta \sim 1$ and only spins with Larmor frequencies such that $|\omega_j - \omega_k| \leq |B_{jk}|$ can interact. Then in sums of the form

$$\sum_{j,k} B_{jk}^2 = N \sum_k B_{jk}^2$$

the final sum, over k , should be weighted by the probability that nuclei j and k can interact. Thus, in calculating the second moment in Equation 14, one makes the replacement

$$\sum_j v_{ij}^2 \rightarrow \sum_j v_{ij}^2 v_{ij} g(\omega_i)$$

For the Suhl-Nakamura interaction

$$M_2^i = \frac{1}{3} I(I+1) g(\omega) \left(\frac{1}{2} A^2 S_A\right)^3 \sum_j B_{ij}^3, \quad (15)$$

since B_{ij} is non-negative, here the i superscript indicates that this is for an inhomogeneously broadened line.

The dipole-dipole interaction can be treated similarly, however, because it is composed of two parts which behave differently, the Hamiltonian is written as

$$\begin{aligned} \mathcal{H}_{dd} &= \mathcal{H}_{ld} + \mathcal{H}_{td} \\ &= \gamma^2 \hbar \sum_{j \neq k} \sum d_{jk} I_j^z I_k^z + \frac{1}{2} \gamma^2 \hbar \sum_{j \neq k} \sum d'_{jk} (I_j^z I_k^z - \vec{I}_j \cdot \vec{I}_k) \end{aligned} \quad (16)$$

where d'_{jk} has the same form as d_{jk} , the prime indicating that the interaction is between like nuclei. Then, since

$$\text{Tr}\{[\mathcal{H}_{dd}, I_x]^2\} = \text{Tr}\{[\mathcal{H}_{ld}, I_x]^2\} + \text{Tr}\{[\mathcal{H}_{td}, I_x]^2\} + 2\text{Tr}\{[\mathcal{H}_{ld}, I_x][\mathcal{H}_{td}, I_x]\}$$

the second moment of the dipole-dipole interaction can be written as

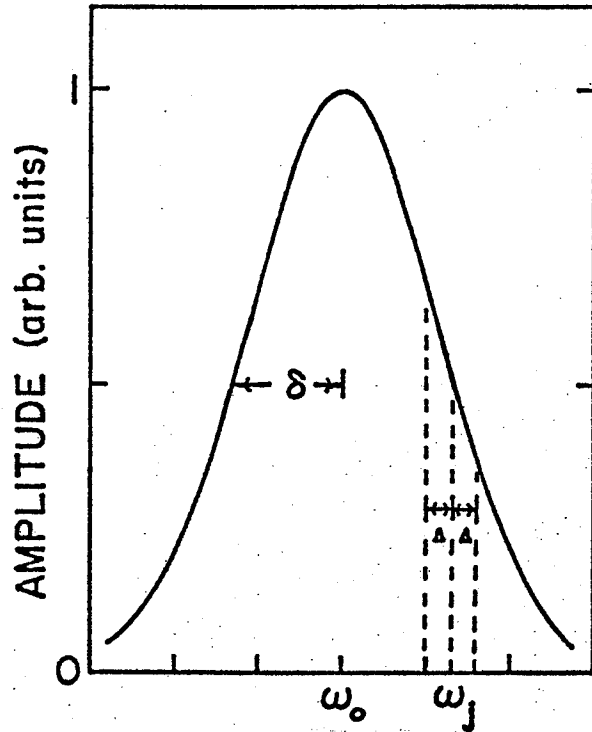


Figure 1. Inhomogeneously broadened resonance line with half-width δ compared to S-N interaction strength Δ .

$$M_2^i = \frac{1}{3} I(I+1) \sum_k d_{jk}^2 + \frac{1}{12} I(I+1) \sum_k d_{jk}^{\prime 2} + \frac{1}{3} I(I+1) \sum_k d_{jk} d_{jk}' \quad , (17)$$

where the sums are over all $k \neq j$, while d_{jk}' indicates that for nucleus j only those k nuclei within the range $|\omega_j - \omega_k| \leq |d_{jk}|$ will interact. In the limiting cases of unlike spin broadening (strictly longitudinal coupling) and strictly homogeneous broadening, Equation 17 gives the expected results⁵⁴. Again, since the probability that spin k has Larmor frequency ω_k within this range is $|d_{jk}|g(\omega_j)$, the total second moment is given by

$$\begin{aligned} M_2^i &= \frac{1}{3} I(I+1) \sum_k d_{jk}^2 + \frac{1}{12} I(I+1) g(\omega) \sum_k d_{jk}^2 |d_{jk}| \\ &\quad + \frac{1}{3} I(I+1) g(\omega) \sum_k d_{jk}^2 |d_{jk}| \\ &= M_2^l + \frac{5}{12} I(I+1) g(\omega) \sum_k d_{jk}^2 |d_{jk}| \end{aligned} \quad (18)$$

where M_2^l is the longitudinal second moment discussed in the previous section.

As mentioned earlier, the Suhl-Nakamura and dipole-dipole contributions to the total second moment should not be treated separately. However, in the present case the Suhl-Nakamura relaxation is far stronger near resonance than the dipole-dipole relaxation is, while far from resonance, only the longitudinal dipole-dipole term needs to be retained.

The treatment of the fourth moment is considerably more involved. For an interaction of the form $B_{jk} (I_j^+ I_k^- + I_j^- I_k^+)$ the normal fourth moment, in the absence of inhomogeneous broadening is^{61,62}

$$M_4^h = \left\{ \frac{1}{3} I(I+1) \right\}^2 \left\{ 5 \left(\sum'_k B_{jk}^2 \right)^2 - 2 \sum''_{k,l} B_{jk}^2 B_{kl} B_{lj} \right. \\ \left. + 3 \sum'_k B_{jk}^4 \left(1 - \frac{1}{2I(I+1)} \right) \right\} \quad (19)$$

where \sum'_k is the sum over $k \neq j$, and $\sum''_{k,l}$ is a double sum with $j \neq k$, and $k \neq l$. The fourth moment for the total dipole-dipole interaction ($\mathcal{H}_{dl} + \mathcal{H}_{dt}$) is^{63,54}, in the absence of inhomogeneous broadening

$$M_4^h = \left\{ \frac{1}{3} I(I+1) \right\}^2 \left\{ 3 \left(\sum'_k d_{jk}^2 \right)^2 - \frac{1}{3} \sum''_{k,l} d_{kl}^2 (d_{jk} - d_{jl})^2 \right. \\ \left. - \frac{1}{5} \left(8 + \frac{3}{2I(I+1)} \right) \sum'_k d_{jk}^4 \right\} \quad (20)$$

where there is assumed to be only one spin species (for the case of two spin species, see Van Vleck⁵³ and Abragam⁵⁴). In the presence of strong inhomogeneous broadening, the expression for the fourth moment given in Equation 19 must be modified to include only those nuclei within the bandwidth $\pm |B_{jk}|$. Since

$$\left(\sum'_k B_{jk}^2 \right)^2 = \sum''_{k,l} B_{jk}^2 B_{jl}^2 + \sum'_k B_{jk}^4 \quad (21)$$

transforming to the inhomogeneous model⁶¹

$$\sum'_k B_{jk}^4 \rightarrow g(\omega) \sum'_k B_{jk}^5 \quad (22)$$

$$\sum''_{k,l} B_{jk}^2 B_{jl}^2 \rightarrow (g(\omega))^2 \sum''_{k,l} B_{jk}^3 B_{jl}^3 \\ = (g(\omega))^2 \left\{ \left(\sum'_k B_{jk}^3 \right)^2 - \sum'_k B_{jk}^6 \right\} \quad (23)$$

yields

$$\left(\sum'_k B_{jk}^2 \right)^2 \rightarrow (g(\omega))^2 \left(\sum'_k B_{jk}^3 \right)^2 + g(\omega) \sum'_k B_{jk}^5 - (g(\omega))^2 \sum'_k B_{jk}^6, \quad (24)$$

Similarly,

$$\sum_{k,l}'' B_{jk}^2 B_{kl}^2 B_{lj}^2 \rightarrow (g(\omega))^2 \sum_{k,l}'' B_{jk}^2 B_{kl}^2 B_{lj}^2 \quad (25)$$

Thus, the fourth moment is now given by

$$\begin{aligned} M_4^i(\omega) = & \left\{ \frac{1}{3} I(I+1) \right\}^2 \left\{ 5 \left(g(\omega) \sum_k' B_{jk}^3 \right)^2 - 2 g^2(\omega) \sum_{k,l}'' B_{jk}^2 B_{kl}^2 B_{lj}^2 \right. \\ & \left. - 5 g^2(\omega) \sum_k' B_{jk}^6 + g(\omega) \left(8 - \frac{3}{2I(I+1)} \right) \sum_k' B_{jk}^5 \right\} \end{aligned} \quad (26)$$

The ratio M_4^i/M_2^{i2} is

$$\begin{aligned} \frac{M_4^i}{(M_2^i)^2} &= 5 - 2 \frac{\sum_{k,l}'' B_{jk}^2 B_{kl}^2 B_{lj}^2}{\left(\sum_k' B_{jk}^2 \right)^2} + \frac{1}{g(\omega)} \left(8 - \frac{3}{2I(I+1)} \right) \frac{\sum_k' B_{jk}^5}{\left(\sum_k' B_{jk}^3 \right)^2} \\ &= \Gamma + \left(\frac{1}{g(\omega)} \right) \left(8 - \frac{3}{2I(I+1)} \right) \frac{\sum_k' B_{jk}^5}{\left(\sum_k' B_{jk}^3 \right)^2} \end{aligned} \quad (27)$$

where $-1 < \Gamma < 5$ ⁶¹. Then, neglecting Γ in the limit of strong inhomogeneous broadening ($M_4^i \gg (M_2^i)^2$), the Suhl-Nakamura relaxation rate is

$$\left(\frac{1}{T} \right)_{S-N} = \frac{1}{6} \pi \sqrt{3} g(\omega) \left\{ \frac{1}{3} I(I+1) \right\}^{1/2} \left(\frac{\left(\sum_k' B_{jk}^3 \right)^{3/2}}{\left(\sum_k' B_{jk}^5 \right)^{1/2}} \right) \left\{ 8 - \frac{3}{2I(I+1)} \right\}^{-1/2} \quad (28)$$

The transverse part of the dipole-dipole interaction will give an identical expression with B_{jk} representing \mathcal{H}_{dt} . Hone, et al.⁶¹ included the total dipole-dipole interaction under the assumption of interactions only between nuclei with $|\omega_j - \omega_k| \leq |d_{jk}|$, finding an expression, analagous to the above, giving

$$\left(\frac{1}{T}\right)_{dd} = \frac{1}{6} \pi \sqrt{3} g(\omega) \left\{ \frac{1}{3} I(I+1) \right\}^{1/2} \left(\frac{\left(\sum_k |d_{jk}|^3 \right)^{3/2}}{\left(\sum_k |d_{jk}|^5 \right)^{1/2}} \right) \left\{ 1.4 - \frac{0.3}{I(I+1)} \right\}^{-1/2}, \quad (29)$$

This equation is at best useful only as an order of magnitude estimate of the strength of the dipole-dipole relaxation rate. A more useful expression, derived by Barak, et al.⁶⁰ is obtained if one writes an effective dipole-dipole interaction as

$$\mathcal{H}_{dd}^{eff} = \sum_{j < k} d_{jk} \left\{ \frac{2}{3} I_j^z I_k^z - C \left(\frac{1}{6} I_j^+ I_k^- + \frac{1}{6} I_j^- I_k^+ \right) \right\}, \quad (30)$$

where C is the average fraction of spins which interact via the spin-flip terms. This gives

$$M_2^C = \left(\frac{2+C}{3} \right)^2 M_2^{dd} \quad (31)$$

where M_2^{dd} is the normal dipole-dipole second moment, and, for the fourth moment,

$$\begin{aligned} M_4^C = & 3(M_2^C)^2 - \left\{ \frac{C}{3N} \left(\frac{4-C}{3} \right) \left(\frac{2+C}{3} \right)^2 \sum_{j,k,l} d_{jk}^2 (d_{kl} - d_{jl})^2 \right. \\ & + \frac{1}{5} \left(\frac{2+C}{3} \right)^2 \left\{ 8 \left(\frac{1+2C}{3} \right) + \frac{3}{2I(I+1)} \left(\frac{8-4C+5C^2}{9} \right) \right\} \\ & \left. \times \sum_{j,k} d_{jk}^4 \right\} \left\{ \frac{1}{3} I(I+1) \right\}^2 \end{aligned} \quad (32)$$

where the constant C depends on frequency. In the limit as $C \rightarrow 1$ this reduces to the usual expression for M_4^h . When $C = 0$, this expression gives the fourth moment for longitudinal dipole coupling only. In the presence of more than one nuclear spin species, as with ^{57}Fe and $^{55}\text{Mn}^{A,B}$ in MnFe_2O_4 , this expression must again be modified⁵³. This, unfortunately, has not been carried out. For manganese ferrites, however, the

estimates for the strengths of the dipole-dipole and Suhl-Nakamura relaxation rates suggest that such a detailed calculation is not necessary. Section 5 discusses the agreement of these relaxation rate calculations with the relaxation time data showing that the model of a frequency dependent Suhl-Nakamura relaxation rate superimposed on a frequency independent background rate is sufficient to explain the observations.

4. Spin-Wave Scattering Processes

The energy absorbed by the nuclear spin system in a nuclear magnetic resonance experiment must eventually be channeled to the lattice via spin-lattice relaxation processes. In ordered magnetic materials the most efficient spin-lattice relaxation mechanism is the scattering of electronic spin-waves via the hyperfine interaction. In Chapter II the hyperfine interaction for Mn^{2+} nuclei on the A-sites was expanded to third order in spin-deviation creation and annihilation operators

$$\begin{aligned}
 \mathcal{H}_{hf} = & -AS_A \sum_n I_n^z + \frac{1}{2} A(2S_A)^{\frac{1}{2}} \sum_k (I_k^+ a_k + I_k^- a_k^+) \\
 & + \frac{A}{N_A} \sum_n \sum_{k_1, k_2} I_n^z \exp\{i(\vec{k}_1 - \vec{k}_2) \cdot \vec{r}_n\} a_{k_1}^+ a_{k_2} \\
 & - \frac{1}{2} A(2S_A)^{\frac{1}{2}} \left(\frac{1}{4N_A^{3/2} S_A} \right) \sum_n \sum_{k_1, k_2, k_3} \{ I_n^+ \exp\{i(\vec{k}_1 + \vec{k}_2 - \vec{k}_3) \cdot \vec{r}_n\} \\
 & \times a_{k_1}^+ a_{k_2}^+ a_{k_3} + I_n^- \exp\{-i(\vec{k}_1 + \vec{k}_2 - \vec{k}_3) \cdot \vec{r}_n\} a_{k_1}^+ a_{k_2}^+ a_{k_3} \}
 \end{aligned} \tag{33}$$

where A is the isotropic hyperfine coupling constant and

$$I_k^\pm = (N_A)^{-\frac{1}{2}} \sum_n I_n^\pm \exp(\pm i\vec{k} \cdot \vec{r}_n)$$

From the form of this expansion one expects, for the n th order term in the expansion, relaxation processes involving the scattering of n spin-waves, subject to the restrictions of conservation of energy and spin angular momentum.

The zero-magnon term can be ignored in a discussion of relaxation processes, while the one-magnon term corresponds to the processes illustrated in Figure 2, where a nuclear spin-flip, designated by the symbol \otimes , is accompanied by the absorption, or emission, of an electronic spin wave. This "direct" process can be neglected because of the large difference between the energy required to create a spin wave and that necessary to flip a nuclear spin ($\hbar\omega_{\vec{k}} \gg \hbar\omega_L$, ω_L the nuclear Larmor frequency).

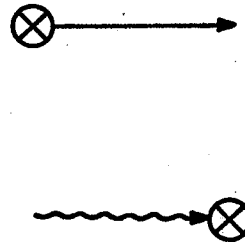


Figure 2. The direct spin-wave process. \otimes represents a nuclear spin-flip, while the arrows represent the magnons.

The two-magnon term in the expansion corresponds to a scattering process in which a spin-wave of wave vector \vec{k}_1 is annihilated, a nuclear spin is flipped, and a spin-wave of wave vector \vec{k}_2 is created. This Raman scattering process is energetically allowed, ($\hbar\omega_{\vec{k}_1} - \hbar\omega_{\vec{k}_2} = \hbar\omega_L$) however, since spin angular momentum cannot be conserved in a system where the electronic and nuclear spin quantization axes are colinear (for the case of an isotropic hyperfine interaction)⁶⁴, for the A-site ⁵⁵Mn resonance in MnFe_2O_4 this process is forbidden and may be neglected.

The three-magnon term in the expansion of the hyperfine interaction, corresponding to a process of the type illustrated in Figure 4, describes a process where both energy and angular momentum can be conserved, $\hbar\omega_{\vec{k}_1} - \hbar\omega_{\vec{k}_2} - \hbar\omega_{\vec{k}_3} = \hbar\omega_L$. This is the lowest order term which can contribute to the spin-lattice relaxation in this system.

4.1 Three-magnon relaxation

The three-magnon term in the expansion of the hyperfine interaction

is given in terms of the spin-wave normal mode operators α_k^+ , α_k , β_k^+ , β_k where

$$\alpha_k = v_k a_k^+ + u_k b_k$$

and

$$\beta_k = u_k a_k + v_k b_k^+$$

as given in Equation II-9. This Hamiltonian includes many processes of the type shown in Figure 4, several of which are not allowed; for example, the terms requiring the simultaneous creation (or annihilation) of all three magnons. The different allowed processes are illustrated in Figure 5 where the wiggly arrows correspond to β -mode magnons and the straight arrows to α -mode magnons, while at the vertex of each process there occurs a nuclear spin flip. Thus, there are only four three-magnon processes which conserve both energy and angular momentum⁶⁵.

With these restrictions the three-magnon Hamiltonian reduces to

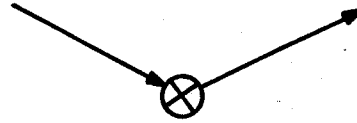


Figure 3. Raman scattering process.

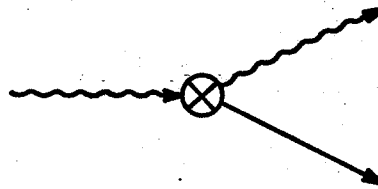


Figure 4. Three-magnon scattering.

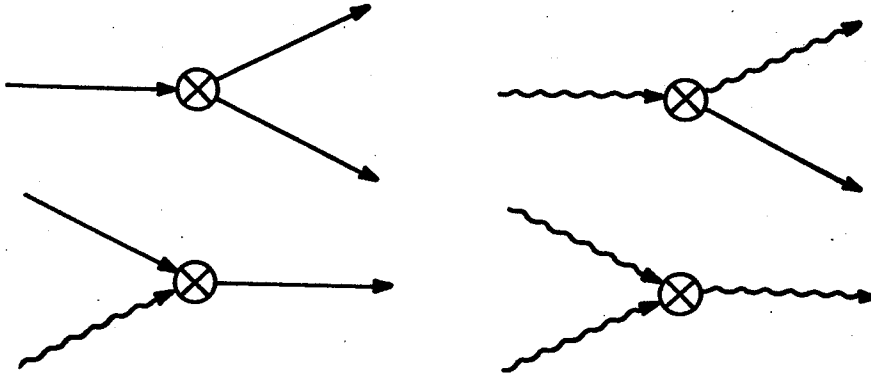


Figure 5. The allowed three-magnon processes

$$\begin{aligned}
 \mathcal{H}^{(3)} &= (2S_A)^{\frac{1}{2}} \left(\frac{A}{8N_A^{3/2} S_A} \right) \sum_n \sum_{k_1, k_2, k_3} \exp\{i(\vec{k}_1 + \vec{k}_2 - \vec{k}_3) \cdot \vec{r}_n\} \\
 &\times I_n^+ \{ -v_1 v_2 v_3 \alpha_1^+ \alpha_2^+ \alpha_3 + u_1 v_2 v_3 \beta_1 \alpha_2^+ \alpha_3 + v_1 u_2 v_3 \alpha_1^+ \beta_2 \alpha_3 \\
 &- v_1 u_2 u_3 \alpha_1^+ \beta_2 \beta_3^+ - u_1 v_2 u_3 \beta_1 \alpha_2^+ \beta_3^+ + u_1 u_2 u_3 \beta_1 \beta_2 \beta_3^+ \} \\
 &= (2S_A)^{\frac{1}{2}} \left(\frac{A}{8N_A^{3/2} S_A} \right) \sum_n \sum_{k_1, k_2, k_3} \exp\{i(\vec{k}_1 + \vec{k}_2 - \vec{k}_3) \cdot \vec{r}_n\} \\
 &\times I_n^+ \{ -v_1 v_2 v_3 \alpha_1^+ \alpha_2^+ \alpha_3 + 2 u_1 v_2 v_3 \beta_1 \alpha_2^+ \alpha_3 - 2 v_1 u_2 u_3 \alpha_1^+ \beta_2 \beta_3^+ \\
 &\quad + u_1 u_2 u_3 \beta_1 \beta_2 \beta_3^+ \}
 \end{aligned} \tag{35}$$

This perturbing Hamiltonian induces transitions between nuclear spin states causing the relaxation of the nuclear magnetization towards its equilibrium value. The probability of inducing a transition from a state with nuclear azimuthal quantum number m to one with quantum number $m+1$ is

$$W = \frac{(2\pi)}{\hbar} \sum_f |\langle f | \mathcal{H}^{(3)} | i \rangle|^2 \delta(E_f - E_i) \tag{36}$$

and the relaxation rate for this process is

$$\left(\frac{1}{T}\right)_{3m} = 2W/(I-m)(I+m+1) \quad (37)$$

yielding finally as the total three-magnon relaxation rate

$$\begin{aligned} \left(\frac{1}{T}\right)_{3m} = & \left(\frac{2\pi}{\hbar}\right) \left(\frac{A^2}{16N_A^3 S_A}\right) \sum_{k_1, k_2, k_3} \{ (v_1 v_2 v_3)^2 (n_{k_1}^\alpha + 1) (n_{k_2}^\alpha + 1) n_{k_3}^\alpha \\ & + 4(u_1 v_2 v_3)^2 n_{k_1}^\beta (n_{k_2}^\alpha + 1) n_{k_3}^\alpha + 4(v_1 u_2 u_3)^2 (n_{k_1}^\alpha + 1) n_{k_2}^\beta (n_{k_3}^\beta + 1) \\ & + (u_1 u_2 u_3)^2 n_{k_1}^\beta n_{k_2}^\beta (n_{k_3}^\beta + 1) \} \delta(\hbar\omega_3 - \hbar\omega_2 - \hbar\omega_1) \end{aligned} \quad (38)$$

where,

$$n_k^\alpha = \frac{1}{\exp(\beta\hbar\omega_k^\alpha) - 1}, \quad n_k^\beta = \frac{1}{\exp(\beta\hbar\omega_k^\beta) - 1}$$

At low temperatures, since the ferrimagnetic optical or β -mode spin-wave branch of the spectrum is at much higher energy than the α -mode branch, it may be assumed that $n_k^\beta \approx 0$. This leaves the first term in Equation 38, which is identical to the result obtained for a ferromagnet^{64,66}.

Thus, the relaxation rate is given by

$$\begin{aligned} \left(\frac{1}{T}\right)_{3m} = & \left(\frac{2\pi}{\hbar}\right) \left(\frac{A^2}{16N_A^3 S_A}\right) \sum_{k_1, k_2, k_3} (v_1 v_2 v_3)^2 (n_{k_1}^\alpha + 1) (n_{k_2}^\alpha + 1) n_{k_3}^\alpha \\ & \times \delta(\hbar\omega_{k_3} - \hbar\omega_{k_2} - \hbar\omega_{k_1}) \end{aligned} \quad (39)$$

The triple sum in this expression can be transformed into a triple integral, yielding in the small-k approximation with $v_i \approx \frac{1}{2} S_A / (S_B - \frac{1}{2} S_A)$,

$$\left(\frac{1}{T}\right)_{3m} = \left(\frac{2\pi}{\hbar}\right) \left(\frac{A^2}{16N_A^3 S_A}\right) \left(\frac{\frac{1}{2} S_A}{S_B - \frac{1}{2} S_A}\right)^3 \times$$

$$X \int \int \int \frac{v(E_1) dE_1}{e^{\beta E_1} - 1} \left(\frac{v(E_2) dE_2}{e^{\beta E_2} - 1} \right) \frac{v(E_3) dE_3}{e^{\beta E_3} - 1} e^{\beta(E_1 + E_2)} \delta(E_3 - E_2 - E_1) \quad (40)$$

where $v(E)$ is the density of states at energy E . Then, using the transformations

$$x_i = (E_i/kT) = x_0 + (\hbar\omega_e/kT)k_1^2 a^2$$

$$x_0 = (g\mu_B H'/kT) \quad , \quad \hbar\omega_e = 2JS_{\text{eff}}(11/32)$$

the relaxation time is given, in the small- k and low temperature approximation, by

$$\left(\frac{1}{T}\right)_{3m} = \frac{2\pi}{\hbar} \left(\frac{A^2}{16S_A \hbar\omega_e} \right) \left(\frac{\frac{1}{2}S_A}{S_B - \frac{1}{2}S_A} \right)^3 \left(\frac{1}{4\pi^2} \right)^3 \left(\frac{1}{N_A} \right)^3 \left(\frac{kT}{\hbar\omega_e} \right)^{7/2} I_{3m} \quad , (41)$$

The integral in this expression

$$I_{3m} = \int_{x_0}^{\infty} \int_{x_0}^{\infty} dx_1 dx_2 \left(\frac{(x_1 - x_0)^{1/2} (x_2 - x_0)^{1/2} (x_1 + x_2 - x_0)^{1/2} e^{x_1 + x_2}}{(e^{x_1} - 1) (e^{x_2} - 1) (e^{x_1 + x_2} - 1)} \right) \quad , (42)$$

is, for $g\mu_B H' \ll kT$, independent of temperature and field and has a value of ~ 7.6 ^{64,66}.

Thus, the three-magnon scattering process provides a relaxation mechanism with a $T^{7/2}$ temperature dependence. The only difference between this result for a ferrimagnet and that for a ferromagnet ⁶⁴ is in the factor $(\frac{1}{2}S_A / (S_B - \frac{1}{2}S_A))^3$.

4.2 Exchange enhancement of the three-magnon process

The presence of the four-magnon scattering terms in the spin-wave expansion of the exchange Hamiltonian, as discussed in Chapter I, Section 4.4-b, leads to a second order relaxation process ^{64,65,67} as illustrated in Figure 6, where, for those processes on the left in

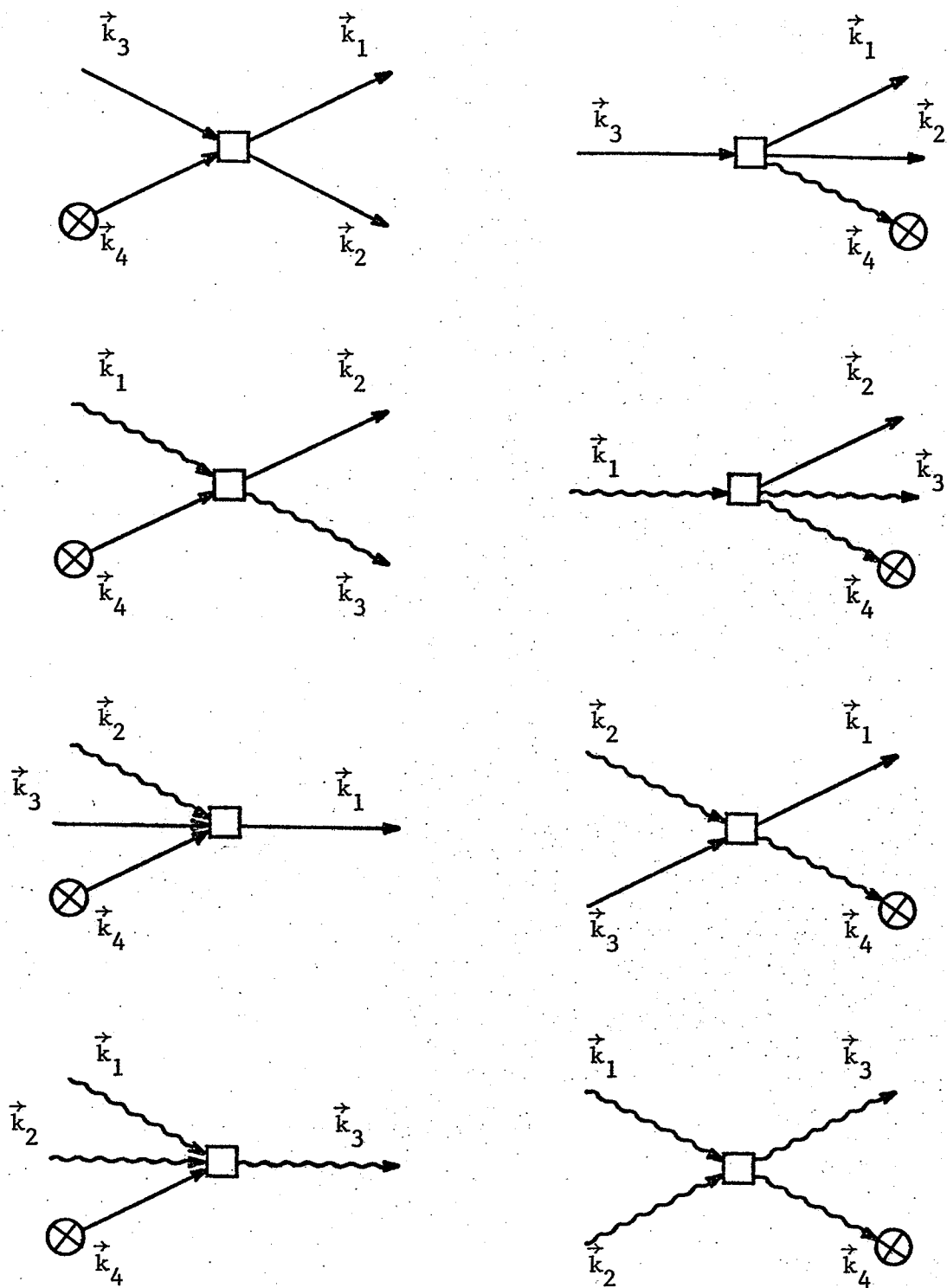


Figure 6. The four-magnon exchange scattering processes. k_4 represents a virtual magnon emitted or absorbed by the nucleus.

the figure, a virtual magnon is created by a nuclear spin-flip which then interacts with the electronic magnons via this four-magnon term, or, for the processes on the right side of the figure, the electronic magnons interact with each other producing, in the final state, one or two magnons plus a virtual magnon which is then absorbed by a nucleus, producing a nuclear spin flip. The initial and final electronic states can be seen to be identical to those for the three-magnon scattering processes illustrated in Figure 5. Thus, these terms must be included in an evaluation of the total three-magnon relaxation process.

The four-magnon terms in the exchange Hamiltonian are given in Equation I.39 (to order $1/S$) . These terms, together with the one-magnon term in the expansion of the hyperfine interaction, given in Equation II.7 , combine to give, in a second order perturbation treatment, an effective three-magnon term such that ^{64,68}

$$\langle f | \mathcal{H}_{\text{eff}} | i \rangle = \frac{\langle f | \mathcal{H}_{\text{ex}}^{(4)} | v \rangle \langle v | \mathcal{H}_{\text{hf}}^{(1)} | i \rangle}{-E_{v \pm AS}} \quad (43)$$

where $|f\rangle$ is the final state, $|i\rangle$ the initial state, and $|v\rangle$ is the intermediate state involving the virtual magnon, and $E_{v \pm AS}$ is the energy of the virtual magnon ($\hbar\omega_{\vec{k}_4}$) $\pm AS$ (the spin-flip energy). $AS \ll \hbar\omega_{\vec{k}_4}$ due to the large energy gap in the spin wave spectrum, and may be neglected.

To obtain the form of this effective interaction explicitly, recalling that only those terms involving only the α_k 's need to be retained since $n_k^\beta \approx 0$, the one-magnon term in the hyperfine interaction is written

$$\mathcal{H}_{\text{hf}}^{(1)} = -\frac{1}{2} A(2S_A)^{\frac{1}{2}} \sum_{\vec{k}_4} (I_{\vec{k}_4}^+ v_{\vec{k}_4} \alpha_{\vec{k}_4}^+ + I_{\vec{k}_4}^- v_{\vec{k}_4} \alpha_{\vec{k}_4}^-) \quad (44)$$

where \vec{k}_4 is taken to be the wave-vector of the virtual magnon. Similarly,

in transforming the four-magnon exchange Hamiltonian in terms of its normal mode operators α_k, β_k only the terms in the α_k 's need to be retained. Then, substituting $a_k = -v_k \alpha_k^+$ and $b_k = u_k \alpha_k$ into Equation I.39, the four-magnon exchange scattering Hamiltonian becomes

$$\begin{aligned}
\mathcal{H}_{\text{ex}}^{(4)} = & -\frac{1}{8} J \sum_{k_1, k_2, k_3, k_4} \delta(\vec{k}_1 + \vec{k}_2 - \vec{k}_3 - \vec{k}_4) \\
& \times \{ 4(Z_A/N_B) \gamma_{-3-4}^A v_1 v_2 u_3 u_4 \alpha_1^+ \alpha_2^+ \alpha_3^+ \alpha_4^+ + 4(Z_B/N_A) \gamma_{3+4}^B u_1 u_2 v_3 v_4 \alpha_{-1}^+ \alpha_2^+ \alpha_{-3}^+ \alpha_4^+ \\
& - Z_A (S_B/S_A N_A N_B)^{\frac{1}{2}} \gamma_{-4}^A \{ v_1 v_2 v_3 u_4 \alpha_1^+ \alpha_2^+ \alpha_3^+ \alpha_4^+ + v_1 v_2 v_3 u_4 \alpha_1^+ \alpha_2^+ \alpha_3^+ \alpha_4^+ \} \\
& - Z_B (S_A/S_B N_A N_B)^{\frac{1}{2}} \{ \gamma_{-2+3+4}^B v_1 u_2 u_3 u_4 \alpha_1^+ \alpha_2^+ \alpha_3^+ \alpha_4^+ + \gamma_{2-3-4}^B v_1 u_2 u_3 u_4 \alpha_1^+ \alpha_2^+ \alpha_3^+ \alpha_4^+ \} \\
& - Z_A (S_A N_A / S_B N_B^3)^{\frac{1}{2}} \{ \gamma_{1+2-3}^A u_1 u_2 u_3 v_4 \alpha_{-1}^+ \alpha_2^+ \alpha_{-3}^+ \alpha_4^+ \\
& \quad + \gamma_{-1-2+3}^A u_1 u_2 u_3 v_4 \alpha_1^+ \alpha_2^+ \alpha_3^+ \alpha_4^+ \} \\
& - Z_B (S_B N_B / S_A N_A^3)^{\frac{1}{2}} \gamma_1^B \{ u_1 v_2 v_3 v_4 \alpha_1^+ \alpha_2^+ \alpha_3^+ \alpha_4^+ + u_1 v_2 v_3 v_4 \alpha_{-1}^+ \alpha_2^+ \alpha_{-3}^+ \alpha_4^+ \} \}
\end{aligned} \tag{45}$$

where v_1, α_3 are short for v_{k_1}, α_{k_3} , and $v_{-k} = v_k, u_{-k} = u_k$.

By interchanging indices on a particular term this expression can be reduced to the following, where for small $k, u_k = u, v_k = v$,

$$\mathcal{H}_{\text{ex}}^{(4)} = -\frac{1}{8} J (u^2 v^2) \sum_{k_1, k_2, k_3, k_4} \delta(\vec{k}_1 + \vec{k}_2 - \vec{k}_3 - \vec{k}_4) \alpha_1^+ \alpha_2^+ \alpha_3^+ \alpha_4^+ \phi_{(3,4)}^{(1,2)}, \tag{46}$$

where the k -dependent function $\phi_{(3,4)}^{(1,2)}$ is given by

$$\phi_{(3,4)}^{(1,2)} = 4\gamma_{-1+4}^A (Z_A/N_B) - \gamma_4^A Z_A (S_A N_A / S_B N_B^3)^{\frac{1}{2}} (u/v) -$$

$$\begin{aligned}
& - \gamma_3^B Z_B (S_A / S_B N_A N_B)^{1/2} (u/v) + 4\gamma_{2-3}^B (Z_B / N_A) - \gamma_{-2}^A Z_A (S_A N_A / S_B N_B^3)^{1/2} (u/v) \\
& - \gamma_{-1}^B Z_B (S_B N_B / S_A N_A^3)^{1/2} (v/u) - \gamma_{-1}^A Z_A (S_B / S_A N_A N_B)^{1/2} (v/u) \\
& - \gamma_4^B Z_B (S_B N_B / S_A N_A^3)^{1/2} (v/u) - \gamma_{-1}^B Z_B (S_A / S_B N_A N_B)^{1/2} (u/v) \\
& - \gamma_4^A Z_A (S_A N_A / S_B N_B^3)^{1/2} (u/v)
\end{aligned} \tag{47}$$

Then, to include those processes which are indistinguishable from the above⁶⁹, i.e., those described by $\phi_{(3,4)}^{(2,1)}$, $\phi_{(4,3)}^{(1,2)}$, and $\phi_{(4,3)}^{(2,1)}$, the Hamiltonian is written as

$$\begin{aligned}
\mathcal{H}_{\text{ex}}^{(4)} = & -\frac{1}{32} J v^2 u^2 \sum_{k_1, k_2, k_3, k_4} \delta(\vec{k}_1 + \vec{k}_2 - \vec{k}_3 - \vec{k}_4) \alpha_1^+ \alpha_2^+ \alpha_3 \alpha_4 \\
& \times \{ \phi_{(3,4)}^{(1,2)} + \phi_{(3,4)}^{(2,1)} + \phi_{(4,3)}^{(1,2)} + \phi_{(4,3)}^{(2,1)} \}
\end{aligned} \tag{48}$$

or,

$$\mathcal{H}_{\text{ex}}^{(4)} = -\frac{1}{32} J u^2 v^2 \sum_{k_1, k_2, k_3, k_4} \delta(\vec{k}_1 + \vec{k}_2 - \vec{k}_3 - \vec{k}_4) \alpha_1^+ \alpha_2^+ \alpha_3 \alpha_4 K_{(3,4)}^{(1,2)} \tag{49}$$

where, since $v/u = \eta(S_A/S_B)^{1/2}$ and $\gamma_{-k} = \gamma_k$

$$\begin{aligned}
K_{(3,4)}^{(1,2)} = & 4(\gamma_{-1+4}^A + \gamma_{-1+3}^A + \gamma_{-2+4}^A + \gamma_{-2+3}^A) (Z_A / N_B) \\
& + 4(\gamma_{2-3}^B + \gamma_{2-4}^B + \gamma_{1-3}^B + \gamma_{1-4}^B) (Z_B / N_A) \\
& - \eta \left\{ (\gamma_1^A + \gamma_2^A + \gamma_3^A + \gamma_4^A) Z_A \{ (N_A / N_B^3)^{1/2} + 1 / (N_A N_B)^{1/2} \} \right. \\
& \left. + (\gamma_1^B + \gamma_2^B + \gamma_3^B + \gamma_4^B) Z_B \{ (N_B / N_A)^{1/2} + 1 / (N_A N_B)^{1/2} \} \right\}
\end{aligned} \tag{50}$$

In the case where $Z_A = Z_B$, $N_A = N_B$, and $\gamma_k^A = \gamma_k^B$, this expression reduces to the usual form given for the ferromagnetic case, for small k , by

$$\mathcal{H}_{\text{ex}}^{(4)'} = (J a_{\text{nn}}^2 / 2N) \sum_{k_1, k_2, k_3, k_4} \alpha_1^+ \alpha_2^+ \alpha_3 \alpha_4 (\vec{k}_1 \cdot \vec{k}_2 + \vec{k}_3 \cdot \vec{k}_4) \delta(\vec{k}_1 + \vec{k}_2 - \vec{k}_3 - \vec{k}_4) \quad (51)$$

By inserting the one-magnon hyperfine Hamiltonian of Equation 44, and the four-magnon exchange scattering Hamiltonian given in Equation 49, into Equation 43 one obtains the effective three-magnon Hamiltonian

$$\mathcal{H}_{\text{eff}}^{(3)'} = - \frac{A}{8SN_A} (2S/N_A)^{\frac{1}{2}} \sum_n \sum_{k_1, k_2, k_3} I_n^+ \exp\{i(\vec{k}_1 + \vec{k}_2 - \vec{k}_3) \cdot \vec{r}_n\} \alpha_1^+ \alpha_2^+ \alpha_3 \quad (52)$$

$$\times \left\{ \frac{(1/8) S J u^2 v^3 N_A K^{(1,2)}(3, 3-1-2)}{\hbar(\omega_{k_3} - \omega_{k_1} - \omega_{k_2})} \right\}$$

where the conservation of linear momentum, represented by the δ -function in Equation 49 has been used, and the spin-flip energy (AS) has been neglected. This may be combined with the direct three-magnon process Hamiltonian to give

$$\mathcal{H}_{\text{eff}}^{(3)} = \frac{A}{8SN_A} (2S/N_A)^{\frac{1}{2}} \sum_n \sum_{k_1, k_2, k_3} I_n^+ \exp\{i(\vec{k}_1 + \vec{k}_2 - \vec{k}_3) \cdot \vec{r}_n\} v^3 \alpha_1^+ \alpha_2^+ \alpha_3 \quad (53)$$

$$\times \{1 - M(\vec{k}_1, \vec{k}_2, \vec{k}_3)\}$$

The relaxation rate due to this total three-magnon process is then calculated by the same method as used in obtaining Equation 41. The factor $M(\vec{k}_1, \vec{k}_2, \vec{k}_3)$, when reduced to a form--such as that corresponding to the special case of identical sublattices given in Equation 51--involving the scalar products of the wave-vectors, can be replaced by a suitable angular average leaving what amounts to an effective enhancement of the three-magnon process. In the case of ferromagnets⁶⁴ this enhancement to the relaxation rate is ~ 8 while in antiferromagnets^{64,68} an enhancement of $\sim 2 - 4$ is expected. Thus, in the present ferrimagnetic case, an

enhancement of a similar magnitude is expected. The calculation has not been carried out due to the complexity of the angular function involved, and also because the three-magnon process is not expected to be the most effective spin-wave relaxation process at very low temperatures.

The presence of the spin-wave energies in the denominator of the expression in Equation 52 introduce a field-dependence into the exchange enhancement process. Thus, there is expected to be a decrease in the effective three-magnon relaxation rate as the applied field is increased. Comparison with the data is left for Section 5 following the discussion of the dipolar induced two-magnon process in the next section.

4.3 Dipolar induced two-magnon process

As discussed in Section 4.1 the Raman or two-magnon scattering process is forbidden in colinear, isotropic spin systems by conservation of angular momentum. However, the terms such as $S^z S^\pm$ in the dipolar Hamiltonian, since they do not commute with S_z^z , need not conserve angular momentum and, therefore, in second order, allow a relaxation process wherein a nuclear spin emits or absorbs a virtual magnon which is scattered by two real magnons via the three-magnon terms in $S^z S^\pm$ given in Equation I.38. These terms ($S^z S^\pm$) connect states whose z-component of angular momentum differ by one unit, thus, the scattering processes which are allowed in a two sublattice system are those shown in Figure 7.

The virtual spin-wave involved in each of these diagrams is either created or destroyed, accompanying a nuclear spin-flip, by the one-magnon term in the hyperfine interaction just as in the case of the exchange-enhanced process discussed in the preceding section. As before, because of the large energy gap separating the two branches of the magnon spectrum

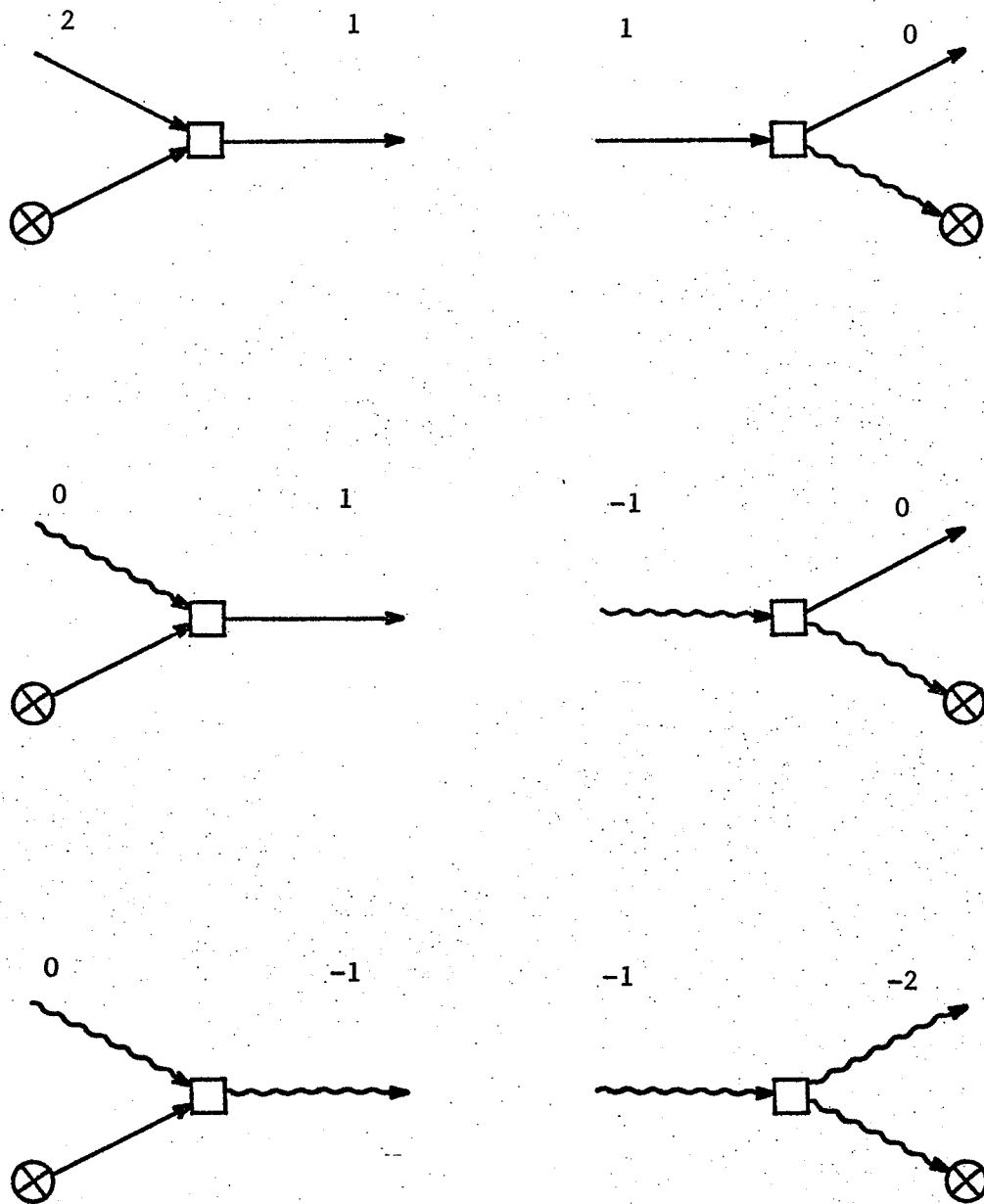


Figure 7. The dipolar-induced two-magnon processes. The numbers above each diagram refer to the z-component of angular momentum of each configuration.

in a ferrimagnet, we need to consider only the process described by the first diagram in Figure 7, that involving only α -mode magnons.

On transforming the Hamiltonian of Equation I.38 to normal mode operators α , β with $a_k = -v_k \alpha_k^+$ and $b_k = u_k \alpha_k$, the three-magnon term in the dipolar Hamiltonian becomes

$$\begin{aligned}
 \mathcal{H}_{dd}^{(3)} = & - \sum_{k_1, k_2, k_3} \delta(\vec{k}_1 + \vec{k}_2 - \vec{k}_3) \left\{ (S_A/2N_A)^{\frac{1}{2}} \left\{ \frac{1}{2} C_{A,A}^{(z,+)}(0) + K_{A,A}^{(z,+)}(\vec{k}_1) \right. \right. \\
 & - \left. \frac{1}{2} (S_B/S_A) (N_B/N_A)^{\frac{1}{2}} K_{A,B}^{(z,+)}(0) \right\} (-v_1 v_2 v_3) + (S_B/2N_A)^{\frac{1}{2}} K_{A,B}^{(z,+)}(\vec{k}_1) (v_1 v_2 u_3) \\
 & + (S_A/2N_B)^{\frac{1}{2}} K_{A,B}^{(z,+)}(-\vec{k}_1) (u_1 u_2 v_3) - (S_B/2N_B)^{\frac{1}{2}} \left\{ \frac{1}{2} C_{B,B}^{(z,+)}(0) \right. \\
 & + \left. K_{B,B}^{(z,+)}(\vec{k}_1) - \frac{1}{2} (S_A/S_B) (N_A/N_B)^{\frac{1}{2}} K_{A,B}^{(z,+)}(0) \right\} (u_1 u_2 u_3) \left. \right\} \alpha_1 \alpha_2 \alpha_3^+ \\
 & + \text{(complex conjugate)} \\
 = & - \sum_{k_1, k_2, k_3} \delta(\vec{k}_1 + \vec{k}_2 - \vec{k}_3) F(\vec{k}_1) \alpha_1 \alpha_2 \alpha_3^+ + \text{c.c.}
 \end{aligned}
 \tag{54}$$

In this expression the factor $F(\vec{k}_1)$ is a function only of \vec{k}_1 , since for small k_i , $u_1 = u_2 = u_3$, $v_1 = v_2 = v_3$. Since this interaction arises from the $S^z S^\pm$ terms in the dipole-dipole Hamiltonian, $F(\vec{k}) \propto k^z k^\pm / k^2$, as discussed in Section I.4.3. A term which is independent of k , due to the $K_B^{(z,+)}(0)$ terms, which is $\sim \Sigma_\delta R_\delta^z R_\delta^- / R_\delta^5$, vanishes in the case of a spinel lattice due to the cubic A-site symmetry and the trigonal axis symmetry of the B-sites.

Then, following the same procedure as used for the exchange-enhancement process, with

$$\langle f | \mathcal{H}_{\text{eff}}^{(2)} | i \rangle = \frac{\langle f | \mathcal{H}_{\text{dd}}^{(3)} | v \rangle \langle v | \mathcal{H}_{\text{hf}}^{(1)} | i \rangle}{-\hbar \omega_{\vec{k}_v}}$$

the effective two-magnon Hamiltonian is given by, (with $S' = (N_B/N_A)S_{\text{eff}}$)

$$\mathcal{H}_{\text{eff}}^{(2)} = -\frac{1}{2} A u^2 v^2 g \mu_B (4\pi M'/V) (S_A/S') \sum_n I_n^+ \sum_{\vec{k}, \vec{k}'} \exp\{i(\vec{k}' - \vec{k}) \cdot \vec{r}_n\} \times \left[\frac{k^+ k^z}{k^2} + \frac{(k' - k)^+ (k' - k)^z}{(\vec{k}' - \vec{k}) \cdot (\vec{k}' - \vec{k})} \right] \left[\frac{1}{E(\vec{k}' - \vec{k})} \right] \alpha_{\vec{k}}^+ \alpha_{\vec{k}'}^+ \quad (55)$$

where $M' = g \mu_B S' \bar{N}_A \{ (N_B S_B - N_A S_A)^2 / N_A S_A N_B S_B \}$, as derived in Chapter I, and $E(\vec{k})$ is the spin-wave energy. The case where magnons \vec{k}_1 and \vec{k}_2 , in Equation 54, have been interchanged, has been explicitly included.

The relaxation rate is given by

$$\begin{aligned} (1/T_1)_{2m} &= \frac{\pi}{\hbar} (v^2)^2 \{A g \mu_B (4\pi M'/V)\}^2 \sum_f |\langle f | \left[\sum_{\vec{k}', \vec{k}} \right. \\ &\times \left. \left(\frac{k^+ k^z}{k^2} + \frac{(k' - k)^+ (k' - k)^z}{(\vec{k}' - \vec{k}) \cdot (\vec{k}' - \vec{k})} \right) \frac{\alpha_{\vec{k}}^+ \alpha_{\vec{k}'}^+}{E(\vec{k}' - \vec{k})} \right] | i \rangle|^2 \delta(E_f - E_i) \\ &= \frac{\pi}{\hbar} (v^2)^2 \{A g \mu_B (4\pi M'/V)\}^2 \sum_{\vec{k}', \vec{k}} \left[\frac{k^+ k^z}{k^2} + \right. \\ &\left. \frac{(k' - k)^+ (k' - k)^z}{(\vec{k}' - \vec{k}) \cdot (\vec{k}' - \vec{k})} \right]^2 \left[\frac{1}{E(\vec{k}' - \vec{k})} \right]^2 n_{\vec{k}}^\alpha (n_{\vec{k}'}^\alpha + 1) \delta(E_f - E_i) \end{aligned} \quad (56)$$

The sums may be replaced by integrals in the usual manner giving, for the angular part, the integral Φ

$$\begin{aligned} \Phi &= \iiint \left[\frac{k^+ k^z}{k^2} + \frac{(k' - k)^+ (k' - k)^z}{(\vec{k}' - \vec{k}) \cdot (\vec{k}' - \vec{k})} \right]^2 \left[\frac{1}{E(\vec{k}' - \vec{k})} \right]^2 d\cos\theta \, d\phi \, d\cos\theta' \, d\phi' \\ &= \left(\frac{1}{g \mu_B \hbar} \right)^2 \iiint \left[\frac{k^+ k^z}{k^2} + \frac{(k' - k)^+ (k' - k)^z}{(\vec{k}' - \vec{k}) \cdot (\vec{k}' - \vec{k})} \right]^2 \times \end{aligned}$$

$$X \left\{ 1 - \frac{4\alpha^2 k^2}{g\mu_B H} \right\} d\cos\theta d\phi d\cos\theta' d\phi' \quad (57)$$

since $E(\vec{k}' - \vec{k}) = g\mu_B H + \alpha^2 (\vec{k}' - \vec{k})^2 \approx g\mu_B H + 2\alpha^2 k^2 (1 - \cos\gamma)$, where γ , the angle between wavevectors \vec{k} and \vec{k}' , is small. With this approximation, to second order in γ ,

$$\Phi = \frac{32\pi^2}{15} \quad (+ O(\gamma^4))$$

Then, the relaxation is given by

$$\begin{aligned} (1/T_1)_{2m} &= \frac{16}{15} \frac{(v^2)^2}{2\pi} (Ag\mu_B M')^2 (1/g\mu_B H)^2 (1/\bar{N}_A)^2 \\ &X \int \int k^2 dk k'^2 dk' n_k^\alpha (n_{k'}^\alpha + 1) \delta(E_{k'} - E_k) \\ &= (A^2/\hbar^2 \omega_e) (g\mu_B M'/\bar{N}_A \hbar \omega_e)^2 (v^2)^2 \frac{2}{15\pi} \left(\frac{kT}{g\mu_B H} \right)^2 \log \left(\frac{\exp(g\mu_B H/kT)}{\exp(g\mu_B H/kT) - 1} \right) \end{aligned} \quad (58)$$

This approximate expression exhibits explicitly the roughly $\sim (T/H)^2$ behaviour obtained graphically by Beeman and Pincus⁶⁴.

The dipolar-induced two-magnon process and the exchange enhanced three-magnon process are the two most effective spin-wave relaxation mechanisms when the direct and Raman processes are forbidden. The characteristic temperature dependences of these two processes suggest that at very low temperatures the two-magnon process will be the stronger of the two, while at higher temperatures, the three-magnon process should dominate. The comparison of the calculated relaxation rates to the experimental values is deferred till Chapter IV since these background relaxation rates could not be measured until a method for the separation of domain and domain-wall components of the signal was devised.

5. Frequency Dependent Relaxation--Comparison with Data--Relaxation of Multiple Echoes

As shown in Section 3, the Suhl-Nakamura relaxation rate shows a strong frequency dependence such that $(1/T_2)_{S-N} \propto g(\nu)$, where $g(\nu)$ is the inhomogeneously broadened lineshape function. The very strong inhomogeneous broadening in manganese ferrite, resulting in a half-width at half-maximum of ~ 1 MHz, allows the direct measurement of this frequency dependent relaxation. Figure 8 gives an illustration of this effect in a single crystal sample⁷⁰ of roughly ellipsoidal shape, of $\text{Ni}_{.03}\text{Mn}_{.62}\text{Fe}_{2.36}\text{O}_4$. These relaxation times were measured by comparing the echo decay envelope to an exponential of known time constant. The open circles are for data taken at $T = 4.2^\circ\text{K}$ in an external field of $H_{\text{ext}} = 3$ kOe, sufficient to effectively saturate this sample, while the solid circles are from data taken at 77°K in the same external field. The error bars for the lower temperature data, and the size of the circles for the 77°K data represent an estimated error of $\sim 10\%$.

The straightforward calculation of the Suhl-Nakamura relaxation time using Equation 28 gives a value which is considerably larger than that measured, suggesting that the asymptotic range function has underestimated the true range function by a factor of $\sim 2 - 3$. The asymptotic range function is good for $r/a_{\text{nn}} \gg 1$. Thus, the short-wavelength (large k) contribution may be underestimated⁶⁰, particularly in cases such as this with a large number of near neighbor identical nuclei (a spinel A-site has 12 next-nearest neighbor A-sites). Then, using the value of exchange energy, $\chi_{\omega_e} = 6 \times 10^{-16}$ ergs, obtained from the spin-wave relaxation time calculation for the two-magnon process (for a MnFe_2O_4 crystal, discussed in Chapter IV, Section 3.2) and, at $T = 4.2^\circ\text{K}$, $H_K = 1.0$ kOe, $H_N = 559.5$ kOe, and with a frequency in-

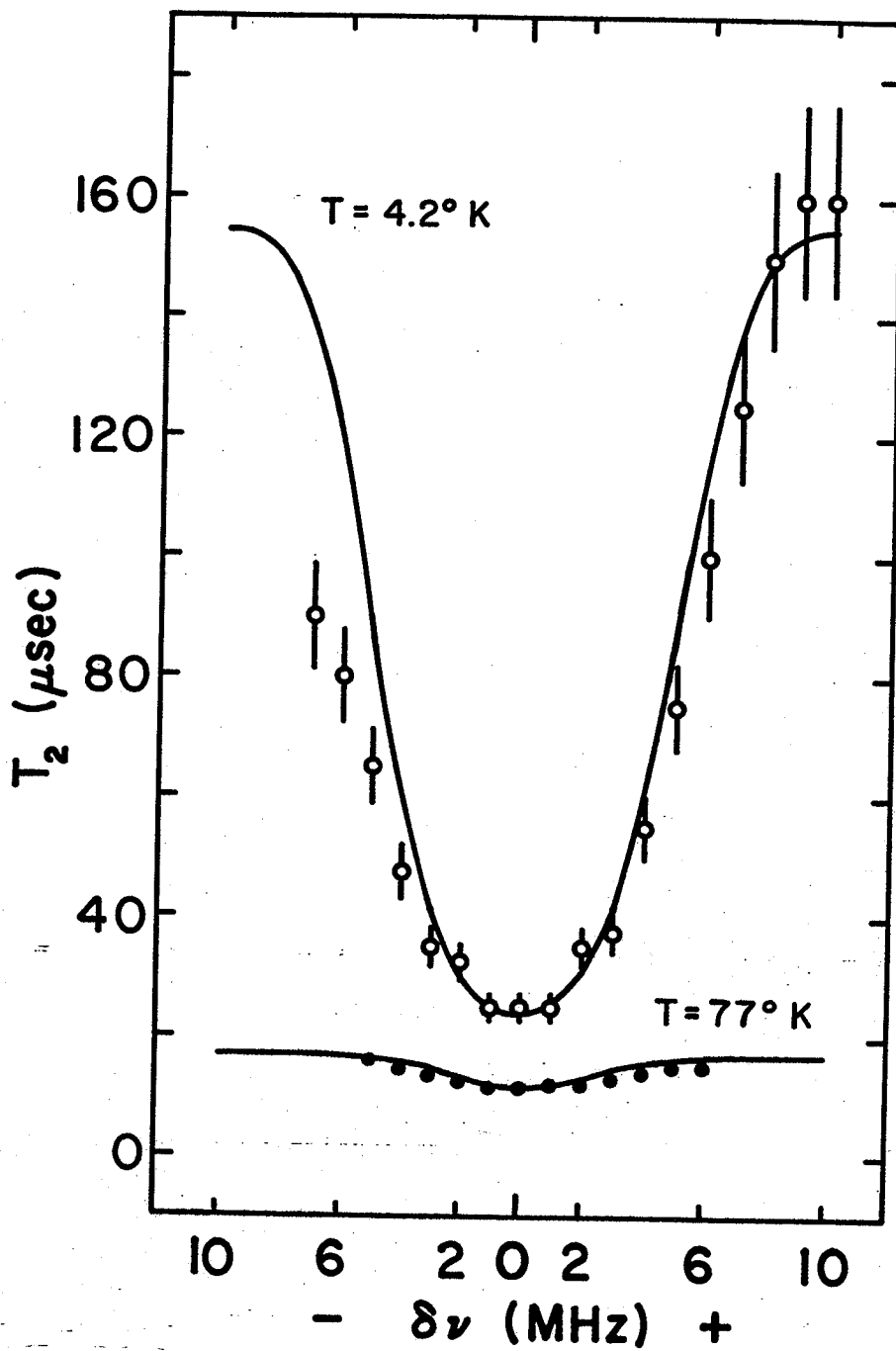


Figure 8. Frequency dependent relaxation in $\text{Ni}_{0.03}\text{Mn}_{0.62}\text{Fe}_{2.36}\text{O}_4$

dependent background relaxation time of ~ 155 μsec , the asymptotic range function, when multiplied by a factor of ~ 2.06 , gives a reasonably good fit to the data, as shown by the upper solid curve in the figure. The fit to the $T = 77$ $^{\circ}\text{K}$ data uses $H_K = 1.5$ kOe, $H_N = 555.4$ kOe, and a background relaxation time of ~ 17 μsec , all other parameters remaining the same, and is shown by the lower curve in the figure. (The necessity of including this numerical factor in the range function points out an error in the calculation of the Suhl-Nakamura relaxation times in reference 51.) A more precise calculation of the range function should yield results more in agreement with experiment, however, the relatively complex lattice structure makes this difficult. The procedure used here is felt to be justifiable since the expression, Equation 28, for the Suhl-Nakamura relaxation time, shows a characteristic field dependence due to the form of the range function, while the transverse part of the dipole-dipole relaxation, which exhibits a frequency dependence much like that of the Suhl-Nakamura relaxation, is independent of field. Figure 9 shows the total relaxation time at the central (or resonance) frequency as a function of external magnetic field, for the same sample as discussed above, at $T = 1.5$ and 4.2 $^{\circ}\text{K}$. The solid curves are the calculated relaxation times at resonance using the same parameters as used in fitting the data in Figure 8 except that at $T = 1.5$ $^{\circ}\text{K}$ the background relaxation time and the anisotropy field were taken to be ~ 250 μsec and 0.7 kOe, respectively. This field dependence completes the identification of the spin-spin relaxation as being primarily due to the Suhl-Nakamura interaction. The transverse dipole-dipole interaction, since it is field independent, should become more important at higher fields, since the Suhl-Nakamura interaction is becoming less effective, and the total relaxation time at resonance is expected to increase less rapidly with field than calculated assuming Suhl-Nakamura relaxation alone.

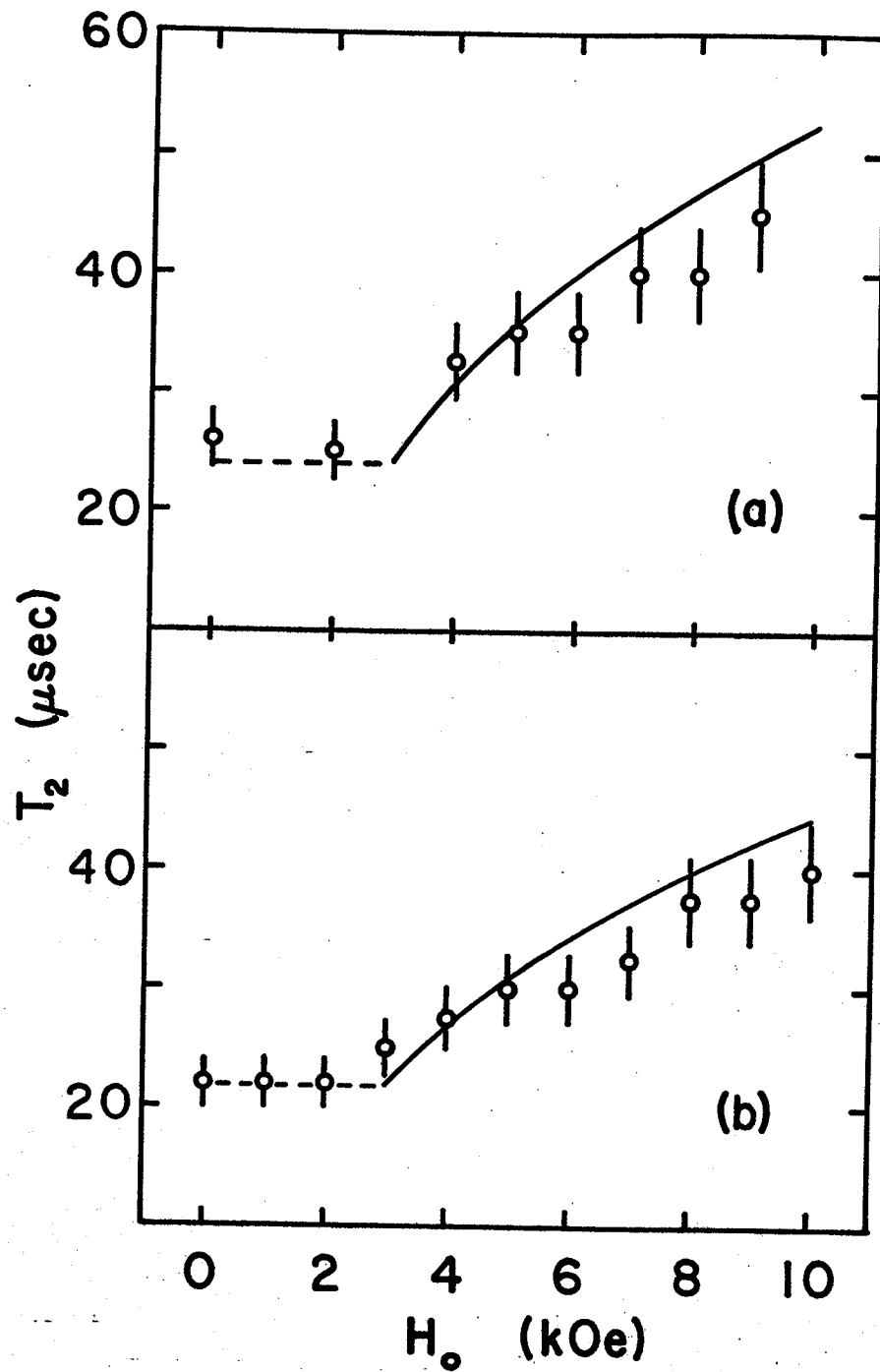


Figure 9. Field dependence of total relaxation time at resonance.

The multiple echoes observed in manganese ferrites, and discussed in Chapter II, exhibit the same frequency and field dependences as the first echo does. The open circles in Figure 10 are the relaxation times for the $\text{Ni}_{.03}\text{Mn}_{.62}\text{Fe}_{2.36}\text{O}_4$ sample at $T = 1.5^\circ\text{K}$, corresponding to the decay envelope of the first echo. The solid curve for this case again is the calculated relaxation time, assuming a background relaxation time of $\sim 250 \mu\text{sec}$. The solid circles in this figure are the decay times of the second echo's decay envelope, at the same temperature. The calculated curve in this case was obtained by a computer calculation based on the density matrix method discussed in Chapter II, where the first echo (i.e., the effective third pulse) was allowed to decrease in amplitude, with pulse separation τ , as $\exp(-2\tau/T_2)$. This naturally leads to the more rapid decay with τ of the higher order echoes. There are no adjustable parameters in calculating the second echo relaxation time, the observed first echo minimum $T_2 \approx 33 \mu\text{sec}$ predicts straightforwardly a second echo minimum $T_2 \approx 20 \mu\text{sec}$, as shown in the figure.

Figure 11 shows the frequency dependence of the amplitudes and relaxation times for the first four echoes in a field $H_{\text{ext}} = 0.0 \text{ kOe}$ at $T = 1.5^\circ\text{K}$. The echo amplitudes show the same lineshape and linewidth for each of the echoes, and the relaxation times show the same behaviour, as expected. It is interesting to note, however, that echoes 2-4 have maxima at $\nu \approx 588 \text{ MHz}$ while echo 1 has its maximum at $\nu \approx 586.5 \text{ MHz}$. This seems to suggest that the first echo has some domain-wall component (since the domain-wall signal occurs at a frequency slightly below that of the domain component), while the higher echoes do not. In Figure 12, which is similar to Figure 11 but for $H_{\text{ext}} = 4.0 \text{ kOe}$, sufficient to effectively saturate the sample, all of the echoes have maxima at

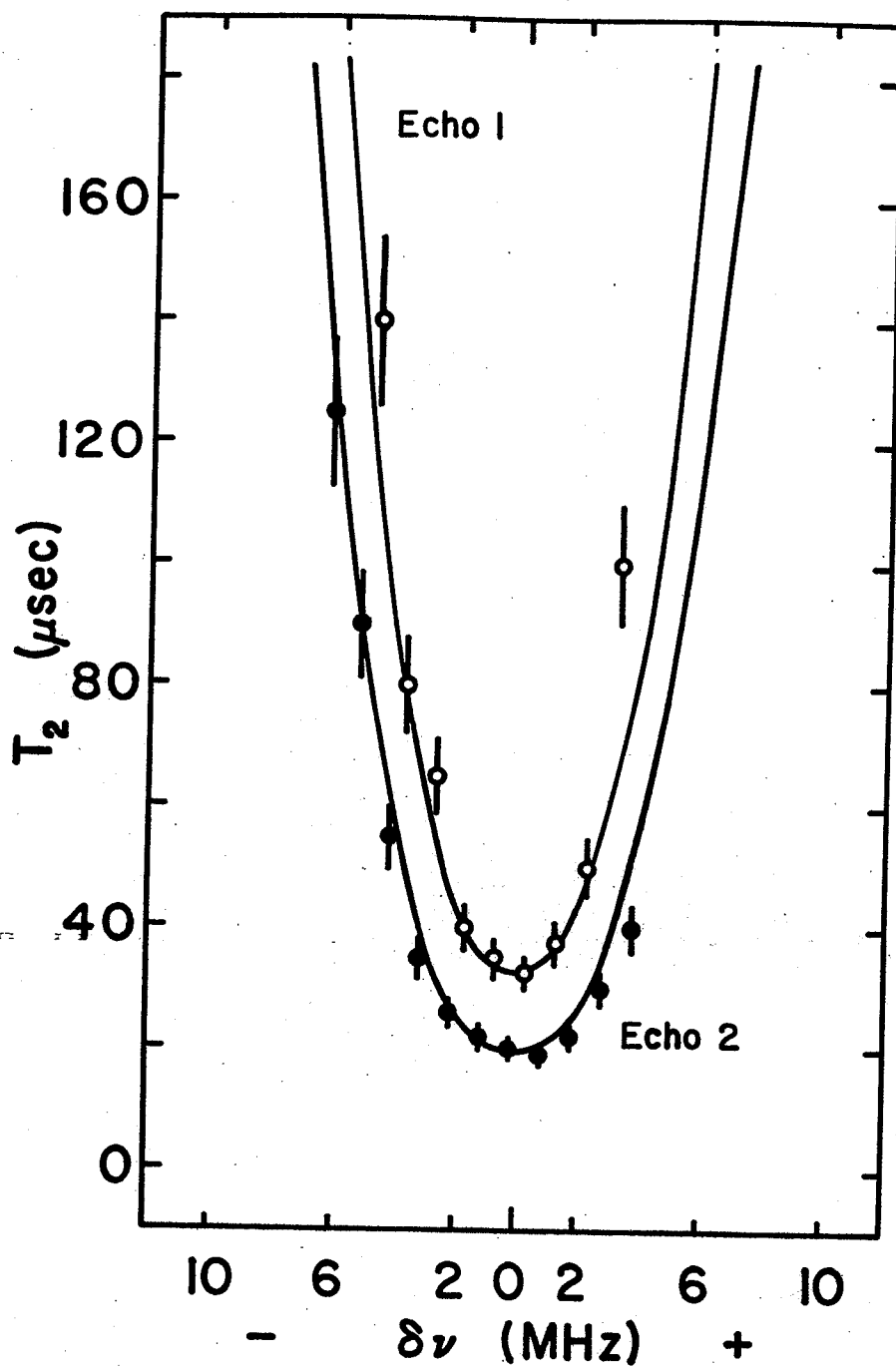


Figure 10. Frequency dependent relaxation of first two echoes at $T = 1.5$ OK.

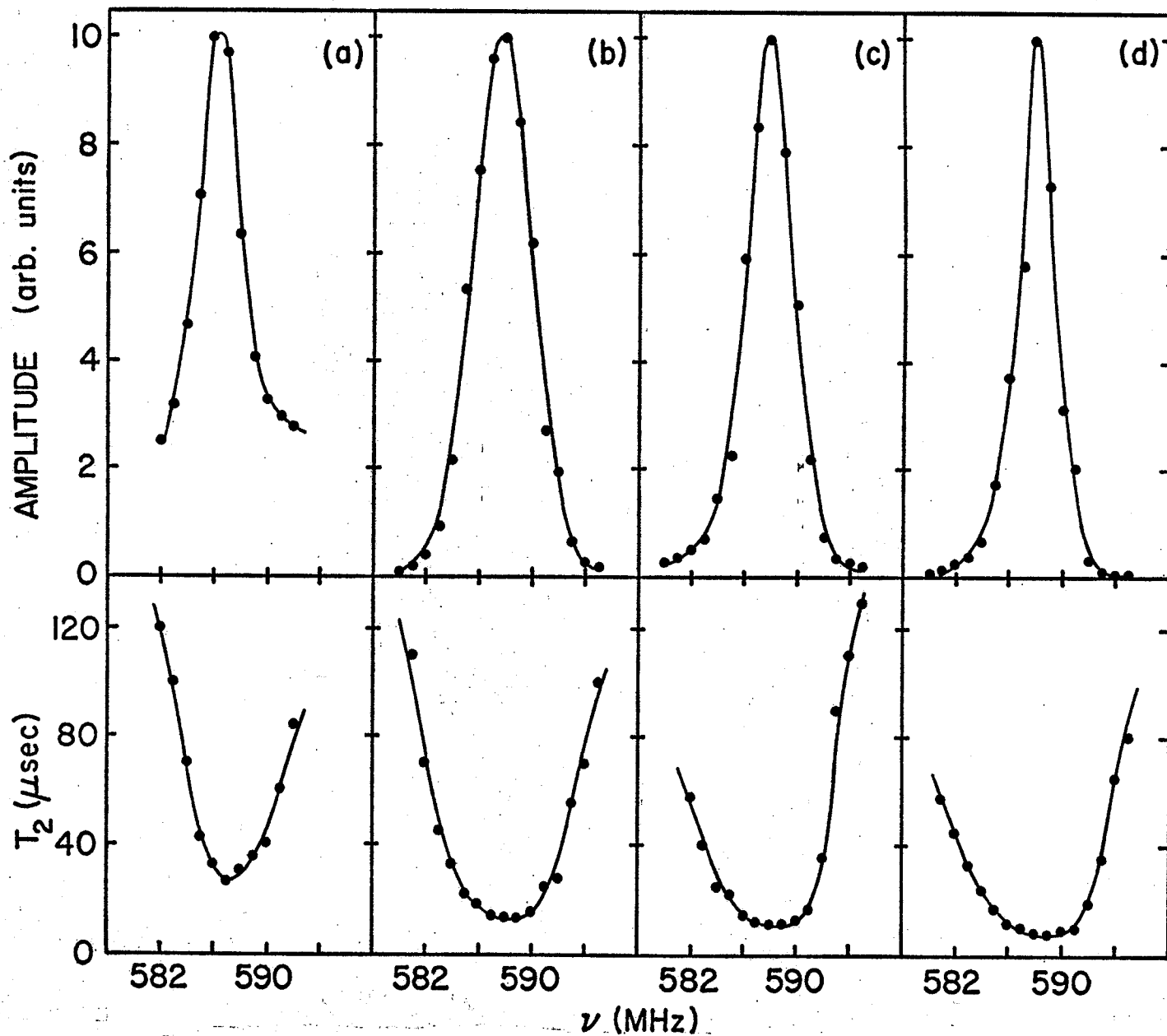


Figure 11. Echo amplitude extrapolated to $\tau = 0$ and relaxation time versus frequency for the first four echoes at $T = 1.5^\circ\text{K}$ in $H_0 = 0$ kOe. a) first echo, b) second echo, c) third echo, d) fourth echo.

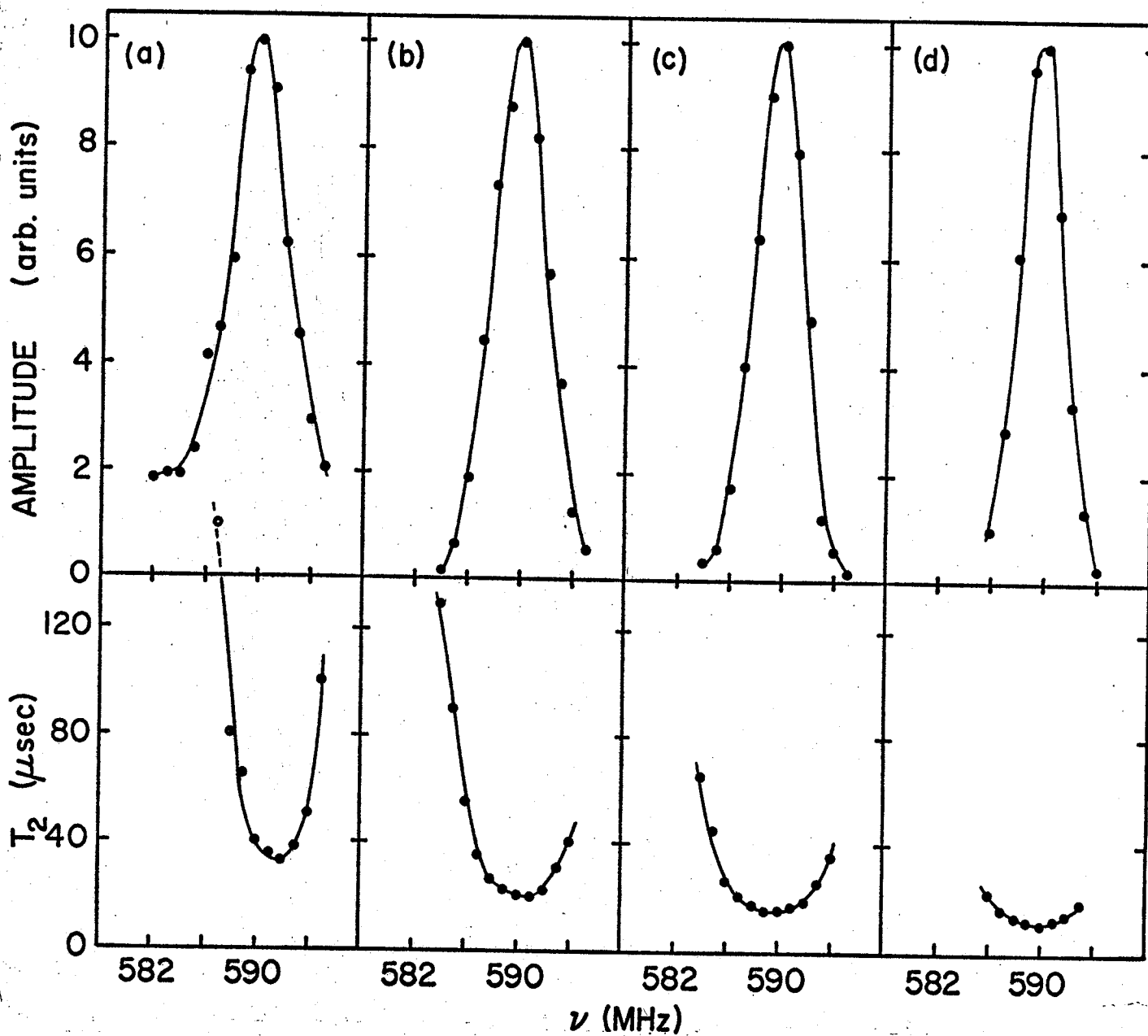


Figure 12. Echo amplitude extrapolated to $\tau = 0$ and relaxation time versus frequency for the first four echoes at $T = 1.5$ °K in $H_0 = 4$ kOe. a) first echo, b) second echo, c) third echo, d) fourth echo.

$\nu = 590$ MHz. Thus, it appears that either the domain-wall component does not contribute to the formation of multiple echoes, or that the relaxation time of the domain-wall component's contribution to higher echoes is so much shorter than that of the domain signal's contribution that it is effectively unobservable. It will be seen in Chapter IV that the domain-wall component of the first echo does have a considerably shorter relaxation time.

The higher numbered echoes will also exhibit a field dependence like that of the first echo. The measured values of the second echo relaxation time as a function of H_{ext} are compared with the values calculated, in the same manner as the frequency dependence of the second echo relaxation time, at $T = 1.5$ °K, in Figure 13-a, and at $T = 4.2$ °K, in Figure 13-b. The calculated values do not quite follow the measured times, particularly at the lower temperature. The third echo relaxation time at these same temperatures are plotted against external field in Figures 14-a,b. The solid curves are the relaxation times calculated neglecting the refocusing effects of the second echo, thus the agreement is not expected to be very good.

The generation and relaxation of multiple echoes, as well as the more basic resonance and relaxation data for the first echo, particularly the frequency and field dependences of the relaxation time, appear to be well explained by the Suhl-Nakamura spin-spin interaction, at least in the single-domain or saturated region. The background relaxation process, which is strongly temperature dependent and therefore likely due to spin-wave scattering, requires a more detailed study to identify the particular mechanism, and will be discussed in the next chapter. In the multi-domain region, however, the nuclei within

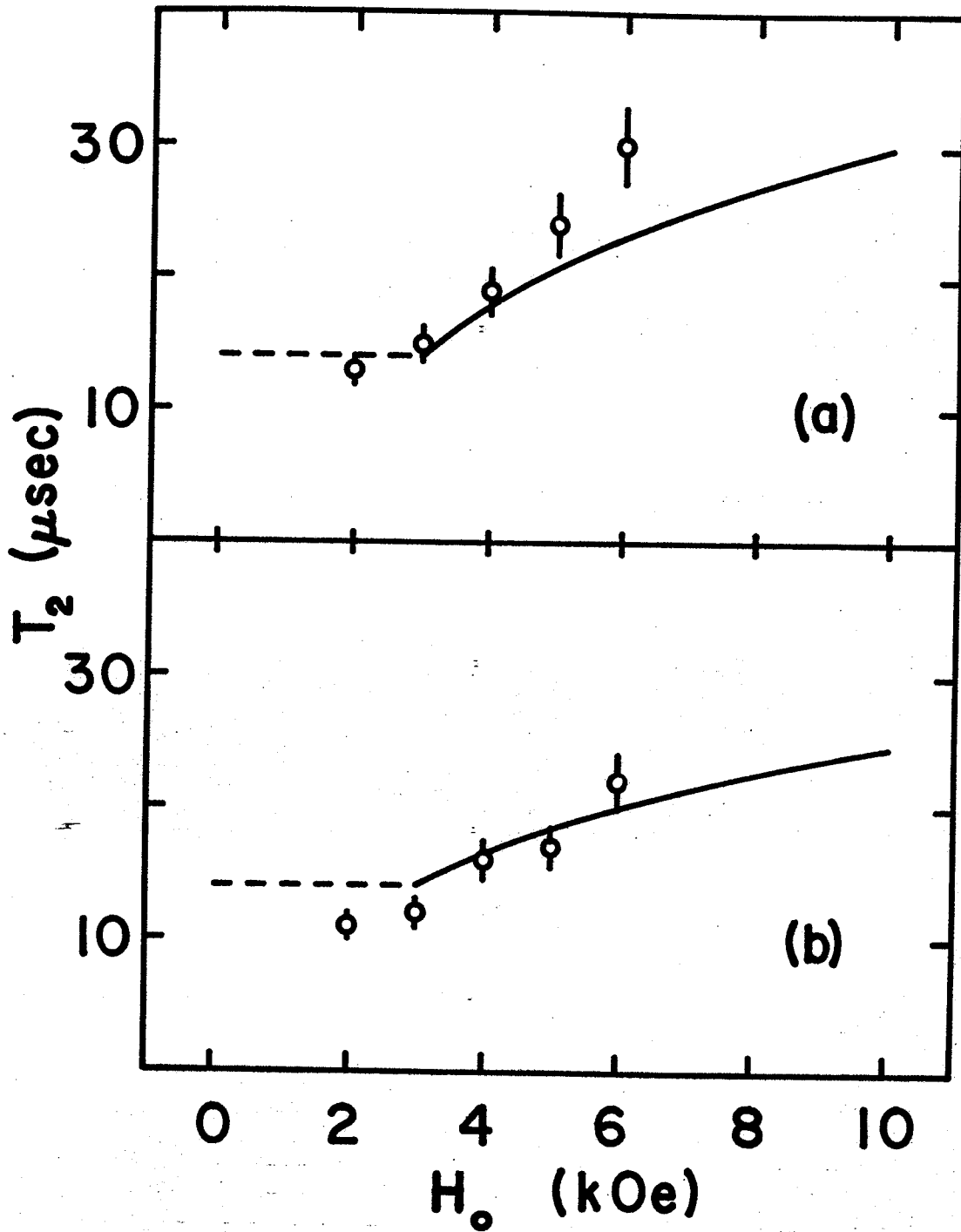


Figure 13. Field dependence of total relaxation time at resonance of the second echo. a) $T = 1.5$ °K, b) $T = 4.2$ °K.

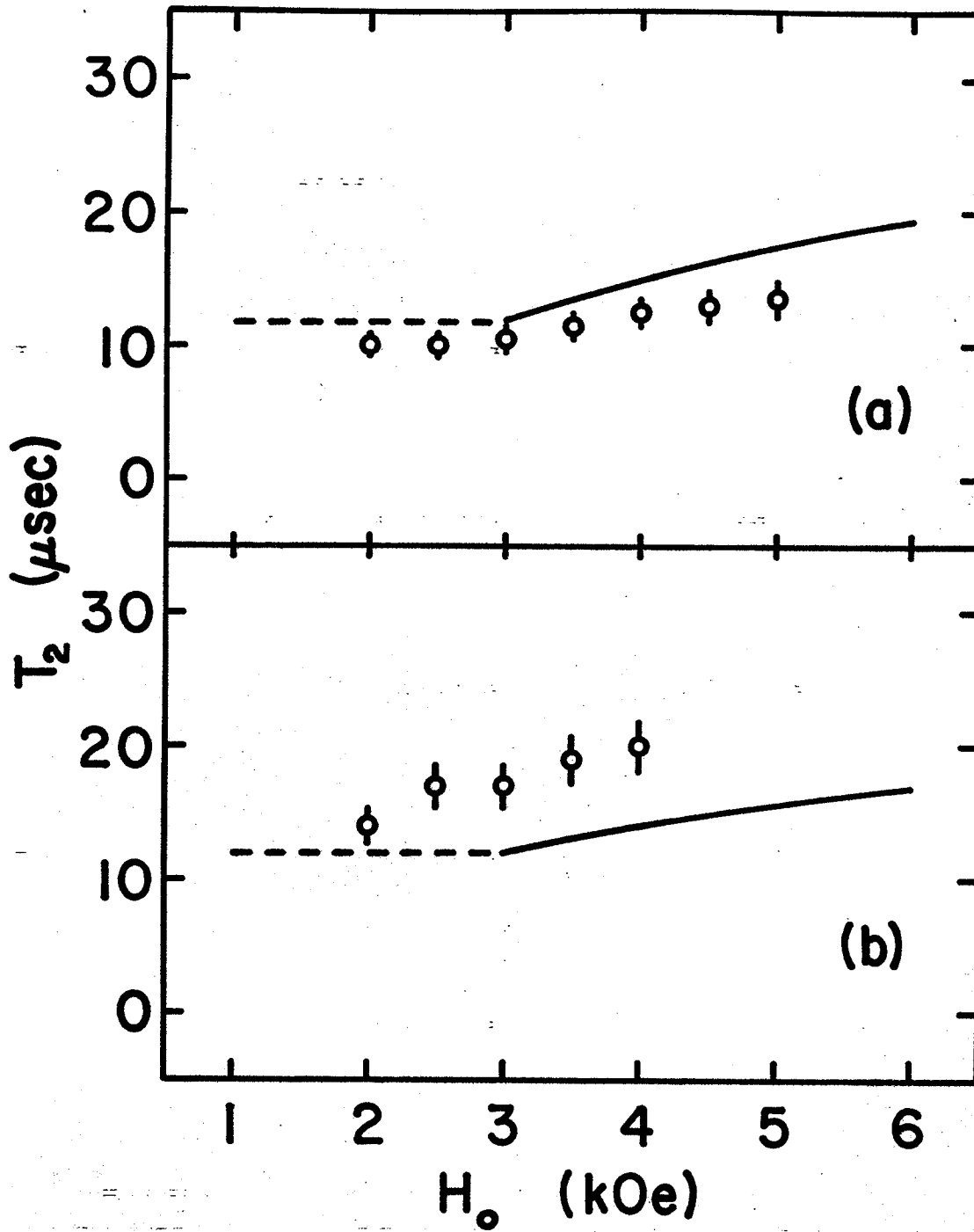


Figure 14. Field dependence of total relaxation time at resonance of the third echo. a) $T = 1.5$ °K, b) $T = 4.2$ °K.

domain walls are expected to give a large contribution to the signal, due to the large enhancement factor (see Chapter I), and the spectrum should consist of two overlapping resonance lines.

6. The Multi-Domain Spectra

The spectrum in Figure 15-a was taken at 4.2 °K in zero field on the $\text{Ni}_{0.03}\text{Mn}_{0.62}\text{Fe}_{1.36}\text{O}_4$ crystal, and shows some indication of the presence of two components to the signal for this sample. The spectra in Figure 15-b,c, taken at the same temperature and field as that in part a of the figure, are for polycrystalline samples of $\text{Mn}_x\text{Fe}_{3-x}\text{O}_4$ with $x = 0.8$ and 1.0 respectively. These spectra show more clearly the two component nature of the signal. In particular, the $x = 1.0$ spectrum in Figure 15-c shows two clear maxima while the relaxation time data gives an indication of the presence of two minima (the echo decay envelopes are quite non-exponential for some frequencies).

Figure 16-a, on the other hand, shows the echo decay envelope of the $x = 1.0$ sample in zero field at 586 MHz and $T = 1.47$ °K. The solid curve is the best fit assuming a single relaxation time, and the decay is quite obviously non-exponential. An obvious explanation for a non-exponential echo decay, in this case, is the presence of two independently relaxing resonance lines. Figure 16-b shows the data of Figure 16-a replotted and fit to the function $A_1 \exp(-2\tau/T_1) + A_2 \exp(-2\tau/T_2)$, where the subscripts on the A's and T's refer to the two signal components. The fit to this function is quite good, suggesting that the echo does consist of two independently relaxing components. However, spectral diffusion^{32,71-73} can also lead to non-exponential decay, in particular, the echo is expected to decay as $\exp(-\kappa\tau^2)$ or $\exp(-\kappa\tau^3)$

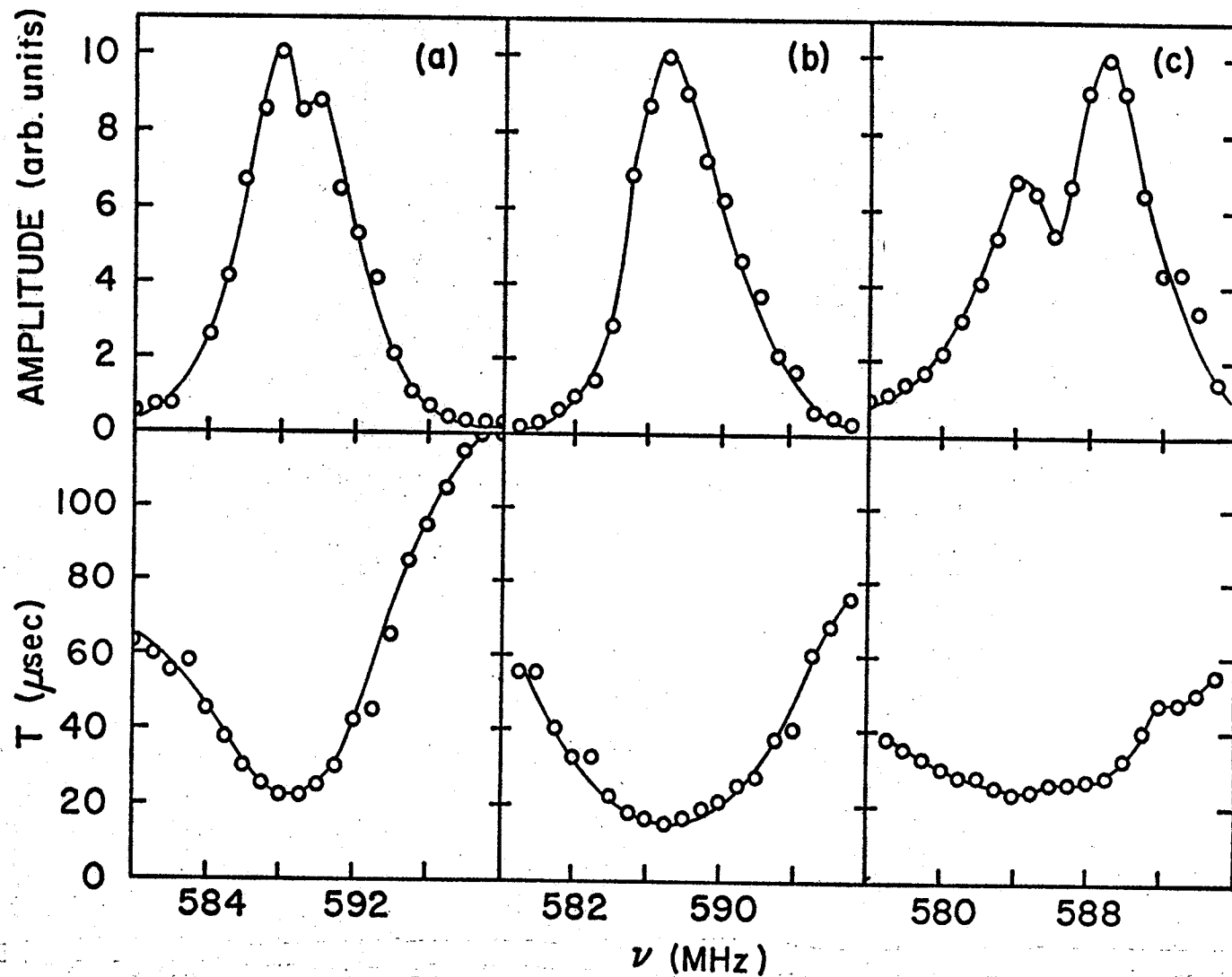


Figure 15. Echo amplitude extrapolated to $\tau = 0$ and relaxation time versus frequency at $T = 4.2$ °K. a) $\text{Ni}_{0.03}\text{Mn}_{0.62}\text{Fe}_{2.36}\text{O}_4$ single crystal, b) polycrystalline $\text{Mn}_{0.8}\text{Fe}_{2.2}\text{O}_4$, c) polycrystalline $\text{Mn}_{1.0}\text{Fe}_{2.0}\text{O}_4$.

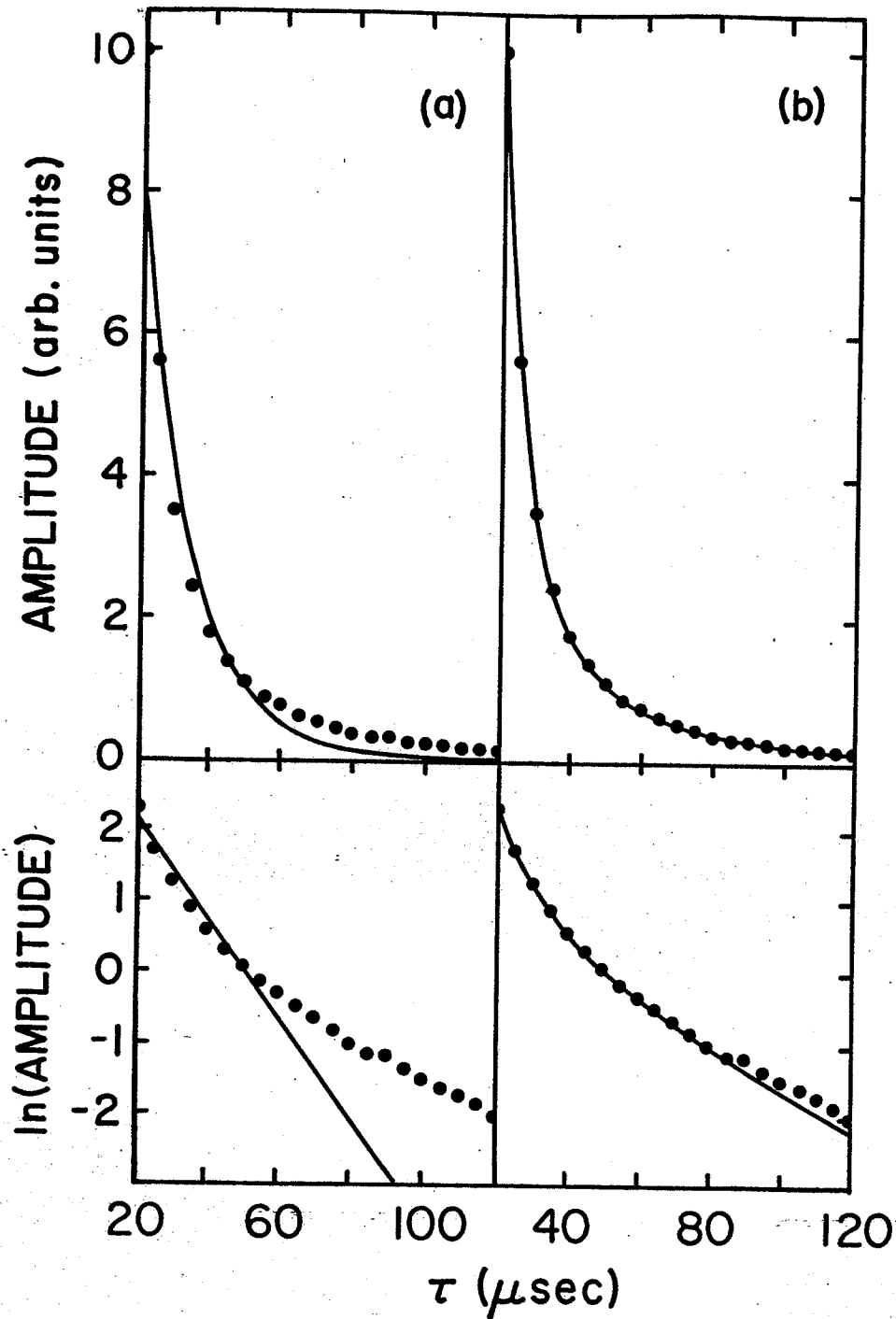


Figure 16. Echo amplitude and $\ln(\text{echo amplitude})$ versus τ at $T = 1.47$ $^{\circ}\text{K}$, $\nu = 586$ MHz, and $H_0 = 0.0$ kOe. a) fit to a single exponential, b) fit to the sum of two exponentials.